University of Washington

Abstract

Reynolds Number Trends in Computational Solutions of Two-Dimensional Airfoils With Taguchi Techniques and Grid Resolution

by Stephen C. Pluntze

Chairperson of Supervisory Committee:　　　　Professor D. Scott Eberhardt

Dept. of Aeronautics and Astronautics

A procedure is proposed which allows the extension of incompressible high Reynolds Number wind tunnel data to even higher incompressible flight Reynolds Numbers using a computational solution about the airfoil. The new procedure is predicated on the performance of different grid refinements and turbulence models versus functions of y^+, the vertical scaling parameter. When the difference between the computational force coefficients and the wind tunnel force coefficients are plotted against the $\log_{10}(y^+)$ or $\log_{10}(y^+/\sqrt{Re})$, the data for the higher wind tunnel Reynolds numbers ($\sim 2 \times 10^6$ - 1×10^7) falls on one line. This behavior is noted for different thicknesses of airfoils at different angles of attack from zero lift to C_{lmax}, although the corrected y^+ ordinate is required only with moderate to high angle of attack. The airfoil is tested in the wind tunnel with enough Reynolds numbers to establish a trend and the computational solution is carried out at the same Reynolds numbers and angles of attack. Corrected flight Reynolds number C_d and C_l values appear to asymptote correctly on a trend curve showing force coefficient with Reynolds number. A statistical measure, adapted from Taguchi Techniques of quality control provides a measure of comparing the importance of turbulence model, angle of attack, Reynolds number, and wall spacing to the analysis. It is used for the first time here to help evaluate the performance of a computational solver. Taguchi results show that wall spacing is often, but not always, the most important parameter, and that the importance of turbulence model and Reynolds number is very dependent on the airfoil and whether lift or drag is being

REPORT DOCUMENTATION PAGE		*Form Approved* *OMB No. 0704-0188*

1. AGENCY USE ONLY *(Leave blank)*	2. REPORT DATE 18 JUN 97	3. REPORT TYPE AND DATES COVERED

4. TITLE AND SUBTITLE
REYNOLDS NUMBER TRENDS IN COMPUTATIONAL SOLUTIONS OF TWO-DIMENSIONAL AIRFOILS WITH TAGUCHI TECHNIQUES AND GRID RESOLUTION

5. FUNDING NUMBERS

6. AUTHOR(S)
STEPHEN C. PLUNTZE

7. PERFORMING ORGANIZATION NAME(S) AND ADDRESS(ES)
UNIVERSITY OF WASHINGTON

8. PERFORMING ORGANIZATION REPORT NUMBER

97-015D

9. SPONSORING/MONITORING AGENCY NAME(S) AND ADDRESS(ES)
DEPARTMENT OF THE AIR FORCE
AFIT/CI
2950 P STREET
WRIGHT-PATTERSON AFB OH 45433-7765

10. SPONSORING/MONITORING AGENCY REPORT NUMBER

11. SUPPLEMENTARY NOTES

12a. DISTRIBUTION AVAILABILITY STATEMENT

12b. DISTRIBUTION CODE

13. ABSTRACT *(Maximum 200 words)*

14. SUBJECT TERMS

15. NUMBER OF PAGES
151

16. PRICE CODE

17. SECURITY CLASSIFICATION OF REPORT	18. SECURITY CLASSIFICATION OF THIS PAGE	19. SECURITY CLASSIFICATION OF ABSTRACT	20. LIMITATION OF ABSTRACT

examined. Excursions carried out include different grid stretchings and a possible extension from 2 to 3 dimensional. Flapped airfoils show similar results, although they may not be consistently valid under this procedure due to the scarcity of suitable data.

VITA

Name: Stephen C. Pluntze

████████████████

████████████████

Ph.D. Aeronautics and Astronautics
University of Washington, June 1997

M.S. Aeronautics and Astronautics
Massachusetts Institute of Technology, January 1987

B.S. Aeronautical Engineering
United States Air Force Academy, June 1982

United States Air Force Active Duty: June 1982 - Present
Current Rank: Major

Experience: Flight Testing GPS on B-52G, F-16A
        Intelligence analysis of future foreign aerospace threats
        Instructor and Assistant Professor, United States Air Force Academy
            Department of Aeronautical Engineering

Registered Professional Aerospace Engineer, Colorado, February 1995, 1997

Senior Member, American Institute of Aeronautics and Astronautics

Reynolds Number Trends in Computational Solutions of Two-Dimensional Airfoils With Taguchi Techniques and Grid Resolution

by

Stephen C. Pluntze

A dissertation submitted in partial fulfillment
of the requirements for the degree of

Doctor of Philosophy

University of Washington

1997

Approved by _____
(Chairperson of Supervisory Committee)

Program Authorized
to Offer Degree   Department of Aeronautics and Astronautics
_____

Date   June 4, 1997
_____

In presenting this dissertation in partial fulfillment of the requirements for the Doctoral degree at the University of Washington, I agree that the Library shall make its copies freely available for inspection. I further agree that extensive copying of this dissertation is allowable only for scholarly purposes, consistent with "fair use" as prescribed in the U.S. Copyright Law. Requests for copying or reproduction of this dissertation may be referred to University Microfilms, 1490 Eisenhower Place, P.O. Box 975, Ann Arbor, MI 48106, to whom the author has granted "the right to reproduce and sell (a) copies of the manuscript in microform and/or (b) printed copies of the manuscript made from microform."

Signature _____

Date _____5 JUN 97_____

University of Washington

Abstract

Reynolds Number Trends in Computational Solutions of Two-Dimensional Airfoils With Taguchi Techniques and Grid Resolution

by Stephen C. Pluntze

Chairperson of Supervisory Committee: Professor D. Scott Eberhardt

Dept. of Aeronautics and Astronautics

A procedure is proposed which allows the extension of incompressible high Reynolds Number wind tunnel data to even higher incompressible flight Reynolds Numbers using a computational solution about the airfoil. The new procedure is predicated on the performance of different grid refinements and turbulence models versus functions of y^+, the vertical scaling parameter. When the difference between the computational force coefficients and the wind tunnel force coefficients are plotted against the $\log_{10}(y^+)$ or $\log_{10}(y^+/\sqrt{Re})$, the data for the higher wind tunnel Reynolds numbers ($\sim 2 \times 10^6$ - 1×10^7) falls on one line. This behavior is noted for different thicknesses of airfoils at different angles of attack from zero lift to C_{lmax}, although the corrected y^+ ordinate is required only with moderate to high angle of attack. The airfoil is tested in the wind tunnel with enough Reynolds numbers to establish a trend and the computational solution is carried out at the same Reynolds numbers and angles of attack. Corrected flight Reynolds number C_d and C_l values appear to asymptote correctly on a trend curve showing force coefficient with Reynolds number. A statistical measure, adapted from Taguchi Techniques of quality control provides a measure of comparing the importance of turbulence model, angle of attack, Reynolds number, and wall spacing to the analysis. It is used for the first time here to help evaluate the performance of a computational solver. Taguchi results show that wall spacing is often, but not always, the most important parameter, and that the importance of turbulence model and Reynolds number is very dependent on the airfoil and whether lift or drag is being

examined. Excursions carried out include different grid stretchings and a possible exten-sion from 2 to 3 dimensional. Flapped airfoils show similar results, although they may not be consistently valid under this procedure due to the scarcity of suitable data.

Table of Contents

List of Figures

List of Tables

List of Symbols

AoA - Angle of Attack

C_d - drag coefficient

C_{do} - drag coefficient at zero lift

C_{dp} - pressure drag coefficient

C_f - friction drag coefficient

C_l - lift coefficient

C_p - pressure coefficient

F - Taguchi confidence level

L - characteristic length

Re - Reynolds number

S_{ij} - shear stress tensor

ST - total sum of squares

Sm - sum of squares due to the mean

Se - sum of squares due to error

S_j - sum of squares due to one factor

u* - friction velocity

V - velocity

Ve - error variance

y^+ - nondimensional vertical boundary layer length

β – artificial compressibility factor

ρ – fluid density and Taguchi percentage significance

τ – shear stress and pseudo time

μ – fluid dynamic viscosity

ν – kinematic velocity

ACKNOWLEDGEMENT

I am deeply indebted to my family for their prayers and patience throughout the times when I wasn't around for them. Brenda is the most wonderful and understanding wife any man could ask for. Grant and Amanda bring joy and satisfaction to my heart; and Kent, who came into this world as a 'Ph.D. Baby', has promised to give me some of his boundless energy and charm. I love them all and am very proud of my family.

I want to thank Professor Scott Eberhardt, my advisor, who had much more to be worried about than this lowly graduate student and yet found the strength to worry a little bit about me anyway. I appreciate the trust of the United States Air Force and the Air Force Institute of Technology who saw fit to send me back to school and who helped guide me through. My fellow faculty members at the United States Air Force Academy were a great source of inspiration - especially Lt Col Wayne "If I Can Do It Anyone Can Do It" Hallgren.

I sincerely thank my father and mother, brother and sisters (and in-laws) and their families, for their support and prayers for my success. It meant a lot to know they were out there pulling for me. And it took quite a bit of pulling but we got through. Thank you all from the bottom of my heart.

Chapter 1   Introduction

1.1 The Problem

A well known and continuing problem in Aeronautical Engineering today is the inability of wind tunnels and Computational Fluid Dynamics (CFD) to duplicate high flight Reynolds numbers (greater than about $30x10^6$) over the test configuration.[31] High enough Reynolds numbers to simulate flight conditions can be entered into a CFD code but associated problems with turbulence modeling will degrade the accuracy. Historically, the yardstick for CFD has been in how well it compares on a case by case basis to wind tunnel solutions, but since neither can handle the high Reynolds number regime, a new way to attack this problem may be necessary. At some point, perhaps the development of new turbulence models will enable CFD to solve problems of high Reynolds number but until this occurs engineers still need a way of obtaining the data. This work will attempt to find a way of using both methods together to compute a high Reynolds number solution and determine a trend of lift and drag coefficient with Reynolds number. Rather than use the wind tunnel data as only a benchmark for comparison, both methods will be connected together with the goal of obtaining high Reynolds number lift and drag data into the flight Reynolds number regime.

We have always wanted our engineering tools to be stronger, or lighter, or more effective and at the same time we remain concerned with more esoteric improvements like supportability, reliability, maintainability - and of course cost. We have always wanted our tools to live up to our expectations of their performance - what we wish they could do - although this does not always happen. The present work and this dissertation should be viewed in that context - it evolves around two particular tools, the wind tunnel and CFD, and a possible way to increase the scope of the data that these tools give us. In order to possibly improve these tools, this work presents a new application of CFD and new ways in which to view the data from both wind tunnels and computers. It represents an entirely new way of examining the relationship between wind tunnels and CFD. It also presents a new way to statistically examine this relationship and the CFD solver itself. Neither CFD

· nor the wind tunnel are perfect tools but working together perhaps they can combine to give a more complete answer in some cases than either is capable of on its own.

The wind tunnel has been a systematic and indispensable design tool for aerospace engineers ever since Orville and Wilbur Wright became frustrated with the data about airfoils available in the literature and so decided to create their own testing lab. Until aircraft started to become very large or to travel at high speeds, the wind tunnel was a perfectly fine way of coming up with the data necessary to design the aircraft. The problem is one of scale. To test a large or fast moving aircraft, the engineer would like to have a full-scale model and/or a full-speed stream of air. But the wind tunnel has to be limited somewhat in size and capability due to budgetary, space, and technological limitations. Since we cannot then test a full-scale model in a full speed tunnel, the next best thing is to build a scale model and test it in a smaller tunnel. Common sense might dictate that the scaled down model be subjected to some sort of scaled down airspeed and Osborne Reynolds in a series of experiments in 1878 determined that scaling the speed of a model with the scale of the dimensions was not necessarily the correct term. Rather, for incompressible tests where Mach number theoretically does not effect the calculations, the Reynolds number (Re) must be matched between the model and the flight test (prototype) aircraft. Assuming geometrically similar models:

$$(Re)model = (Re)prototype \tag{1.1}$$

$$\frac{V_m L_m}{\nu} = \frac{V_p L_p}{\nu} \tag{1.2}$$

where ν is the kinematic viscosity (approximately 1.57×10^{-4} ft^2/sec for air at STP). Assuming the working fluid remains the same, viscosity cancels and

$$V_m = \frac{V_p L_p}{L_m} \tag{1.3}$$

So only in the case where the fluid remains the same (usually air or water) in an incompressible test can the velocity be scaled by the same amount as the dimensions. If the

model is 1/10 scale, the equation above becomes $V_m = 10(V_p)$. The wind tunnel velocity must be 10 times the flight velocity. Even at low speeds for landing or taking off, the wind tunnel velocity can quickly become compressible which invalidates the test. A simple solution is to build a larger or full-scale model but for reasons already given this is probably impractical (although it has been done) and of course is expensive. Another solution would be to change the working fluid in the wind tunnel so that we now have:

$$V_m = \frac{V_p L_p \nu_m}{L_m \nu_p} \tag{1.4}$$

Now the ratio of kinematic viscosities, if small enough, can balance a large dimension ratio. But what working fluid to use? It must be inexpensive, non-toxic, non-corrosive and easily portable. It must also have a kinematic viscosity appreciably smaller than that of the prototype, (which is probably air) and if possible it should obey some sort of perfect gas law as air does. Since all of these requirements are hard to find in one fluid, the wind tunnel fluid usually remains air and it is pressurized or heated or cooled or in some way treated to lower its kinematic viscosity. In some cases gases such as Helium or Nitrogen are used but the point is that it is very awkward to match the Reynolds numbers of the wind tunnel model and the flight vehicle for all but the lowest Reynolds numbers. If flight velocity or prototype size remain small, the wind tunnel velocity can remain low and the air does not have to be treated. At any rate the wind tunnel eventually runs out of Reynolds number. If the aircraft flies at a Reynolds number above that, the engineer needs another way to get the data. In 1950, Abbot and Doenhoff wrote their definitive work on wings and wing sections. As part of a discussion about the drag coefficient of two different airfoils they offer the following quote which illustrates their frustration with this problem: "These data [Fig 1-1 here] illustrate the inadequacy of low Reynolds number test data either to estimate the full-scale characteristics or to determine the relative merits of wing sections at flight values of the Reynolds number"[51]. In other words, low Reynolds number behavior in the wind tunnel alone is not necessarily a good predictor of high Reynolds number data because there was no way to investigate higher Reynolds numbers. And high Reynolds

number wind tunnel data is hard to come by. Perhaps CFD can help to close this gap, at least over certain flight regimes and geometries.
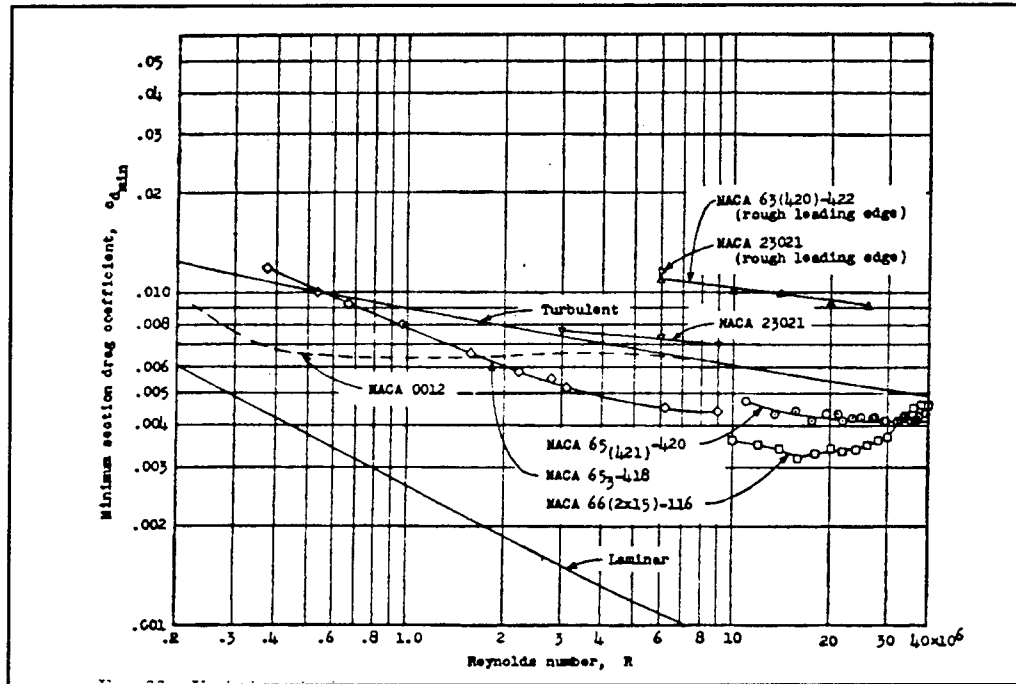
Fig. 1-1   Wind Tunnel C_{d_o} Trends with Reynolds number, circa 1950

As an example, consider the NASA Langley Low-Turbulence Pressure Tunnel (LTPT). Several of the test runs for airfoils used in this work were completed there and it is one of the premier low to medium speed wind tunnels in the United States[59]. The airfoils used in this work are not necessarily designed for low speed flight per se, but they will all have to go through take-offs and landings - two very important off-design points - and engineers would like to have accurate data at these points. At Mach 0.22 (an incompressible test) the maximum Reynolds number of the LTPT is about 15 x 10^6 per foot[7]. This means for an airfoil model in the tunnel with a two foot chord, it would be seeing air with a Reynolds number of about 30 x 10^6. If the flight prototype is a B-747 (average wing chord is about 35 feet) landing at 150 KTAS at sea level, the flight Reynolds number the tunnel is supposed to match is about 60 x 10^6. The tunnel is short by a factor of 2. This

` does not sound so bad until you consider that this Reynolds number was reached in the wind tunnel only by pressurizing the entire tunnel to 10 atm - the Reynolds number cannot get any closer. A very expensive proposition and it still cannot match the flight Reynolds number of a large transport aircraft in a low speed environment. A large percentage of the aircraft designed or modified by engineers today are large, transport-type aircraft. The more accurate the data at every design or off-design point, the lighter the engineering community should be able to make the airframe, which is the key for aircraft design. Figure 1-2 shows the performance of several low speed wind tunnels. UWAL is the wind tunnel at the University of Washington. Ames is a NASA Center and RAE is a British tunnel. None of them are able to handle the low speed flight regimes of large transport aircraft.
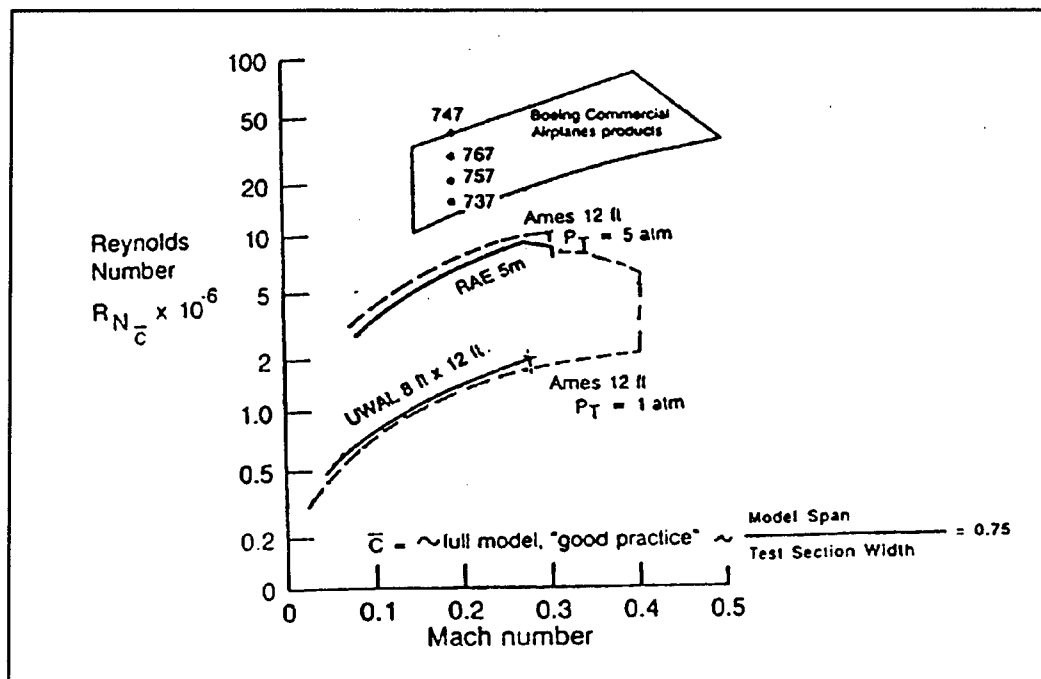
Fig. 1-2   Low Speed Wind Tunnel Performance[31]

Can Computational Fluid Dynamics help to close the Reynolds number gap? Is there a way to extend wind tunnel data in general using CFD? After all, the programmer can enter any flight parameters he wants into the computer program so any Reynolds num-

ber should be able to be computed within the CFD code. In theory this is correct, but like wind tunnels, CFD has its share of problem areas. A good summary of both is found in Reference 32. High among these potential problem areas are the equations that are being modeled by the computer. The Navier-Stokes equations are correct enough for aircraft design and supposedly all of the airflow effects are contained within them. However, in order to solve these equations on a computer, approximations must be made. The domain of interest is somehow divided into many discrete points, areas, and/or volumes if three dimensional. This is the grid on which the CFD calculation is performed. The final answer given by the code is highly dependent on the locations of the discrete points in the domain because the location of the points helps to determine the gradients within the flow. Depending on the number of points, their locations and how they are spread out, the solution may diverge, it may converge correctly, or it might converge to an incorrect solution. This is independent of any computational errors the solver may have. The impact of grid construction will play a major role in the present work.

Whatever difficulties the wind tunnel may have, at least it has real air going over a real airfoil surface. Turbulence, transition, separation bubbles, reattachment, vortex shedding, and separation can all happen naturally. These effects are almost impossible to pick up accurately with the computer because of the fine scale over which they begin and the computer's inability to realistically work with grids small enough to pick up these phenomenon. The ratio of large to small turbulent eddy size is $RE^{-3/4}$. In three dimensions the smallest grid size would need to be $RE^{-9/4}$ - too small to be computed in a finite time in the foreseeable future.[54,60] The current "world record" for DNS, Direct Numerical Simulation, is the flow around an object about the size of a BB[59]. The Reynolds number is small enough here (~1000) to allow eddies to form on a large enough scale to be picked up by very fine grids. On a normal airfoil problem, (Re ~ 10^6 or higher) the computer has to somehow model the turbulent flows in an attempt to match the forces created by them (the grid construction will impact the turbulence model also). For this reason the incompressible momentum equations are written in Reynolds Averaged form, Equation 1.5, using the

Boussinesq Approximation: the fluid viscosity is divided into μ and μ_t where μ_t is the turbulent viscosity.

$$U_j \frac{\partial U_i}{\partial x_j} = \frac{1}{\rho}\left(-\frac{\partial P}{\partial x_j} + 2(\mu + \mu_\tau)(S_{ij})\right) \tag{1.5}$$

$$S_{ij} = \frac{1}{2}\left(\frac{\partial U_i}{\partial x_j} + \frac{\partial U_j}{\partial x_i}\right) \tag{1.6}$$

Turbulent viscosity adds another unknown to the normal set of equations and requires at least one other equation (the turbulence model) to solve. In fact some turbulence models add more than one equation. The point, though, is that the CFD code is relegated to approximating one of the main aerodynamic effects on the wing surface and it is no wonder that CFD results are better in lift (a pressure effect mainly) than drag (pressure and shear stress). The literature reports lift results much more often than drag because of this. There seems to be some inclination to believe that since "it can't be done" drag should be secondary to lift. When comparative studies are performed, the C_p envelope is used to compare codes and turbulence models more often than C_d. Calculated C_d is rarely reported. One way or another though, the engineer needs these data and (s)he needs them at high Reynolds number. This study will include drag as just one parameter that can perhaps be obtained at higher Reynolds numbers using both wind tunnels and CFD together.

Other CFD effects such as accuracy considerations, boundary conditions, and the flow solving algorithm will impact the CFD solution but these two effects, grid and turbulence model will represent the majority of the controllable solution variances in this work. A related problem to turbulence is that of transition. In the wind tunnel, the boundary layer transitions when it is ready. Inside the CFD code, the programmer must tell the code when to transition or the code must be sophisticated enough to compute transition. Because we rarely have any idea when this is going to happen, it is usually easier to begin turbulent flow right from the beginning of the airfoil and leave it at that, although transition models are being developed. The codes used in this study did not have transition models. In this

case, if the CFD solution is to be compared to that of a wind tunnel, the wind tunnel model should be one that has some roughness applied close to the leading edge at around 0.05c to trip the boundary layer.

When validating a CFD code, separate test points are chosen to try to match the CFD solution with detailed wind tunnel data. Often this takes the form of trying to match details of the flow physics, which is very important in our search for better CFD models.[26,27] What the engineer actually needs are the force and moment coefficients along the flight profile. Specifications for matching drag and lift coefficients extend to the fourth decimal place during CFD code validation. This is understandable because we *want* the codes to be as accurate as possible but is this really what the engineer *needs*? Certainly this accuracy is required at times but in the search to eliminate all errors perhaps we sometimes lose sight of the forest for the trees. Certainly better CFD models are desirable and will result in better answers over a larger flow regime in the future, but what can we do for engineers with the technology available today? It is with this motivation that some of the current research was undertaken. Code developers may also find the Taguchi Techniques of interest as an independent way of pinpointing areas of physics or significant modules of the solver.

Because of all of these fixes, CFD has been more of a point design tool. The grid may or may not be valid over a wide range of flow speeds and angles of attack but the turbulence model rarely is, for example. The models are designed for certain circumstances and the designer hopes the off design performance (of both the turbulence model and the code) is satisfactory. Within the scope of their limitations (incompressible or not, no transition prediction, limited separation accuracy) the turbulence models produce reasonable data over a fairly large flow regime but researchers have been most comfortable reporting on the performance of a particular CFD code to one wind tunnel test of one airfoil at several angles of attack and accepting the limitations on extending the operating envelope of the code. CFD codes have been used to reverse engineer wing sections, i.e., given a desired pressure distribution they will generate an airfoil shape, but this still is only valid for the one pressure distribution given. Even though the underlying equations (Incom-

pressible Navier-Stokes) are valid for all slow speed flight conditions, for one reason or another our two main ways of solving these equations, empirical wind tunnels or numerical CFD, have limitations which prevent them from being used as wide-Reynolds number, wide-angle of attack, wide-airfoil-type design tools. The wind tunnel and the computer both have their areas of "expertise" and yet they have never been used to improve each others' results except through comparison. In Ref 34 the authors postulate in the recommendations section that: "CFD can provide analysis of data from flight and/or wind tunnels to bridge the gap between experimental results obtained at different Reynolds number conditions.".

1.2 Present Work

Engineers require data for their aircraft over a wide range of conditions as has been shown. What data do they need, how accurate does it have to be, and where will it come from? Wind tunnels alone cannot do it, nor can CFD. This effort will attempt to give engineers a new tool by attempting to answer some of these questions.

Aeronautical Engineers require force and moment coefficients and stability derivatives to design the airframe. Of course weights, internal structure, cost, etc. are also required but the engineer needs at least forces and moments from the wind tunnel or CFD to set the loads on the airframe. Ultimately this data is required for a three dimensional body in flight. Major airframe company engineers have indicated that if this data was consistently within 5% of the actual wind tunnel value they would be satisfied[17]. As indicated, wind tunnels cannot measure flight Reynolds number values and CFD cannot get them consistently within 5% over a broad range of configurations at once. To be completely fair, a test of a two dimensional object (the airfoil) in a wind tunnel will not give the flight values but hopefully more widely applicable two dimensional data can only help the design of three dimensional models.

The goal of the present work is to break this problem down to two dimensional, incompressible wing sections and try to discover if there is a way to extend the correct data from the wind tunnel at lower Reynolds number to flight Reynolds numbers using

CFD in some way - not directly because we already know that CFD cannot calculate high Reynolds number data well - but through some new indirect method. Even though two dimensional wing sections and incompressible flow do not give the entire data package desired by the engineer, perhaps this work will serve as a building block to more complex cases. No Mach effects will be considered. It is well known that even at theoretically incompressible velocities the value of C_{lmax} changes with Mach number after the Mach number passes $M = 0.20$ or so. The computer codes used in this study do not even have Mach number as an input variable because in practice any transient compressibility effects are not considered until $M > 0.3$. Most of the wind tunnel data collected for use in this study were taken at approximately $0.1 \leq M \leq 0.2$ so the results of this study should be interpreted as being purely incompressible.

It should also be pointed out that this work will not be a theoretically based new CFD algorithm. It will attempt to take what is readily available to today's engineer, i.e., wind tunnel data at some Reynolds number range, an appropriate CFD solver/turbulence model combination and a grid generator; and create a new tool to help the engineer in his task by extending the wind tunnel data to higher Reynolds numbers. Tools of this type have always been used in engineering to compensate for some inability of prevailing methods for design. For example, linear airfoil theory (lifting line theory) was an early attempt to compensate for a lack of accurate predictive tools for lift and drag. The Moody Diagram does the same thing for pipe flow. Industry has used proprietary drag curves for things such as landing gear and nacelles. In an interesting engineering tool development effort[24], Boeing engineers developed a way to predict lift and moment over a 3-D wing using the solution over an airfoil by adding the right amount of camber and thickness to a CFD solution of the airfoil. The bottom line is that we need to get the best possible data in the hands of the designer while at the same time not increasing the complexity or costs of his job. The engineer does not care if he can predict the forces on an airfoil based on the flow around a coffee mug as long as the data is correct, consistent, and cost effective.

The following original contributions will be presented in this research:

1. A new way of considering the data collected from wind tunnels and CFD

- wind tunnels and CFD used in a combined fashion instead of adversarial

2. Establishment of y^+ across Reynolds number to establish a trend for the NACA0012.

- highest absolute accuracy at higher truncation errors

- repeatable across Reynolds number and evidently angle of attack

- constant y^+ is two orders of magnitude lower than recommended

3. Tracking absolute accuracy (defined as the absolute value of the difference between wind tunnel and CFD solutions for lift and drag) using grid y^+ across different Reynolds numbers and angles of attack.

4. General method to connect wind tunnel to CFD solution in order to establish high Reynolds number data and trends of lift and drag coefficients with Reynolds number

- development of areas of consistency between wind tunnel and CFD data

5. Excursions on basic method

- different airfoils

- different turbulence models

- different grids

6. First application of Taguchi Techniques to evaluate solver performance

- reinforce conclusions of general trend method

- investigate use of Taguchi Technique as a tool to aid code development

7. Apply method to high lift complex airfoils

In order to demonstrate these items this work is presented and organized as follows:

Chapter 2 will focus on the early work for this effort and will explain the search for parameters to govern the comparison of CFD and wind tunnel data as well as the relevant CFD parameters for running the available codes.

Chapter 3 will describe the development of the research ideas.

Chapter 4 will investigate some excursions from the basic method.

Chapter 5 will present a statistical snapshot of the results using the methods of Taguchi and postulate these methods for other CFD uses as well.

Chapter 6 will present the results as they apply to high-lift airfoils.

Chapter 7 will present the conclusions.

Chapter 2   Initial CFD/Wind Tunnel Efforts

2.1 Introduction

In order to compare wind tunnel and CFD results you must first have the wind tunnel results. This seems so obvious as to be ridiculous but a little research shows why this needs to be said. Over the years many, many airfoils have been tested in various wind tunnels under widely varying conditions and it would seem a simple matter to uncover the required results. However, for the present work to be successful, several things must be true about the wind tunnel tests themselves.

The wind tunnel tests will be accepted as "truth" (hereafter referred to as baseline data) because this is the data we are trying to extend. This data will be the lower Reynolds number data that is assumed to be already in place for the engineer to use. These tests are expected to have been taken carefully in a controlled test where the appropriate wind tunnel data corrections have been made. The errors that can occur in wind tunnel testing, even at (or especially at) low speeds are well documented[32] and will not be repeated here. A good tunnel with improper corrections gives poor data. Remember that the final goal is to come up with "the right answer" for lift and drag at higher Reynolds numbers. If the data at the lower Reynolds numbers are wrong, it would be against all odds to expect the high Reynolds number data will somehow be correct.

The data must cover an adequate Reynolds number range. Some wind tunnel tests, when used for design purposes, cover only narrowly selected regions of the flight envelope. The goal of the present work is to uncover trends of forces, or force coefficients, with Reynolds number. If there are not groups of data at several lower Reynolds numbers, there will be no trend information to extend to the higher Reynolds numbers. This work is not an extrapolation but enough data must exist to allow the consistent data to converge (see Chapter 3) and to allow conclusions to be drawn. If the lowest Reynolds number the wing will see in flight is higher than the wind tunnel's capability this may require some extra testing because some tests at lower than required Reynolds numbers may be needed to

help establish the trend. Recall the B-747 example of Chapter 1. The lowest Reynolds number this wing will see in normal flight is take-off and landing. In those configurations it is just above the higher end of today's low speed wind tunnels. The wind tunnel testing would have to be run at several Reynolds numbers leading up to some high value, perhaps three or four different Reynolds number tests, i.e., spanning a range of perhaps several million in Reynolds number, covering all of the configurations and angles of attack of interest. Assuming a method can be proposed, perhaps less testing could be done as confidence increases. Ordinarily these wind tunnel tests probably would not be run because they are nowhere near the flight Reynolds number and would not give correct answers for C_d and C_l. This may or may not add extra costs to the design stage depending on how many other wind tunnel tests have to be performed anyway. If the final result of the entire wind tunnel/CFD process as presented in this study is a reasonably correct high Reynolds value for lift and drag coefficients, it may be worth some limited added costs.

The wind tunnel model and the CFD solver should have the same transition point. It makes sense that the closer the CFD model comes to the conditions on the airfoil, the closer it can match the data. Since transition was not a focus of this study, the flow is assumed to be completely turbulent. To cause this turbulence in the wind tunnel requires some sort of boundary layer trip, usually some grit attached with adhesive. If the wind tunnel tests do not have this trip they may not match the computer results consistently enough to provide any correlation for a trend to develop. As turbulence models improve, presumably transition models will also and data matching will only improve in the future. Figure 2-1 shows that perhaps this problem may not be as bad as it may appear. At the higher Reynolds numbers of interest in this study, the gap between tripped and natural transition comes closer naturally due to turbulence occurring sooner at higher Reynolds numbers for shallow angles of attack. In general we can conclude that higher Reynolds number CFD data is better than lower Reynolds number data as far as transition to turbulence goes.
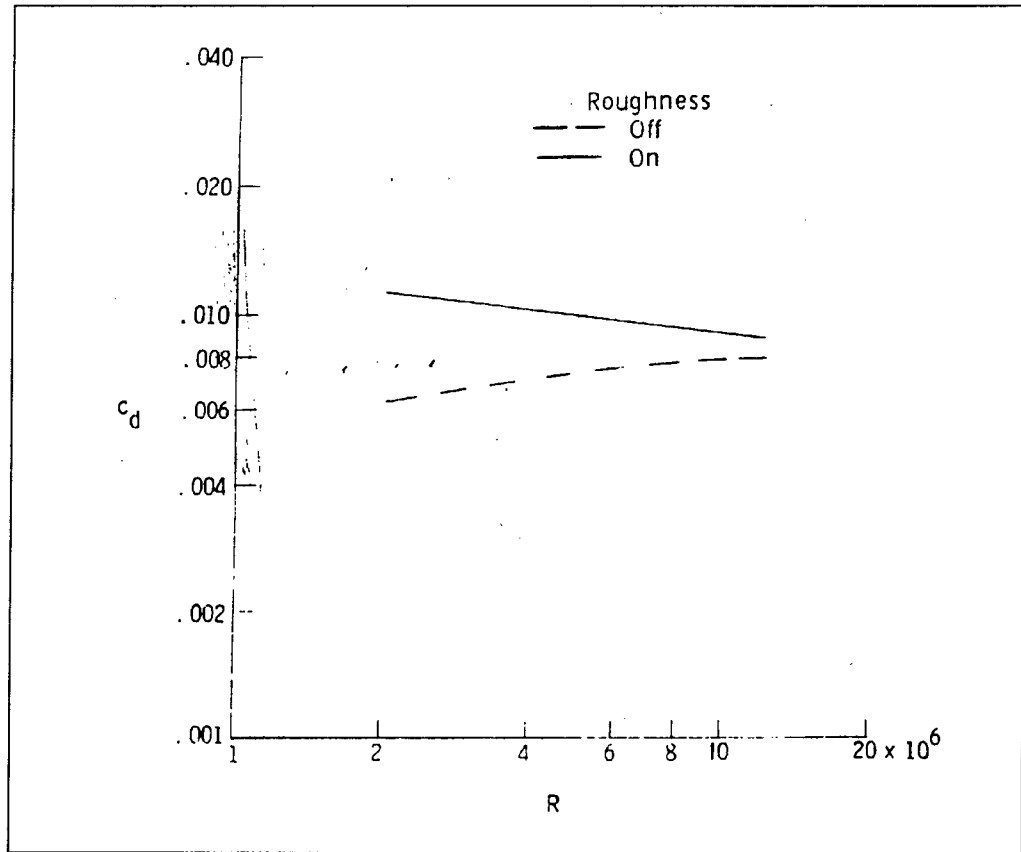
Fig. 2-1 Free versus Forced Transition at Increasing Reynolds number for an NACA0012 Airfoil at Zero Lift[10]

The CFD solver must be one capable of performing on the conditions similar to those of the wind tunnel model. In this case this requires incompressible Navier-Stokes solvers. For the present work two flow solvers will be used; one written in the University of Washington's CFD Lab and the other developed by NASA. ITANS2D[1] is a two dimensional pseudo-compressibility solver written at the University of Washington specifically for cases with large amounts of separation. INS2D[3,4,5] is a NASA code which also uses pseudo-compressibility. Pseudo-compressibility is a method whereby a fictitious time derivative of pressure is added to the continuity equation to turn the entire system of Navier-Stokes equations into a hyperbolic system which can then be marched forward in

fictitious (or pseudo-) time (because the added term is a fictitious term) for ease in calculating and coding. The incompressible continuity equation then appears as

$$\frac{1}{\beta} \cdot \frac{\partial p}{\partial \tau} + \nabla \bullet \vec{V} = 0 \qquad (2.1)$$

At steady state this derivative disappears and divergence free flow is maintained. Time accurate problems can also be completed with this method as long as pseudo time derivatives are also added to the momentum equations (the energy equation is not required in incompressible flow calculations) and integration is performed in pseudo-time for all equations. For the problem at hand, it should not matter what kind of flow solver the engineer has at his disposal, other than for his own cost/time constraints. As long as the solver is capable of converging to a correct solution for the given airfoil configuration and input conditions, the results should be satisfactory insofar as the solution for two or more proven codes running under the same conditions should give nearly the same answers.

What will matter is the turbulence model. The Reynolds Averaged Navier Stokes Equations (Equ. 1.5) are written with ($\mu + \mu_\tau$) multiplying the velocity derivatives in the shear tensor. Turbulence models try to assign a value to μ_τ, the turbulent viscosity, which is then used in the momentum equations. To do this they may create a production equation in much the same way as momentum is produced and convected by forces in the momentum equation. Some models are algebraic and more empirical in nature and are not formed this way. The equation(s) is(are) [some models have two] either in terms of μ_τ directly or some other parameter that can be used to calculate μ_τ. The models try to take into account the production of turbulent energy in the main flow stream and the damping effect of any walls (turbulence is zero at the wall). The difference between the models lies in how these terms are constructed and then how they are calibrated. Each model has some arbitrary constant coefficients which must be assigned values through calibration. These arbitrary constant values might be assigned using a flat plate test or a conglomeration of other types of turbulent tests but no matter how the models are calibrated, each turbulence model is only "best" over the region in which it was derived and then calibrated. The fact that they give reasonable results in other regimes is helpful. In this work, the ITANS2D code uses

the Baldwin-Lomax model and the INS2D code uses both the Spalart-Allmaras or Baldwin-Barth models. The availability of this spectrum of models can help to gain more understanding of their effect over a range of Reynolds numbers, especially in the statistical tests of Chapter 5.

For the initial work on this problem, which aims to determine only if CFD can match a known Reynolds number trend and what it takes to do so, a NACA0012 airfoil was selected as representing a broad cross section of airfoils satisfying the above conditions. It has been widely tested over the years and supposedly large amounts of data exist for wind tunnel tests of this airfoil. However it can be rather difficult, as stated previously, to find quality tests over a wide Reynolds number range with boundary layer trip.

2.2 NACA0012 Tests

McCroskey[10] has written an excellent paper summarizing many different wind tunnel tests for the NACA0012. By examining different classifications of tests, i.e., tripped vs. non-tripped, compressible vs. incompressible, he was able to come up with empirical relations governing the trend of C_{do} with Reynolds number for this very common airfoil. This trend compilation has only been done for this airfoil and it provides a solid foundation from which to begin CFD comparisons with wind tunnel results. It should be stated that the goal of this work is not to generate empirical "curve fits" for C_d and C_l with Reynolds number. Rather, the goal is to find an independent, consistent relationship to a parameter of some kind that when properly used will show the desired relationships. It is not possible with current methods to accurately predict viscous high Reynolds number data either with numerical or analytical methods directly.

McCroskey's empirical relationships took the form of a function of the inverse log(Re) and were quite different depending on whether the data was from a tripped or non-tripped test. His resulting equations were:

$$C_{do} = 0.0017 + \frac{0.91}{\log(Re)^{2.58}}$$

(2.1)

for tripped tests and:

$$C_{do} = 0.0044 + \frac{0.018}{\log(Re)^{0.15}}$$ (2.2)

for the non-tripped version. Other airfoils would of course have different relations if known. The nature of an inverse logarithm of Reynolds number to a power may help lead toward a more universal parameter because the general behavior of most airfoils should be similar, at least for the incompressible subclass of flows. The NACA0012 wind tunnel tests with tripped boundary layers, (Equ 2.1), now provide a goal for the CFD code to match. This curve is shown in Fig. 2-2.
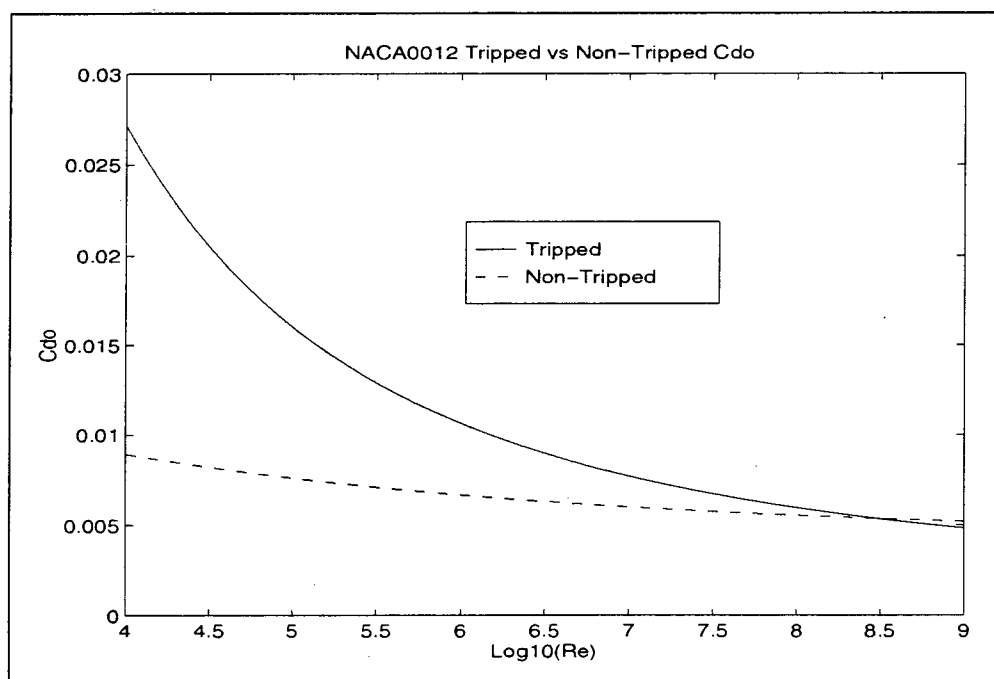
Fig. 2-2   Wind Tunnel C_{do} Trend Data for NACA0012 from Equations 2.1 and 2.2

If this were an unknown airfoil, the engineer would have wind tunnel test results for the lower Reynolds number end of the curve (perhaps $\sim 10^5$ to $\sim 10^7$) and we would hope to use CFD to help extend the data to the higher end of the curve. It may seem a sim-

ple matter to "connect the dots" in some sort of extrapolation fashion beyond the highest experimental data point. However, there are an infinite number of paths the data could take toward the higher Reynolds numbers. An independent and consistent tie between the lower and upper Reynolds numbers would give more confidence in extending the data. In McCloskey's paper the highest Reynolds number of an actual data point was about 10^7. The goal of the initial work is to discover how well CFD can extend the wind tunnel solutions beyond the highest Reynolds number and what CFD and physical parameters are important in doing so. Contrary to some CFD literature, the CFD results do not have to exactly lay on top of the wind tunnel data in order to consider it "matched". This work aims to improve engineering tools and aeronautical engineers do not need, nor do they expect, perfect data from CFD. Researchers who are developing new algorithms sometimes feel the need to match wind tunnel data as exactly as possible and this is essential for new algorithms, but the algorithm then will work exactly under only the conditions of the reported tests with no assurance that extensions of the validated code will be accurate without adjusting various code parameters. It may not be a general predictive design tool for engineers. This effort is attempting to find a new application of CFD across a wide spectrum of conditions and improve its use for design. It is very significant to get one algorithm and one grid to match up exactly with one test but it may be more useful to somehow use CFD to apply to many different tests if possible.

At this point, the engineer has the airfoil, some lower Reynolds number data, the flow solver, and a grid generator. The various inputs to the flow solver and the grid generator can be very numerous. The flow solver inputs are generally of two types - the flow conditions, which are determined by the problem; and the code variables, which are generally modified to make the code converge or converge more quickly or converge more accurately - an example would be the artificial viscosity coefficients which help to damp the low frequency errors. Since changing all of the possible variables would quickly make the current problem of finding consistent relationships intractable and inefficient, it is assumed that the engineer knows enough to set up the code to run correctly and then leaves it alone. Especially at the high angle of attack conditions there may be some tweaking required, but modern codes that satisfy the conditions of this effort are very robust.

The runs generated for this effort were made with the CFD solvers' variables constant for all cases. The only variables that change are the turbulence model, the grid, the angle of attack, the airfoil and the Reynolds number.
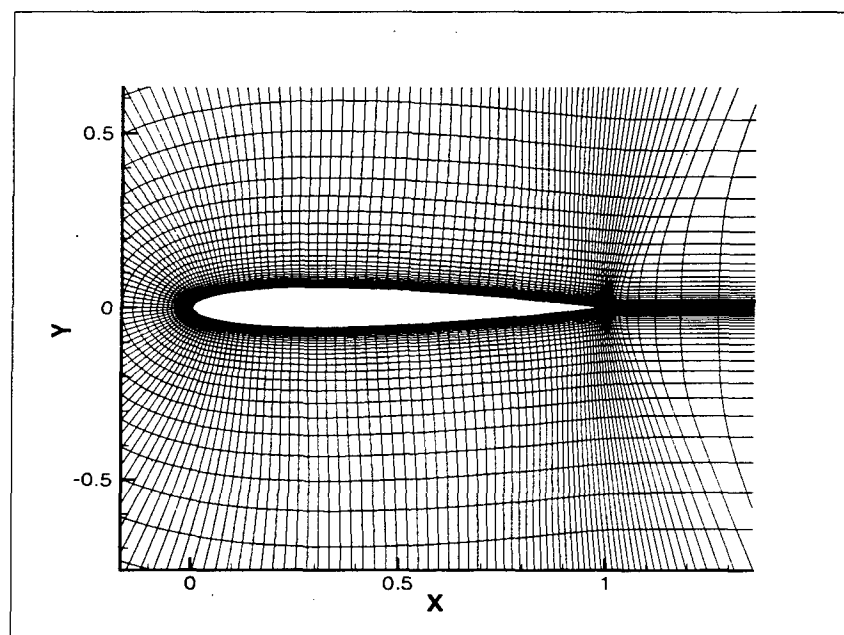
Fig. 2-3   NACA0012 Airfoil Grid

The grid, however, has a more profound effect on the final answer than the CFD parameters. Figure 2-3 shows a possible grid for the NACA0012. The word "possible" is used because there is no guarantee what the engineer will pick for grid density or grid spacing. It is possible that the user may keep the values from whatever grid was generated an hour or a day ago with the same grid generator. The engineer would be familiar with the general guideline that he needs "a lot of grid points" clustered in the viscous regions of high gradients and that there should not be "too many" points or his problem would take forever to run. Figure 2-3 was created with 201 points circumferentially around the wake and the airfoil and 62 points radially outward, for a total of 12,462 grid points. This is a "reasonable" number of points based on current papers and standard usage with which a design engineer is presumed familiar. Jameson[38] lists 512 x 64 as sufficient and Zingg[35] indicates 249 x 49 is acceptable. The variations even among researchers in the field is

obvious. This work will attempt to determine important grid parameters too but the difference is that the goal here is consistent trends rather that point calculations.

An engineer may be less familiar with how far away from the surface to put the first point. Once this distance is determined, the spacing of the remaining points is automatic within the grid generator. For the first NACA0012 runs, the initial distance of the first point from the wall was set by simply using the last value remaining in the grid generator from the previous user, 0.3×10^{-5}. This is certainly a "small" number and appears reasonable for boundary layer-type distances. Viscous rules of thumb such as keeping $y^+ = 1.0$ may or may not be applicable to trend information but provide a good start to placing the first point. To get trend data, the engineer chooses, say, four, Reynolds numbers: 1×10^6, 1×10^7, 5×10^7, and 1×10^8. Then, using the given flow solver (ITANS2D in this case) and the created grid, four values of drag coefficient are created at zero degrees angle of attack to get C_{do}. In Figure 2-4 these four CFD values are plotted versus the log of the Reynolds number and McCroskey's tripped NACA0012 curve. While it appears that at least two of the resulting values are somewhat close to baseline data, the trend is totally incorrect. In the absence of the known trend curve, with only these four scattered data points, and with known data stopping at a Reynolds number of $\sim 10^7$ or so, the two high Reynolds number CFD points in this figure may have been considered satisfactory. This is a good illustration of the requirement for complete wind tunnel data. Again, these values were created with a proven solver for these conditions and grid values that appear reasonable, at least at first glance.
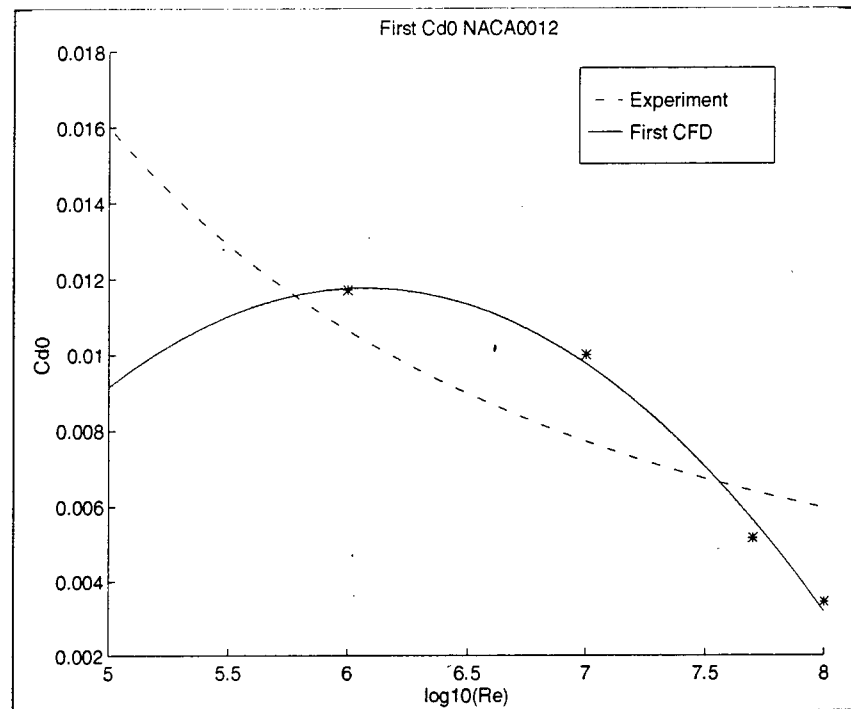
Fig. 2-4   Initial NACA0012 C_{do} Results with Given Grid Parameters

Figure 2-5 shows all CFD runs on the same airfoil and on the same grid but at different angles of attack. The point here is to show that the performance of the code/turbulence model combination is consistent for more highly stressed conditions. Although the trend was already shown to be incorrect (and the drag values certainly are at these angles of attack), it is incorrect in a consistent manner. This is vital and holds promise that any predictive technique that may be developed from this work will give consistent readings at the higher angles of attack where larger amounts of separation and turbulent flow render the turbulence models at least questionable.
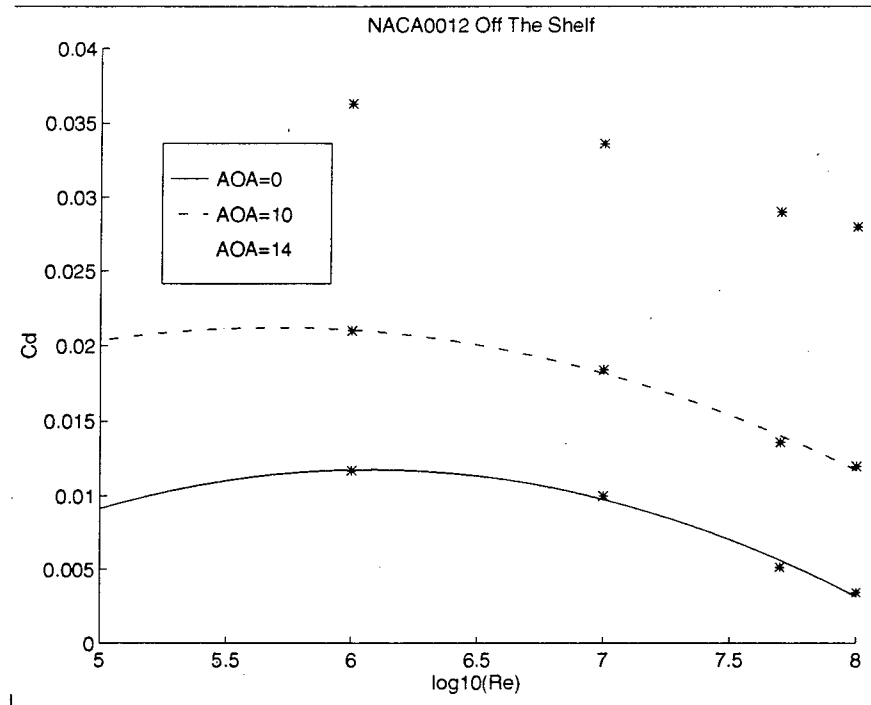
Fig. 2-5   Initial NACA0012 Airfoil Result over Higher Angles of Attack

Clearly, something needs to be changed. The inputs to the flow solver that pertain to the flow cannot be changed, nor should those which affect the convergence of the flow solver since presumably it works just fine. The turbulence model is fixed with this code. The grid is the only remaining variable to try. One of the knocks against CFD over the years has been that to make a particular run work almost perfectly, the parameters of the flow solver are massaged to a point where the solver will run *only* the one case. For this work, the flow solver inputs are left alone and only the grid is changed. This should be more appealing from an engineering point of view since the grid must change for each new airfoil anyway and the engineer's basic tool, the flow solver, can hopefully remain constant over many configurations.

It is entirely possible that there is a perfect grid for each problem. A grid that allows the solver to calculate the correct answer to that specific problem either because it happens to capture the right flow information or it just gets lucky by ending up with the

right answer as a result of the distribution of grid points. It seems impractical to search for this magic grid for every problem due to the number of iterations that might be required to find it. Statistical methods (Chapter 5) can help to determine the correct grid parameters to concentrate on but not where to put all of the points.

The grid has a major affect on the CFD solution because the relative nearness of points affects the value of the gradients of velocity and pressure. It is these gradients which make up the governing equations, so the grid spacing and density will affect the accuracy, convergence, and eventually the trends of the data. Grid density refers to the number of points on the actual grid. In theory, if the entire space domain around an airfoil had a grid point assigned to it, the flow solver would get the right answer, at least in the absence of round-off error or modeling error. Since this is not practical, the user decides where to place the grid points. Grid spacing as used here will refer to the distance from the surface of the airfoil to the first point in the radial direction. It will also be referred to as wall spacing. The spacing between adjoining grid points is controlled by the grid density and the stretching conventions built into the particular grid generator. Conventional wisdom in the CFD community states that if the user keeps adding points in the interest of accuracy, eventually the grid will become so full of points and they will become so tightly spaced that the solution will become independent of the grid. Consistent performance between low and high Reynolds number regions may not occur in grid independent situations. It may be acceptable to be inaccurate as long as the inaccuracies are consistent.

In this initial work on the NACA0012, the grid density will remain the same. Its effect will be considered later in Chapters 3 & 4. The parameter that will be changed is the wall spacing. In effect, we will attempt to replace the effects of increased grid density by modifying the spacing at the surface. Reference 36 touches on this briefly for transonic flows, but this is an incompressible study and nothing is known about the importance of this point for trend information. Other studies have also referred to the importance of this distance.[35,36,37] This has the effect of changing the definition of the boundary layer which in turn will change the value of the skin friction coefficient which will result in a new value of the drag coefficient. As the first point from the surface is moved in or out by the

engineer, all of the remaining points in the radial direction are changed because of the stretching algorithm in the grid generator. This algorithm sets the relative spacing between rows of points as the grid is marched away from the surface during construction. For example, imagine a Δy at the surface doubling from one grid attempt to the next. Each successive row of grid points in the radial direction would not double but would be set according to a formula within the grid generator. Therefore the ratios between the Δy values of one grid and the next would remain the same, even though the absolute "y" values would change. The distance of the outer boundary might change also depending on the grid generator and is another grid parameter which may have an effect on trend information but it was not studied in this research. The distance to the outer boundary remains at 15 chords in this study. Since any change in Reynolds number will affect the viscous nature of the flow, and with it the boundary layer, the optimum wall spacing for each case may be different. The next three figures show the effect of wall spacing on C_{do} for the NACA0012 at three of the four Reynolds numbers used for the trend data.
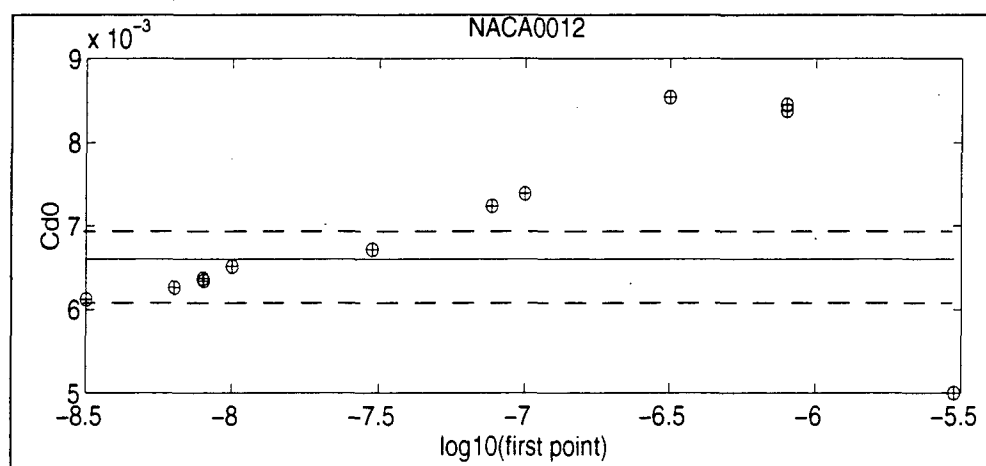
Fig. 2-6 NACA0012 Wall Spacing versus C_{do} at Re = 5 x 10^7

Figure 2-6 shows the result of decreasing the wall spacing at a Reynolds number of 5 x 10^7. The solid line represents the baseline data from McCroskey's curve and the dashed lines represent a 5% error bound. Not only is there significant drag variation with

wall spacing but the minimum spacing is not the optimum. (At this point it was still believed that drag should be matched as closely as possible but this was later found to be unnecessary, [see Chapter 3], especially since drag cannot be matched exactly at higher angles of attack.) Also there seems to be no tendency toward grid independence at this Reynolds number when only changing the wall spacing. Figure 2-7 shows the same case at a Reynolds number of 1×10^6. Similar behavior is observed with decreasing wall spacing but at this lower Reynolds number there is some evidence of grid independence until the spacing becomes too small. The true C_{do} value on this figure is 0.0106, the bottom of the graph. The dashed line again is a 5% error bound.
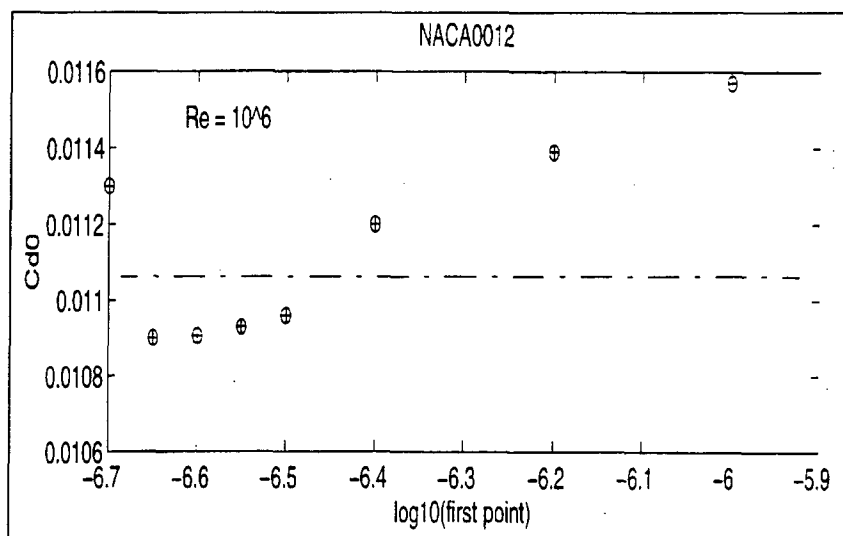
Fig. 2-7   NACA0012 C_{do} with Wall Spacing at RE = 1×10^6
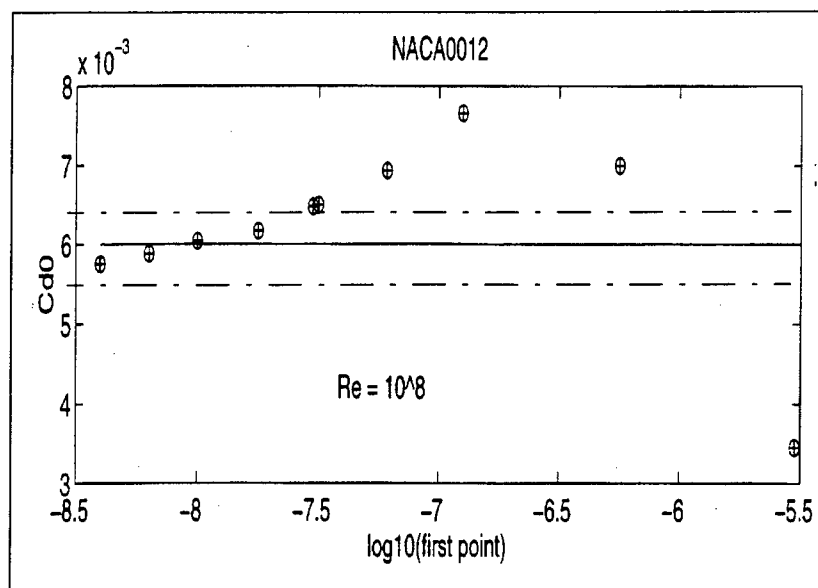
Fig. 2-8   Initial Wall Spacing at a Reynolds number of 1 x 10^8

Figure 2-8 is again the same case run at a Reynolds number of 1 x 10^8. With this very high Reynolds number more viscous activity is contained in a region closer to the airfoil so the optimum spacing is narrower than that of Fig 2-6 or 2-7. The drag value closest to the true value is again not at the minimum spacing, although the values here fall in a narrower percentage range than the lower Reynolds numbers. Several things can be noted from these figures:

1. The minimum wall spacing is not necessarily the optimum (closest to baseline) spacing.

2. As Reynolds number increases, the required wall spacing becomes lower and the percentage drag variation of the lowest spacings becomes narrower.

3. Grid independence is not completely in evidence for each of these three Reynolds numbers when only changing wall spacing.

4. Since the optimum wall spacing varies at least with Reynolds number, we need a better indicator of optimum spacing which hopefully will stay relatively constant with Reynolds number.

5. These results are for one turbulence model and one angle of attack. (The code used only the Baldwin-Lomax model and McCroskey's paper covers only C_{do}.)

Grid independence for this case may be a poor criteria to mention. In this work, any drag improvement caused by changing the wall spacing is attempting to compensate for grid density. In other words, the total number of grid points does not change and yet we hope to approach the true value of drag only by changing the grid spacing at the surface. It may be that under these conditions grid independence is not reached before the code halts due to the extremely small distances causing floating point errors. It may even be possible to decrease the grid density even further (recall it remains at 201 x 62) and still compensate by finding the optimum wall spacing. However it is best to err on the side of caution and a reasonable amount of grid density must remain. At some point, too few points will remain in the grid and no amount of spacing changes would overcome it. The case for fewer points is that the computing time is less as the number of points decreases. Lessening the time required is a commendable goal, but some minimum threshold of grid points must be maintained to assure a reasonably good chance of getting an optimum value of drag. The literature recommends more points in the interest of lower truncation errors but in this case the goal is matching a trend, no matter what the errors inherent in the solver. If this inaccuracy is consistent, there may be some confidence in extensions to higher Reynolds numbers.
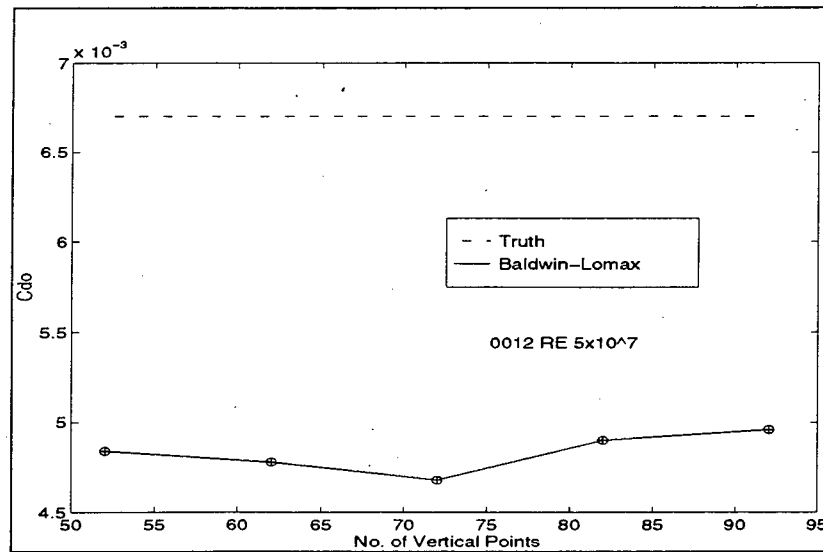
Fig. 2-9   ITANS2D Behavior With Increased Grid Density at a Wall Spacing of 0.3×10^5

Figure 2-9 shows that increased grid density with the original wall spacing in the absence of other changes is not necessarily the answer either. Presumably, decreased spacing at the wall can compensate for decreasing density, but the reverse is not true, at least not for the current case. The reason is that by decreasing the initial spacing more points are pulled into the boundary layer to add definition regardless of whether or not any more points are added. Some mention of this phenomenon is made by researchers in high speed flows where speed[36,37] and temperature gradients must be well resolved but incompressible researchers do not go into too much detail about creating their grids. It seems that the grid can hold much promise in providing accurate drag answers from incompressible CFD, or at least pointing to a way of getting an optimum drag value. Hopefully this will also apply to matching trend data. Zingg has presented a very interesting work along these lines.[35] This paper will be discussed in detail later in this chapter.

Note that no mention has been made yet of spacing *along* the surface or of trying to match lift. These will be investigated in the next, more detailed phase, but in the initial work it seemed prudent to investigate the parameter hardest for CFD to match (drag) and the grid spacing parameter having perhaps the greatest effect (the direction through the

boundary layer). It is entirely possible that different angles of attack and/or turbulence models would affect the nature of these conclusions. This will again be the subject of Chapter 3. For this initial part of the research we desire only to discover if the trend data can be matched and if so how. We have already seen that spacing at the wall can somehow be used to find an optimum drag value. What remains is to find a better parameter to pinpoint this optimum spacing - some physical parameter that is related to spacing but stays constant over the Reynolds number range. A natural choice of a non-dimensional parameter related to vertical spacing in the boundary layer is y^+.

2.3 The Use of y^+

` Y^+ is a parameter somewhat akin to the Reynolds number. It scales normal spacing in the lowest parts of the boundary layer. Y^+ is defined by:

$$Y_L{}^+ = \frac{yu^*}{\nu} = \frac{yU_\infty\sqrt{\frac{C_f}{2}}}{\nu} = yRe_L\sqrt{\frac{C_f}{2}} \qquad (2.3)$$

where

$$u^* = \sqrt{\tau_w/\rho} \qquad (2.4)$$

is the friction velocity. The last equality in Equ 2.3 follows from the fact that at the end of the airfoil L=1.0 and in this equation y^+ is calculated at the end of the airfoil. At each point along the surface the shear changes so y^+ would also be different for a given "y" distance above the surface. It seems reasonable to use an average y^+ which is the value of y^+ calculated at the trailing edge using the C_f value for the entire airfoil as opposed to local values.

$$\overline{Y^+} = \frac{1}{N}\sum_{i=N} y_i Re_L\sqrt{\frac{C_{fi}}{2}} \qquad (2.5)$$

$$= \frac{\left((NyRe_L)\sqrt{\frac{C_f}{2}} \right)}{N} \tag{2.6}$$

$$= y^+_L \tag{2.7}$$

as long as the "y" value is the same at each point. Unless otherwise noted, y^+ and y^+_L will now refer to the same thing.

Other researchers using turbulence models refer to using a y^+ value of about 1.0 for the first point from the surface. This seems to be a generally accepted value that gives good drag results for a wide class of problems. However, there is no record of any systematic tests of the type done here to discover if there is an optimum y^+ value for airfoil trends and if it applies across a Reynolds number spectrum. Merely setting y^+ of around 1.0 may not be the best way of assigning wall spacing, nor may it necessarily give an optimum answer for trend data. The value of $y^+ = 1.0$ is often set by matching C_f but drag also has a pressure component and it may be that y^+ of 1.0 is not the best value over wide angle of attack or Reynolds number regimes.

The previous figures showed drag data plotted versus the log of the spacing of the first point from the surface. Knowing the Reynolds number, it is easy to turn these plots into graphs of drag versus y^+ once the codes are modified to calculate and output the value of C_f for the airfoil. The value of "y" in equation 2.3 is the value of desired initial grid spacing entered into the grid generator by the user. The next series of figures will show what happens to the data when it is plotted versus y^+.
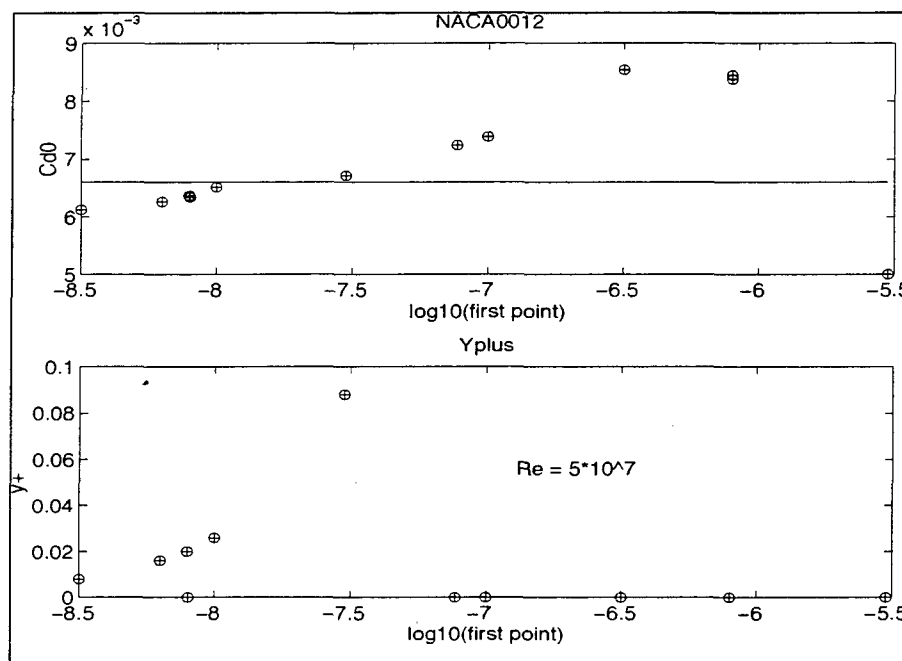
Fig. 2-10   Comparison of C_{do} versus y^+ and the Wall Spacing, Re = 5 x 10^7

Figure 2-10 is a comparison of the data originally presented in Figure 2-6. At a Reynolds number of 5 x 10^7, the top graph shows C_{do} against Wall Spacing and the bottom shows y^+_L against the same wall spacing. The zeros on the y^+ chart are points that were not calculated so they would not distort the vertical axis of the y^+ graph. Those points would have been at high values of y^+ and would mask the low y^+ data which is what we need to see. Notice that because the upper graph uses a log scale for wall spacing, the y^+ distances increase rapidly in orders of magnitude. The two points in the upper plot closest to the true drag value from McCloskey's curve are an order of magnitude apart in y^+. The three points clustered together in a tight band around a wall spacing of 1 x 10^{-8} all fall at a y^+ of around 0.02. Figure 2-11 shows this same comparison at a Reynolds number of 1 x 10^6.
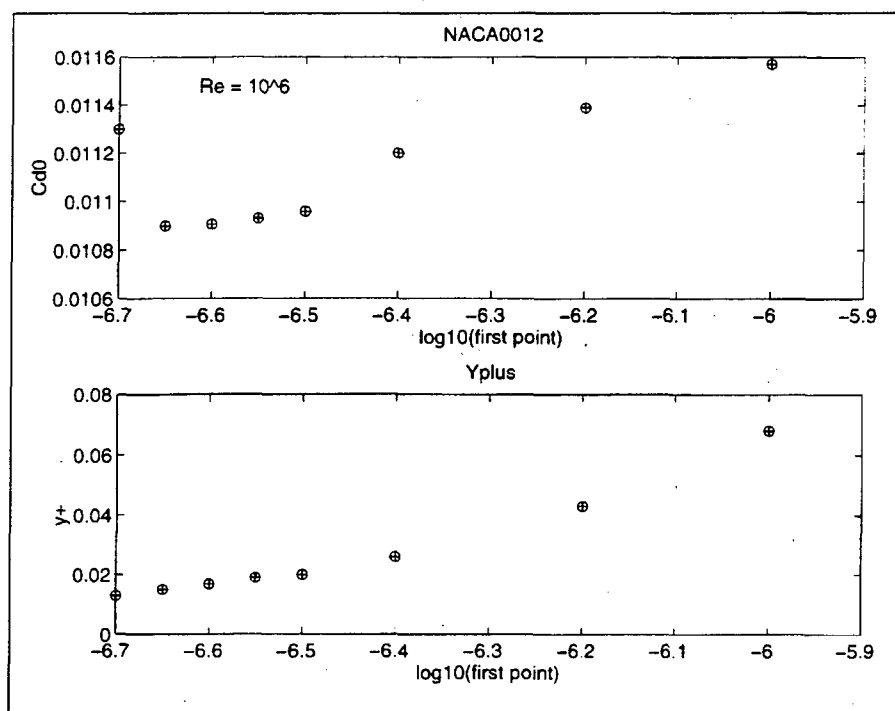
Fig. 2-11   Comparison of C_{do} versus y^+ and the Wall Spacing, Re = 1 x 10^6

In this case, the graph is the extension of Figure 2-7, with the baseline data for C_{do} at 0.0106 for this Reynolds number. The drag data is flatter at the lower spacings but the optimum C_{do} value seems again to occur at a y^+ value of approximately 0.02. Similar results appeared in the remaining two Reynolds number cases, 1 x 10^7 and 1 x 10^8. It appears, at least for this airfoil and this Reynolds number range that an approximately constant value of y^+ = 0.02 is a satisfactory indicator of the grid spacing required at the surface to get optimum drag. Although this an initial look at the problem of predicting trends, it may be that y^+, or a parameter involving y^+ could be the physical parameter we seek to allow the engineer to find the optimum value for drag across a wide Reynolds number range. This is a new concept. Nothing is yet said about lift, other turbulence models, or an angle of attack range. When a y^+ value of 0.02 is applied at each of the four Reynolds numbers, and the resulting grid spacing is used to generate a grid of density 201 x 62, the

result appears in Figure 2-12. Note that this optimum value of y^+ is two orders of magnitude smaller than that considered acceptable for most turbulence models.
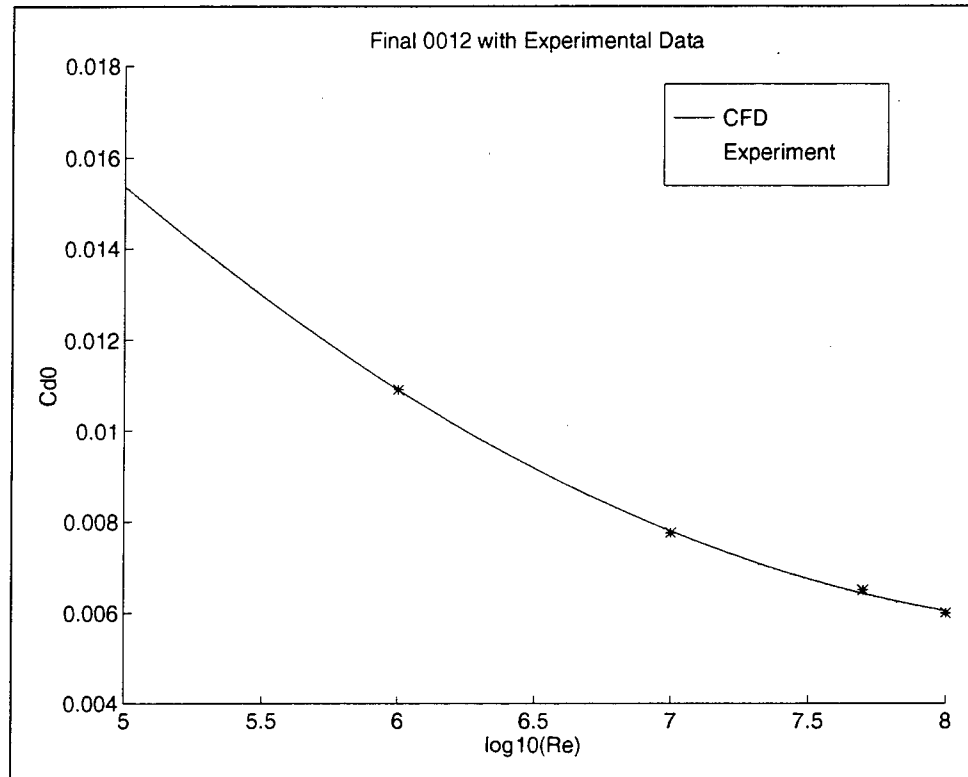
Fig. 2-12 Final Result of NACA0012 with $y^+ = 0.02$

The CFD matches the trend curve well because the curve was the accepted baseline data. If the individual test data points from McCloskey were placed around the experimental curve there would be more variance but the CFD data would still appear to match the data. Other airfoils will not have a trend curve laid for them out so the CFD data will attempt to match a trend based on scattered raw data points.

It may appear that the engineer has to know C_f ahead of time by running several grids to target the optimum grid spacing. A simple calculation using assumed values of C_f and a known y^+ will give target grid spacings. Assuming a y^+ of 0.02 and a C_f value of 0.006 at a Reynolds number of 1×10^6 and a C_f value of 0.004 at a Reynolds number of 1

$x10^8$ gives initial grid spacings of 3.7×10^{-7} and 4.5×10^{-9}, respectively, from equation 2.3, which are generally of the correct magnitude. A few grids and runs may then be required to fine tune the optimum value of y^+.

By way of comparison, Figure 2-13 shows the effect of grid density at a y^+ of approximately 1.0 for the Baldwin-Lomax turbulence model at a Reynolds number of 5×10^7 on the NACA0012. More of a tendency toward grid dependence is observed but no grid density gives as accurate a drag value as that from the previous discussion with $y^+ = 0.02$.
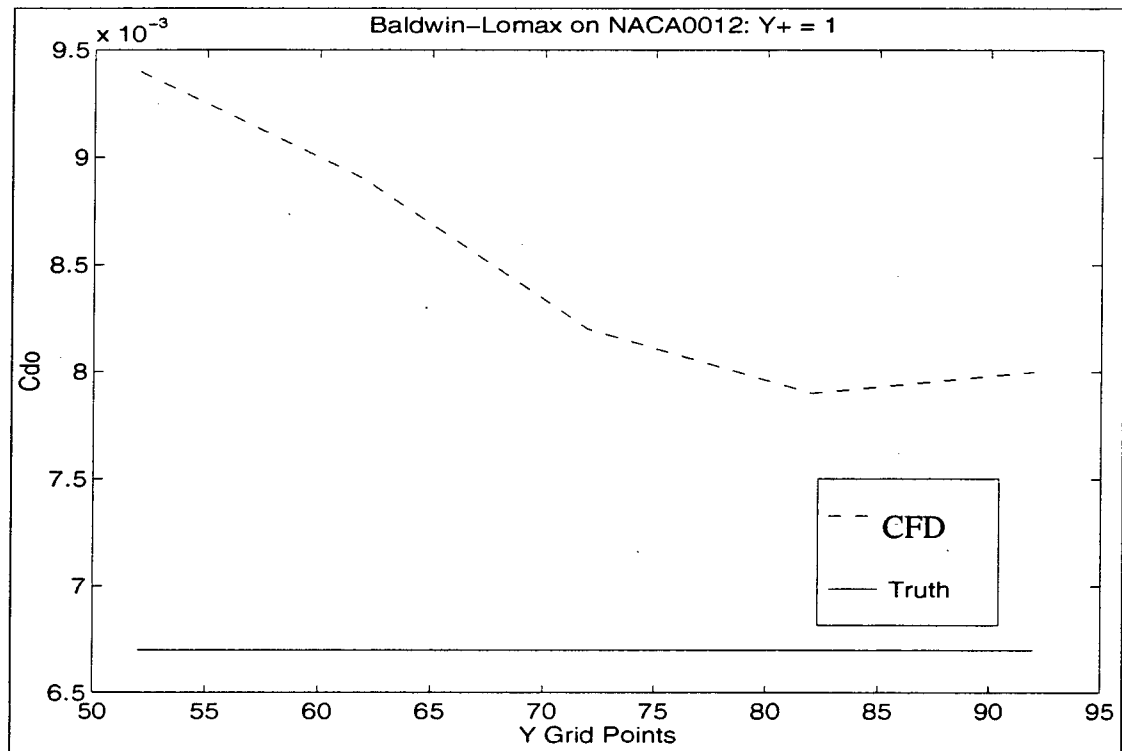
Fig. 2-13   Behavior of Baldwin-Lomax Turbulence Model at $y^+ = 1.0$

In contrast, Figure 2-9 shows what happens when no attempt is made to decrease wall spacing while increasing the grid density. The number of points in the grid has relatively no effect on the solution at all if the gradients are poorly resolved in the boundary layer. This result is similar to one of the conclusions reached in reference 36 but this is an

incompressible case and has been translated to y^+ across two orders of magnitude in Reynolds number. Some researchers[35,38,41] have reported that y^+ values less than 0.2 or so take longer to converge because of the large grid cell aspect ratios. No problem with convergence was noticed at this point in the study but certainly higher y^+ values would decrease the number of iterations required to reach a point where either the solution converges or the C_d and C_l values are changing by less than a percent. Perhaps higher values of y^+ would be sufficient to establish the trend but not give accurate drag values. In other words, if $y^+ = 1.0$ is chosen and *every* drag value is in error by, say, 12% (this is the consistency we are looking for) the trend is still established and all high Reynolds number values are corrected to the trend. It just so happens that for this airfoil under these conditions a y^+ of 0.02 matches the trend *and* calculates drag correctly. We do not necessarily need both. During the initial research, finding a y^+ that accurately matched the drag gave more confidence in the trend information at this single angle of attack.

In a Technical Note in 1992, Zingg[35] reported values of C_l, C_d, C_{dp} and C_f for an NACA0012 airfoil under wind tunnel conditions similar to the current work (M=0.16 Reynolds number=2.88 x 10^6, angles of attack of 0°, 6° and 12°). The overall conclusions were drawn that favored grids with upwards of 95,000 grid points and achieved spatial discretization (truncation) errors of less than 1% in lift and drag using Richardson extrapolation. But the actual resulting lift and drag coefficients were better (as compared to the wind tunnel results) for grids that happen to be of the same order in size (249 x 49 Zingg, 210 x 62 here) and y^+ (0.015 Zing, 0.02 here) as the current work using the same turbulence model (Baldwin-Lomax) on a different solver (ARC2D). No mention is made of difficulty with convergence. What the paper fails to point out is that the best absolute accuracy (wind tunnel - CFD) was obtained on the same grid and y^+ for all three angles of attack. This is true for both lift and drag and was not obtained on the grid with the lowest truncation errors. This is the type of consistency that will hopefully allow the development

of trends regardless of numerical errors. The following tables show this result using values reported by Zingg.

Table 1: $\%\,C_d$ Errors

Grid	0°	6°	12°
497 x 97	13.8	19.4	19.2
249 x 49	4.3	8.3	13.8

Table 2: $\%\,C_l$ Errors

Grid	0°	6°	12°
497 x 97	N/A	1.2	4.8
249 x 49	N/A	0.6	2.2

Several references have been made concerning the engineer having to do several CFD runs. This is a good time to discuss costs that may be associated with this method. The method as it exists at this point is as yet immature and we do not yet know if y^+ is the parameter we seek for other airfoils at other angles of attack. But whatever the parameter, it seems certain the engineer will have to do several computer runs to find his optimum values. Is this too expensive? In the not-too-distant past it may well have been. Today there are PCs that can do each of these airfoil runs in about an hour. And this is done in background while the engineer is free for other tasks. The grid generation takes only seconds. Compare this to the cost of building new wind tunnels, which the US Congress recently decided not to do because of the cost, or modifying new ones. It costs $10,000 per week to run the NASA LTPT[59]. If some of the higher Reynolds number tests can be scaled back due to some sort of predictive method like the one to be presented in this work then perhaps a few extra computer runs are worth it.

2.4 Boeing 737-200 Airfoil

To test whether or not y^+ is a good indicator of trend information, the Boeing 737-200 airfoil was chosen because the ITANS2D code had been used on it as part of an icing program at the University of Washington[23] and some limited baseline data was available. Figure 2-14 shows the airfoil with a 201 x 62 grid.
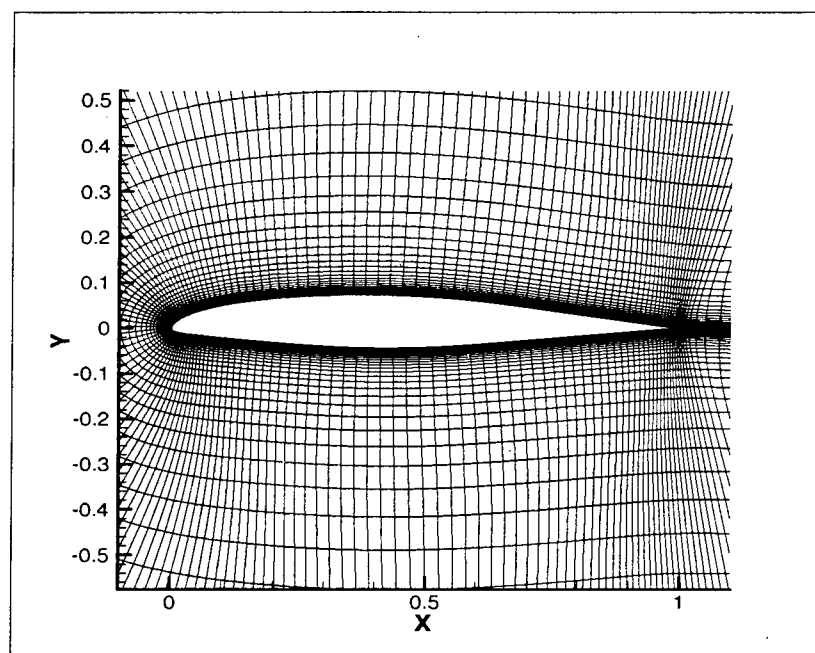
Fig. 2-14   Boeing 737-200 Airfoil Grid

This time no comparison of baseline data (i.e. wind tunnel data) was made beforehand to set the grid spacing at the wall. Wind tunnel data was only used to set flow parameters and Reynolds numbers. A y^+ value of 0.02 was used based on the analysis of the previous section. The same four Reynolds numbers were used to create the trend curve. Figure 2-15 shows the result.
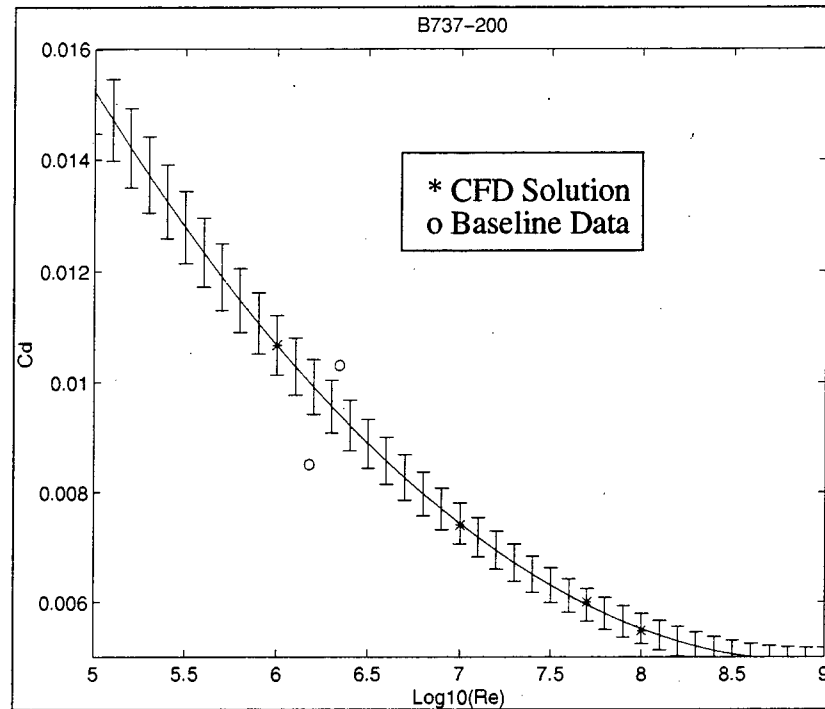
Fig. 2-15   Possible Boeing 737-200 Trend Curve at $y^+ = 0.02$

The circles on the figure are the baseline data at two different Reynolds numbers and a 5% error band has been placed on the trend curve. The scattered and limited baseline data for this airfoil are an accurate representation of what an engineer may face if he uses an airfoil tested in the literature. An airfoil under design by an airframe company would have many data points over a larger Reynolds number band. The results look reasonable, especially considering the limited baseline data upon which to base any trend. The two baseline points could well be part of a trend that is matched. More tests on airfoils with more baseline data are required.

It also may be that y^+ is not the best choice across other airfoils, other angles of attack, and other Reynolds number ranges. Also no conclusions have been drawn for lift, other turbulence models and possibly other grid parameters. This will be the subject of the next chapter. What has been shown is that there does appear to be a physical parameter pointing to optimum usage of a CFD flow solver to compute drag over an airfoil at a wide

Reynolds number range and a method to follow in order to perform that task. One new concept has been put forth in this Chapter:

1. The use of y^+ not to match friction drag or total drag coefficient at one test condition but to predict trend data of drag coefficient across two orders of magnitude in Reynolds number. The trend appears promising to extend to higher Reynolds numbers beyond the reach of the wind tunnel.

Chapter 3   Creating the CFD Trend Procedure

3.1 Multiple Airfoils

In the next phase of the work, we will try to determine if the procedure of the previous chapter is valid and whether or not the y^+ value of approximately 0.02 is applicable to other airfoils. There is no guarantee that the value of $y^+ = 0.02$ on the NACA0012 airfoil will necessarily work on other airfoils. The results for the Boeing 737-200 were inconclusive, although this is partly due to the fact that there was little high quality baseline data available for the 737-200 airfoil.

Abbot and von Doenhoff's book on airfoil theory is widely read by aeronautical engineers and contains a wealth of data on airfoils. Unfortunately, the data does not span a large Reynold number regime for the tripped airfoils. Usually the tripped airfoils are only tested at one Reynolds number. Still, it is perhaps the widest range of airfoil data available for a quick comparison of this type. Several different airfoils were chosen, gridded with the same size grid as before, and run over several different values of y^+ at an angle of attack of zero. This is not necessarily the value of the zero lift angle of attack as it was for the NACA0012. In each case, the value of y^+ which gives the best answer for C_d was found over several wall grid spacings. The table below shows the results:

Table 3: Multiple Airfoil y^+ Results

NACA Airfoil	Re	y^+
2412	5.7×10^6	0.49
4412	6.0×10^6	0.70
65-212	6.0×10^6	0.95
2415	6.0×10^6	0.4
63-009	$1.0 \times 10^6 - 2.0 \times 10^7$	0.06

The point is not so much that the y^+ value is whatever it is but that each airfoil seems to have a different y^+ value that is optimum. This may also be dependent upon angle of attack and/or Reynolds number. The y^+ value seems to be a function of camber and perhaps thickness, which might be another interesting research project. If optimum y^+ were equal to the same value at the same Reynolds number for each different airfoil this would provide a consistency we seek between wind tunnel and CFD data to tie low Reynolds numbers to higher ones, but there could be others. For example, the last airfoil, 63-009, had a constant y^+ value for the optimum drag over its entire tested Reynolds number range, similar to the NACA0012 of Chapter 2. Optimum drag does not mean exact drag, just the value of drag closest to the wind tunnel result. If this holds over other airfoils then perhaps trends could be identified because high Reynolds number CFD tests could then be run at the same y^+ value. Unfortunately, this is all the tripped wind tunnel data on these airfoils so we must search for other tests.

3.2 Test Airfoils

Fortunately, several quality airfoil tests do exist upon which to test any new methods of investigating trends. These four were chosen:

Table 4: Selected Test Airfoils

Airfoil	Purpose	Re Range	Test Location
MS(1)-0313	Medium Speed	$2 \times 10^6 - 12 \times 10^6$	NASA LTPT
MS(1)-0317	Medium Speed	$2 \times 10^6 - 12 \times 10^6$	NASA LTPT
LS(1)-0421	Low Speed	$2 \times 10^6 - 9 \times 10^6$	NASA LTPT
Super 9.3%	Supercritical Wing	$2.9 \times 10^6 - 16.8 \times 10^6$	NASA LTPT

These airfoils span a wide range of uses, thicknesses, cambers and shapes. A method that could be useful across these four airfoils might hold some hope of working for most any airfoil. Again, the goal is to find a way, through the use of the correct consis-

tent parameter choice, of identifying a trend of C_d and C_l with Reynolds number for these four airfoils at several angles of attack. The four following figures show these airfoils.

In this phase of the research we will attempt to tie one parameter to several airfoils over a wide Reynolds number range and several angles of attack. The initial method will be worked out on the 13% thick airfoil (from now on referred to as the MS13) and then try it on the others. Three different turbulence models will be tried and grid effects such as stretching in the "x" and "y" directions will also be investigated.
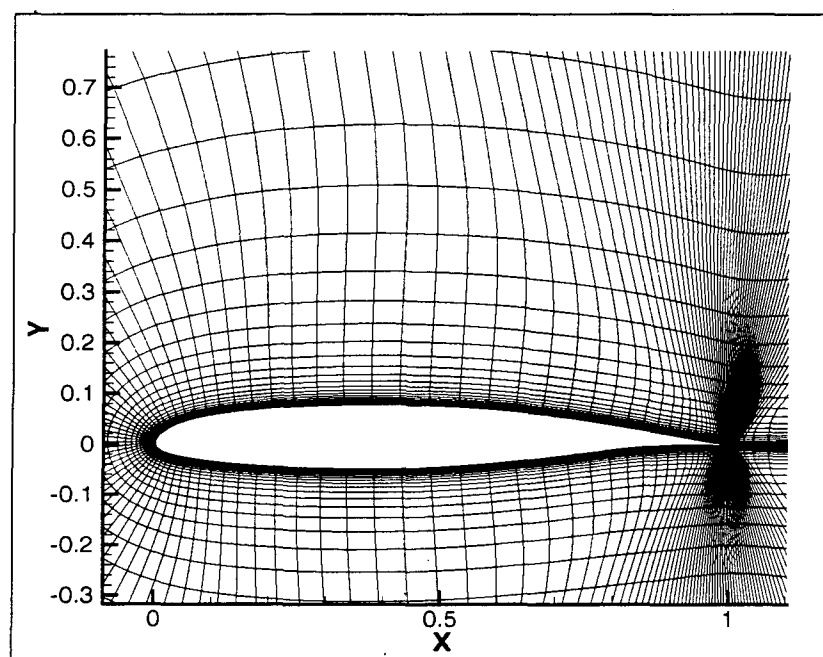
Fig. 3-1   MS-13 Airfoil
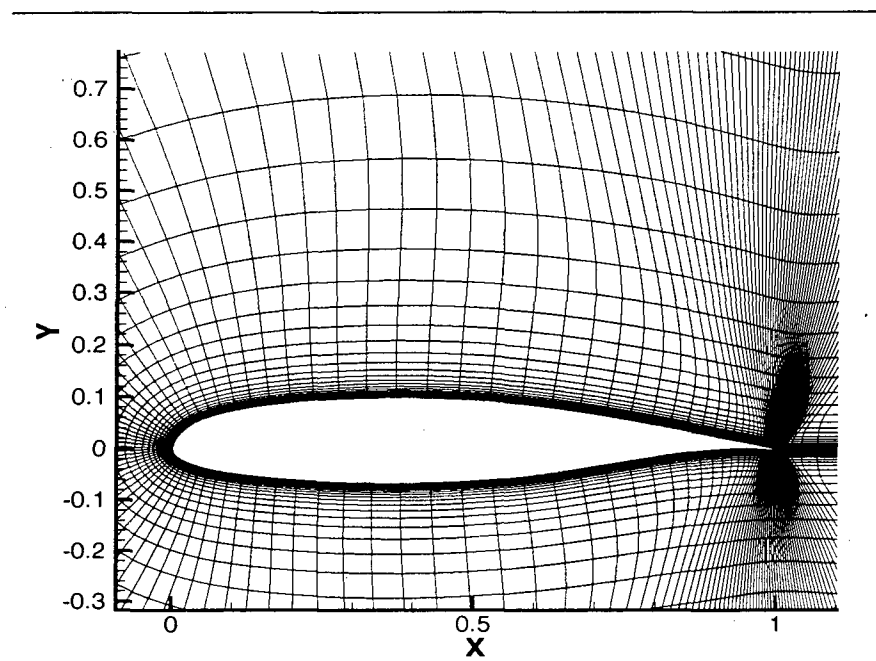
Fig. 3-2   MS-17 Airfoil
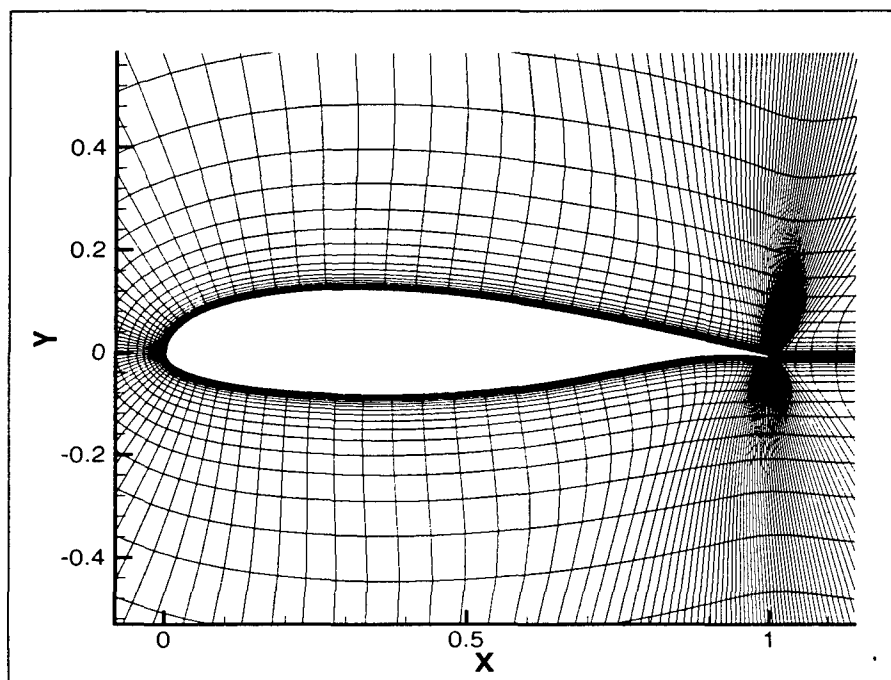
Fig. 3-3   MS-21 Airfoil
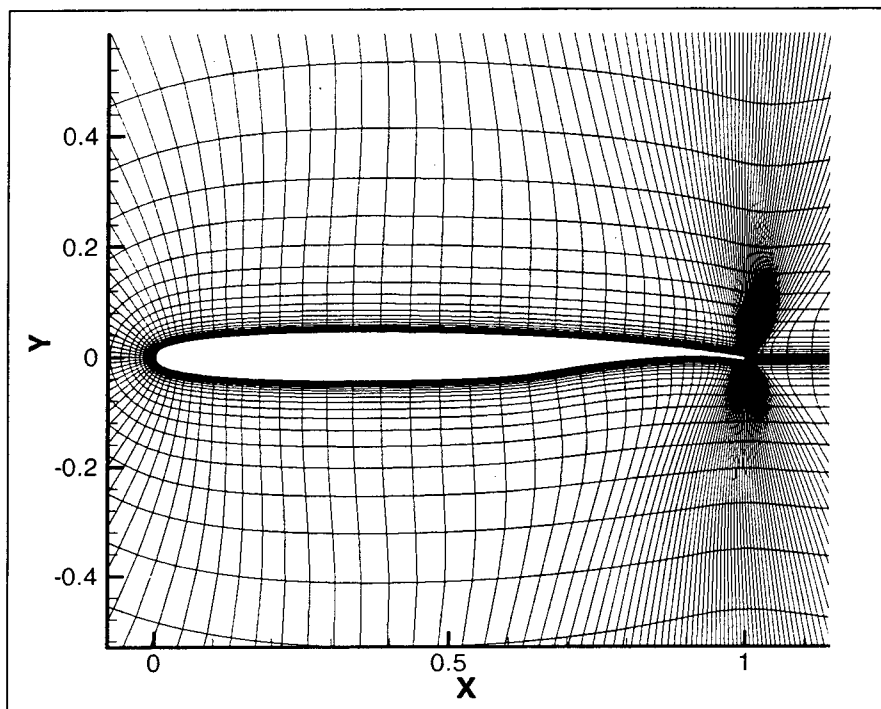
Fig. 3-4   MS-93 Airfoil

3.3 Turbulence Models

This is not a study of turbulence models themselves but since they play such an important role in the calculation of the force coefficients and may impact any trend method it seems worthwhile to introduce them.

3.3.1 Baldwin-Lomax[42]

The original report by Baldwin & Lomax came out in 1978. It is an attempt deal with the calculation of compressible turbulent separated flows and as with all other turbulence models, it has been tried in many cases that do not conform to this norm. It uses a two-layer approach where μ_τ is calculated differently depending upon the nearness to the wall; i.e., an inner and outer layer. The Baldwin-Lomax model is an algebraic model that is uncoupled to the governing equations. The other two turbulence models are partial differential equations which are coupled to the governing equations through the velocity gra-

dients. The arbitrary constants that occur in the equations were calibrated using a formulation for constant pressure (i.e. flat plate) boundary layers at transonic speeds. Reported wall spacing used in the original report were set so that $y^+ = 2.0$ or less. Although almost 20 years old, it continues to be a mainstay in the technical literature.

3.3.2 Baldwin-Barth[43]

This is a one equation model that was first published in 1991. This model is derived from an older, standard k - ε model, where k represents the turbulent kinetic energy and ε is the turbulence dissipation rate.

$$2k = (\overline{u^2} + \overline{v^2} + \overline{w^2})$$ (3.1)

$$\varepsilon = \nu \left(\frac{\partial u_j}{\partial x_i} \bullet \frac{\partial u_j}{\partial x_i} \right)$$ (3.2)

This model was calibrated from the flow over a flat plate. According to its authors, one of the motivations for creating the model was the inability of other models (including the Baldwin-Lomax model) to predict viscous flows over transonic airfoils. The model begins with one equation for both k and ε and combines them through the turbulent Reynolds number,

$$R_T = \frac{k^2}{\nu \varepsilon}$$ (3.3)

and then derives one equation using the turbulent Reynolds number. Turbulent kinematic viscosity is then calculated from turbulent Reynolds number. For zero pressure gradient boundary layers, such as that over a flat surface, the authors recommend a $y^+ < 3.5$ which they indicate is comparable to that required by the Baldwin-Lomax model. Basic k–ε models are reported to require wall spacing such that $y^+ = 0.2$ or less.

3.3.3 Spalart-Allmaras[44]

This model was presented in 1992 as another one equation model with similarities to the Baldwin-Barth model. The difference in this model is that it does not treat the boundary layer as a single entity and therefore should perform better with detached, or separated, flows. It is derived from first principles and is not based on any previous turbulence model. The one resulting equation solves for turbulent kinematic viscosity directly without any intervening variables. The free shear term (the model without wall damping effects included) is calibrated using mixing layers and wakes. The near wall term is calibrated using the turbulent solution over a flat plate. There is also a term to account for more highly viscous, lower Reynolds number flows. No recommendations were made in the original report about values of y^+, although researchers using the model report results with y^+ approximately equal to 1.0.

None of the three models was designed for incompressible flow outright but all three are used for many flight regimes other than what they were designed for.

3.3.4 Turbulence Model Performance

As a check on the possible comparative merits of these three turbulence models for the current work, they were tested on the sharp and blunt NACA0012 airfoil using the previous grid density (201 x 62). Blunt trailing edges appear on all four of the tested airfoils and are more realistic from a practical and a research standpoint than a sharp trailing edge that ends in a point. For manufacturing reasons, real airfoils cannot truly end in one point. The upper and lower skins of the wing are made from sheet aluminum that are riveted together at the trailing edge to form an approximately flat ending to the airfoil that is approximately between 1 - 3% of the chord thick. Fig. 3-5 shows a blow-up of the trailing edge of the MS13 airfoil. It also shows how the grid lines join the body in this one block grid (not all lines are shown). Some CFD studies using blunt trailing edges use two blocks or zones of grid lines at the trailing edge, one block going around the airfoil from lower to upper trailing edge and the second block covering the wake. One block construction eliminates the need for boundary conditions and interpolations between the two blocks.
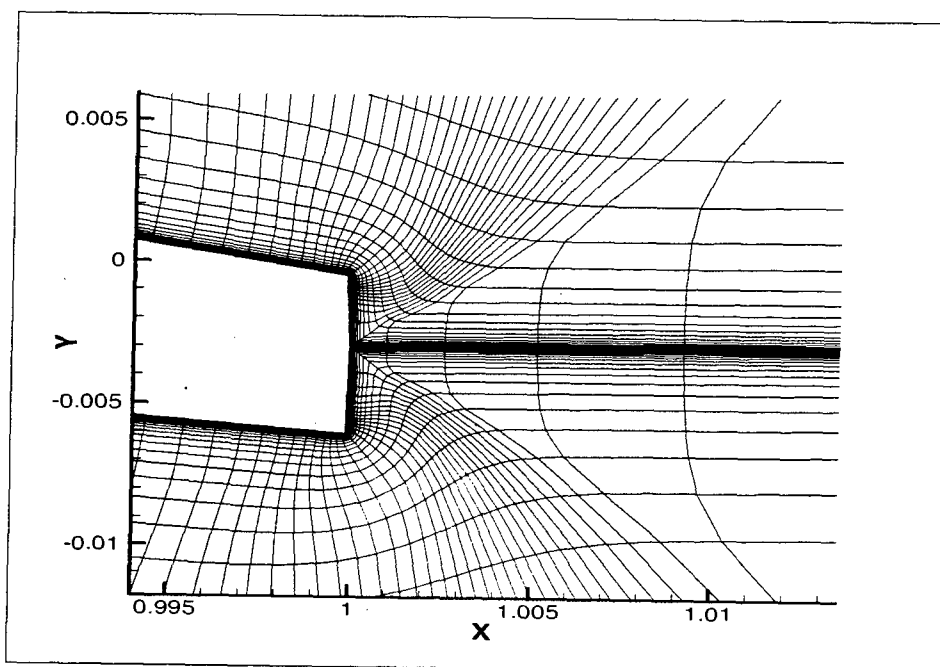
Fig. 3-5   Trailing Edge of Blunt MS13 Airfoil
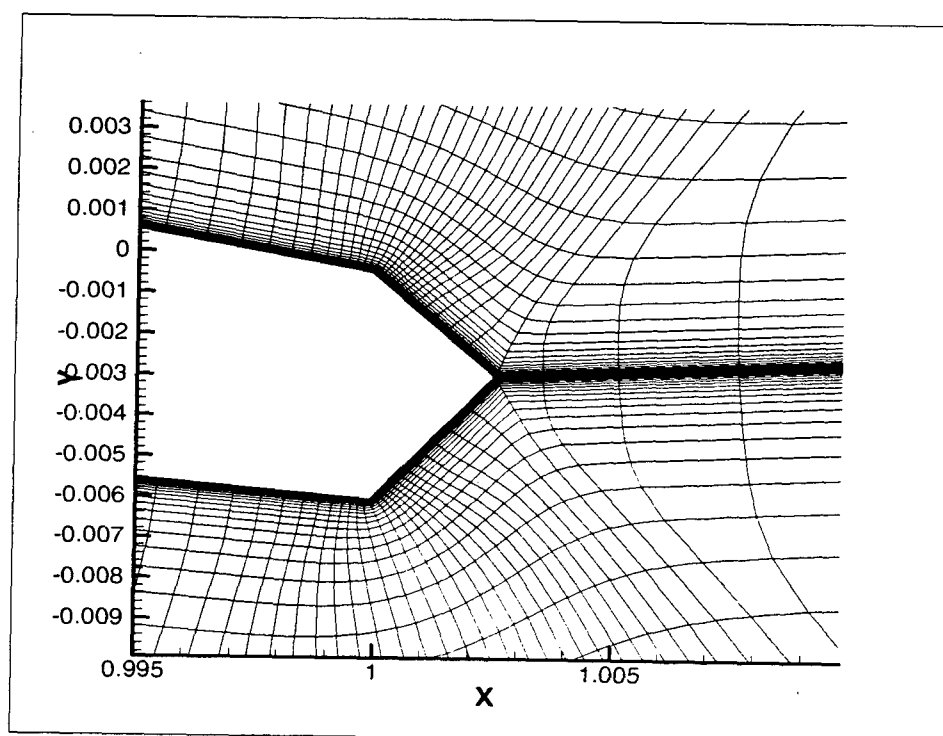
Fig. 3-6   Rounded Trailing Edge, MS13 Airfoil

Fig. 3-6 shows a "rounded" trailing edge which some researchers suggest[40]. This configuration is not how the airfoils actually appear, but it allows the CFD solution to give a better answer in some cases. Sharp edges have been used on all tested airfoils through Table 3. Blunt trailing edges (both flat and round) will be used on the test airfoils of Table 4. The presence of the blunt trailing edge causes vortices to form on the rear of the airfoil, even when separated flow is not present anywhere else on the surface. In addition to the manufacturing realities, this vortex formation allows a relaxed pressure boundary condition on the trailing edge. Because of this, the pressure gradient is not so steep on the aft end of the airfoil and this helps the boundary layer to stay attached. Since the pressure distribution changes and the boundary layer dynamics also change, both lift and drag are affected. In studies for this work it was found that the lift coefficient on the blunt airfoils calculated by CFD increases from between 33 - 50% at an angle of attack of zero degrees for the four tested airfoils. At this angle of attack, that represents a delta on the order of about 0.1 for C_l. Assuming this 0.1 delta in C_l was constant with angle of attack, which it may not be, there would be about a 5 - 7% increase in calculated C_{lmax} over a sharp edged airfoil. The drag effects would also vary with angle of attack; at zero degrees the effect is just about a wash because the skin friction drops slightly and the base drag increases. Although an interesting phenomenon in its own right, the impact to this study is that the blunt end must be represented in the grid structure. Pointed trailing edges cannot correctly model all of the changes that occur due to the bluntness and the wind tunnel and CFD tests would not correlate. It is a result of this research that blunt end effects will change the y^+/ C_d interactions. The trends can be calculated for sharp ends but the data must be held separately from those of blunt airfoils.

The next series of figures illustrate the both the effect of this bluntness and the turbulence on the drag of the NACA0012 airfoil as the grid density varies. Abbot and von Doenhoff publish airfoil coordinates for both blunt and sharp trailing edges of some airfoils although they do not indicate which models were used in the wind tunnel tests in their book. The baseline data for the 0012 is not taken from Abbot and von Doenhoff but this does serve as a caution to the CFD and experimental communities that blunt trailing

edges (even small ones) make a large difference in the solutions over aerodynamic shapes and they must be handled appropriately. Some tests have shown that bluntness as small as 0.07%[39] of the chord can have an appreciable effect.

Figure 3-7 shows the Baldwin-Lomax (BLO) performance at various grid densities when the $y^+ = 1.0$. This figure is for a Reynolds number of 5 x 10^7. The BLO performance at large y^+ was discussed in Chapter 2 (Figure 2-9). Recall that one of the keys to establishing a CFD trend of lift or drag (or any parameter) with Reynolds number is that the drag (or lift) performance be consistent with given flow and grid parameters. Because of this, we do not want to have to vary the grid and flow solver parameters for each Reynolds number. Since the at least drag varies quite a bit with grid density, Chapter 2 indicated that perhaps we can achieve the optimum accuracy, greatest computational efficiency, and predictable performance across a Reynolds number range by fixing the grid density and manipulating the wall spacings. The next series of figures (3-7 thru 3-11) show not only relative turbulence model performance on but also the variance with grid density.
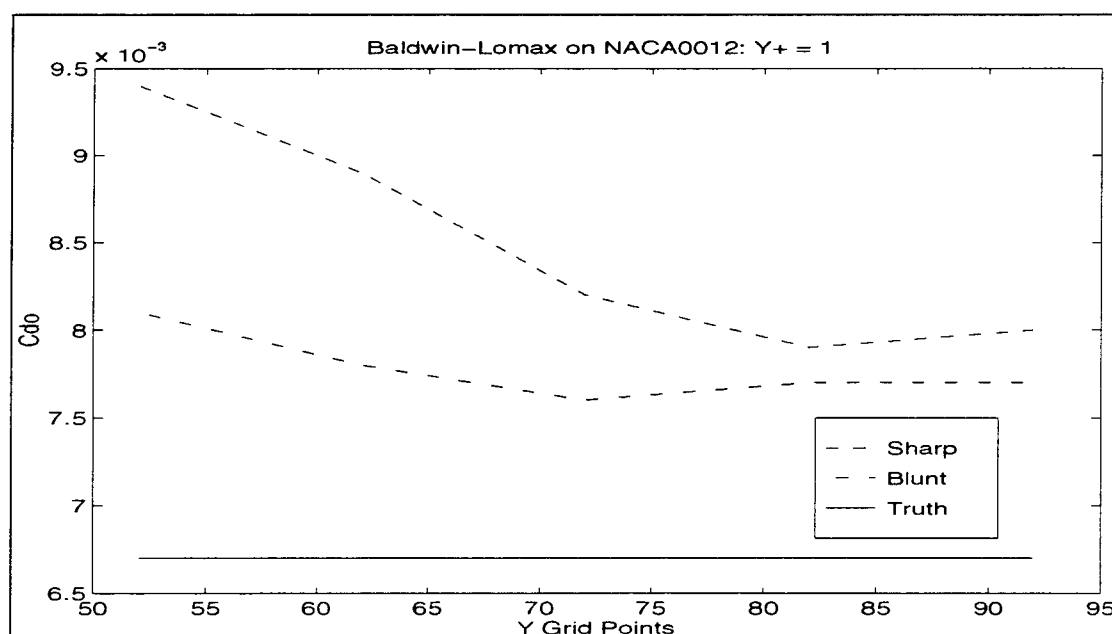
Fig. 3-7   Baldwin-Lomax on NACA0012 Airfoil, $y^+ \sim 1.0$

Figures 3-8 and 3-9 show the Baldwin-Barth (BBT) performance at $y^+ \gg 1$ and y^+ ~ 1.0, respectively. Figures 3-10 and 3-11 show the same data using the Spalart - Allmaras (SPT) model. Note the scale of the large y^+ plots compared to the $y^+ = 1.0$ plot. The BLO model (Figure 2-13) and the SPT model show approximately twice as much error on a percentage basis than BBT over the entire range of grid densities. When y^+ is about equal to 1.0, BBT again seems to be more accurate on blunt airfoils. The scale of BLO in Figure 3-7 is higher than that of the other two and the SPT model actually gets slightly worse with grid density at y^+ of about 1.0. At the highest grid densities when y^+ ~ 1.0, the blunt BBT result is within 5% of the true value over the entire grid density range. Other research has shown that the BBT model and SPT models both have their strengths in different flow areas on the same problem[39] and that the BLO model may be unsatisfactory (when compared to the other two) in separated flows.
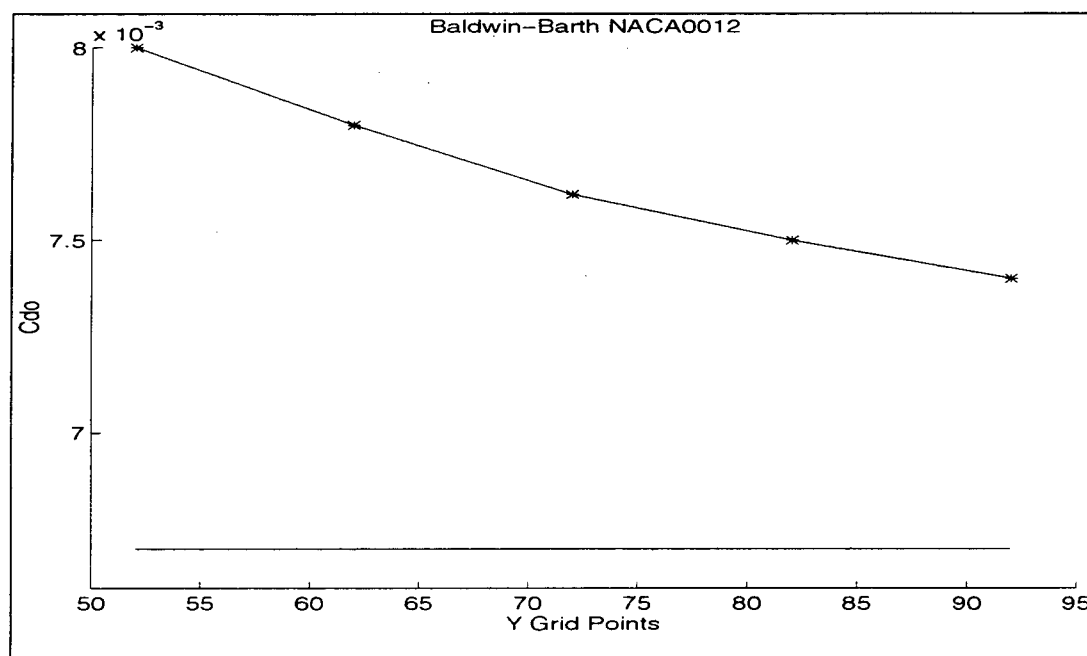
Fig. 3-8   Baldwin-Barth Model at $y^+ \gg 1.0$
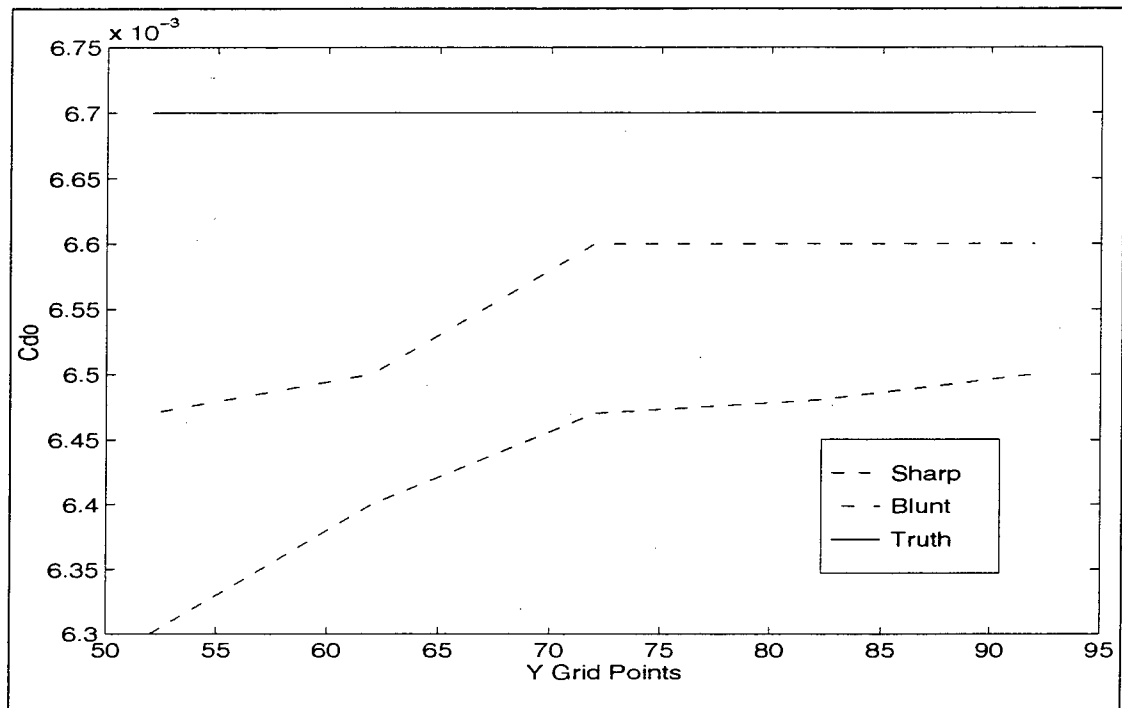
Fig. 3-9   Baldwin-Barth Model at y+ ~ 1.0
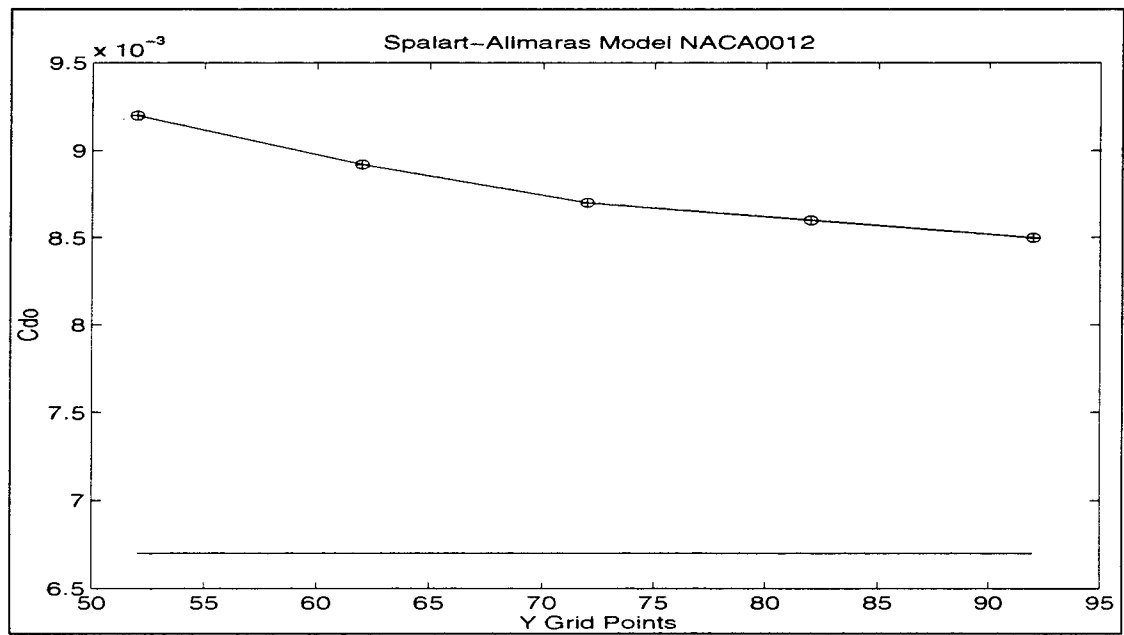
Fig. 3-10   Spalart-Allmaras Model at $y^+ \gg 1.0$
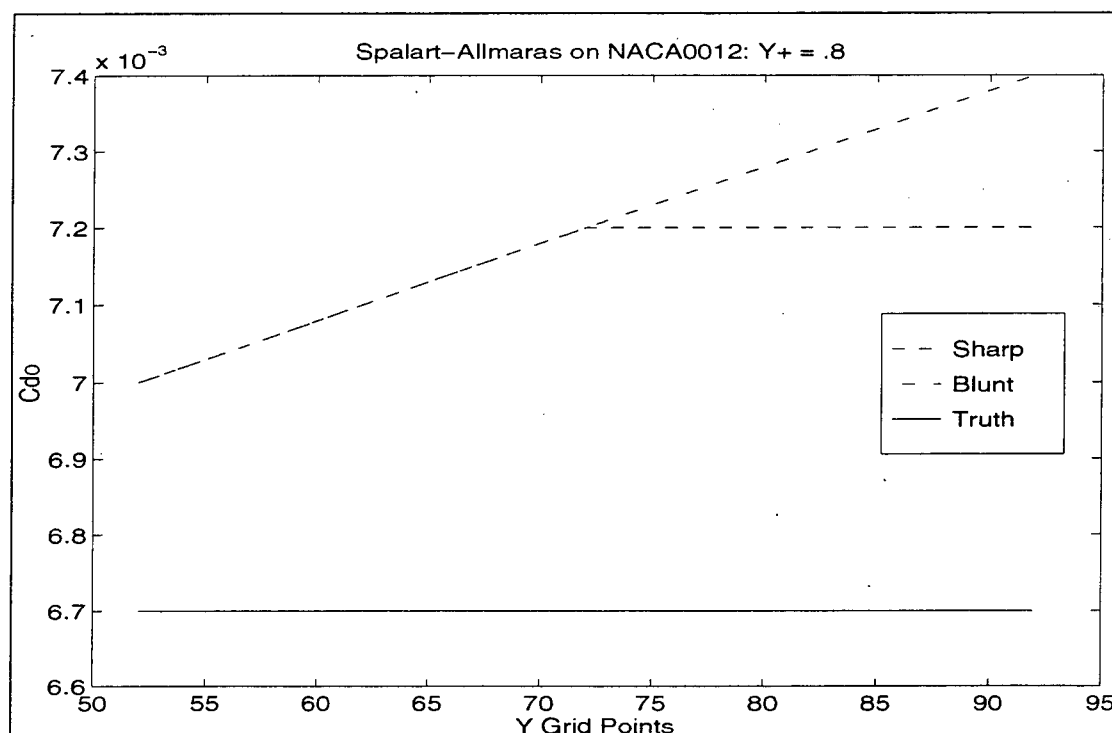
Fig. 3-11   Spalart-Allmaras Model at $y^+ = 0.8$

These figures also indicate that 62 grid points in the normal direction is sufficient, which agrees with Jameson[38]. More grid density is not justified by enough improved performance in any of the three models. By keeping the same grid density and decreasing the wall spacing, we have already shown that the BLO model can be within 5%, at least for zero lift on the sharp NACA0012. It does not do as well as the other two models when confronted with the new vortices at the trailing edge of the blunt airfoil. However, each turbulence model and each flow situation must have a constant parameter over a Reynolds number range if the new method is to be valid. Of the three models tested, Baldwin Lomax may have difficulty with performance across wide Reynolds number and angle of attack ranges. The other two seem comparable for this task. Fig. 3-12 is a streamtrace of the CFD-calculated flow at the trailing edge of this blunt airfoil at 12°. The small vortex is easily seen. Fig. 3-13 shows a small region of separation at 15°.
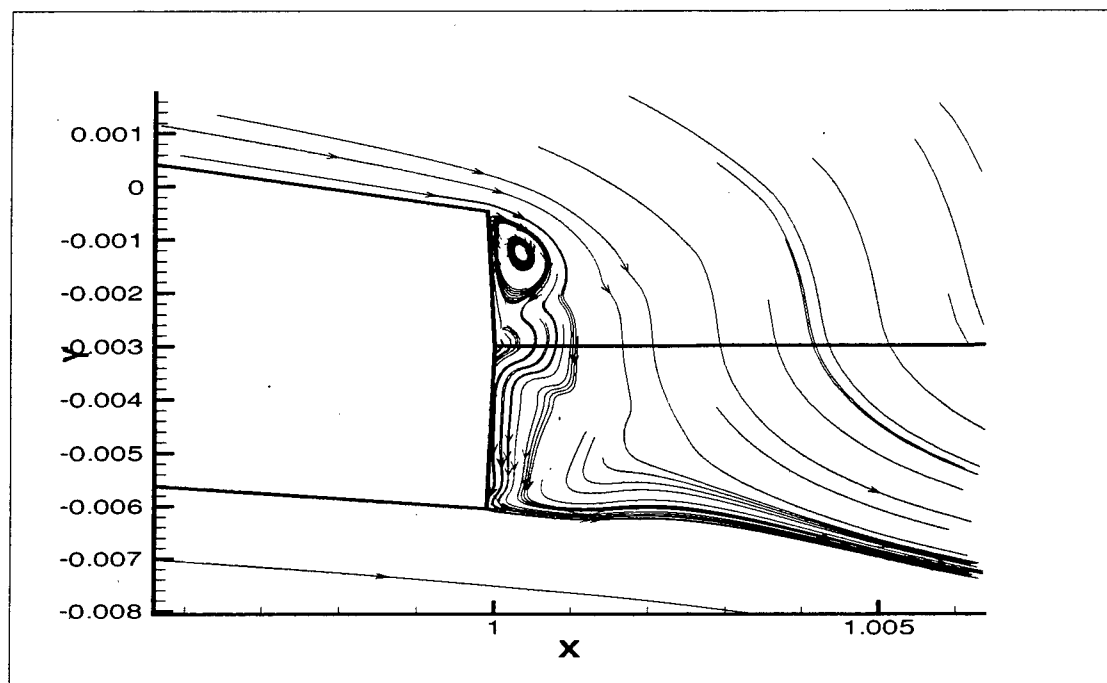
Fig. 3-12   Streamtrace of Blunt MS13, Wall Spacing = 5 x 10⁻⁷, Re= 6 x 10⁶, AoA = 12°
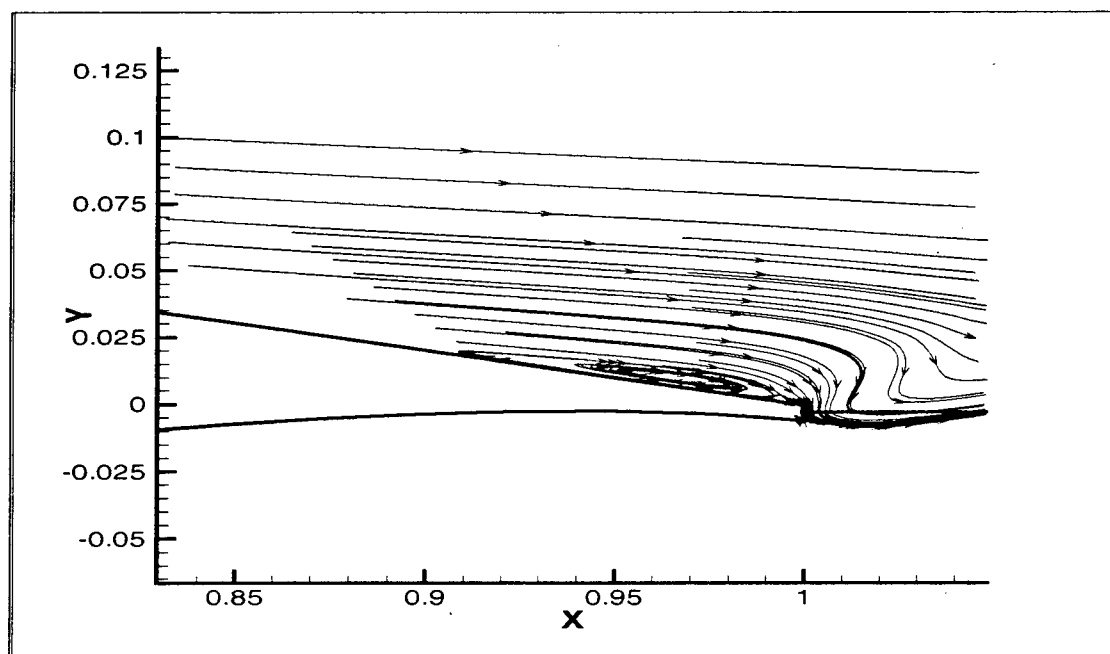
Fig. 3-13   Streamtrace of Blunt MS13, Wall Spacing = 5 x 10⁻⁷, Re= 6 x 10⁶, AoA = 15°

3.4 MS13 Results

3.4.1 Spalart-Allmaras (SPT) Model.

Of the four tested airfoils, the 13% thick model was selected for the initial work because it is "middle-of-the-road" as far as airfoils go. No extreme thickness or camber to worry about and certainly representative of airfoils used for all types of low to medium speed aircraft. Thirteen different grids were created, each of the same grid density (201 x 62). The wall spacing varied from 1.0×10^{-7} to 1.0×10^{-4} in thirteen increments approximately equally spaced apart in $\log_{10}$-space. The CFD solution was run at angles of attack from -3° (the zero lift angle of attack) to as high an angle of attack as desired (usually the stall angle of attack for the highest Reynolds number). Reynolds numbers tested in the wind tunnel for this airfoil included 2, 4, 6, 9 and 12 million resulting in y^+ values of approximately 0.01 at the smallest spacings to about 60 at the largest. Since each airfoil and each Reynolds number has a different stalling angle, the maximum angle of attack will change with each airfoil. Solution values of C_l, C_d, C_f, C_{dp}, and y^+ were used as the main parameters for analysis. Several modifications were made to the solvers and the turbulence models but only in the area of CPU timing and calculation post-processing, such as calculation of drag coefficients and y^+. The grid generator, flow solver, and turbulence model are all as they might appear off the shelf, with any problem specific modifications held constant throughout testing.
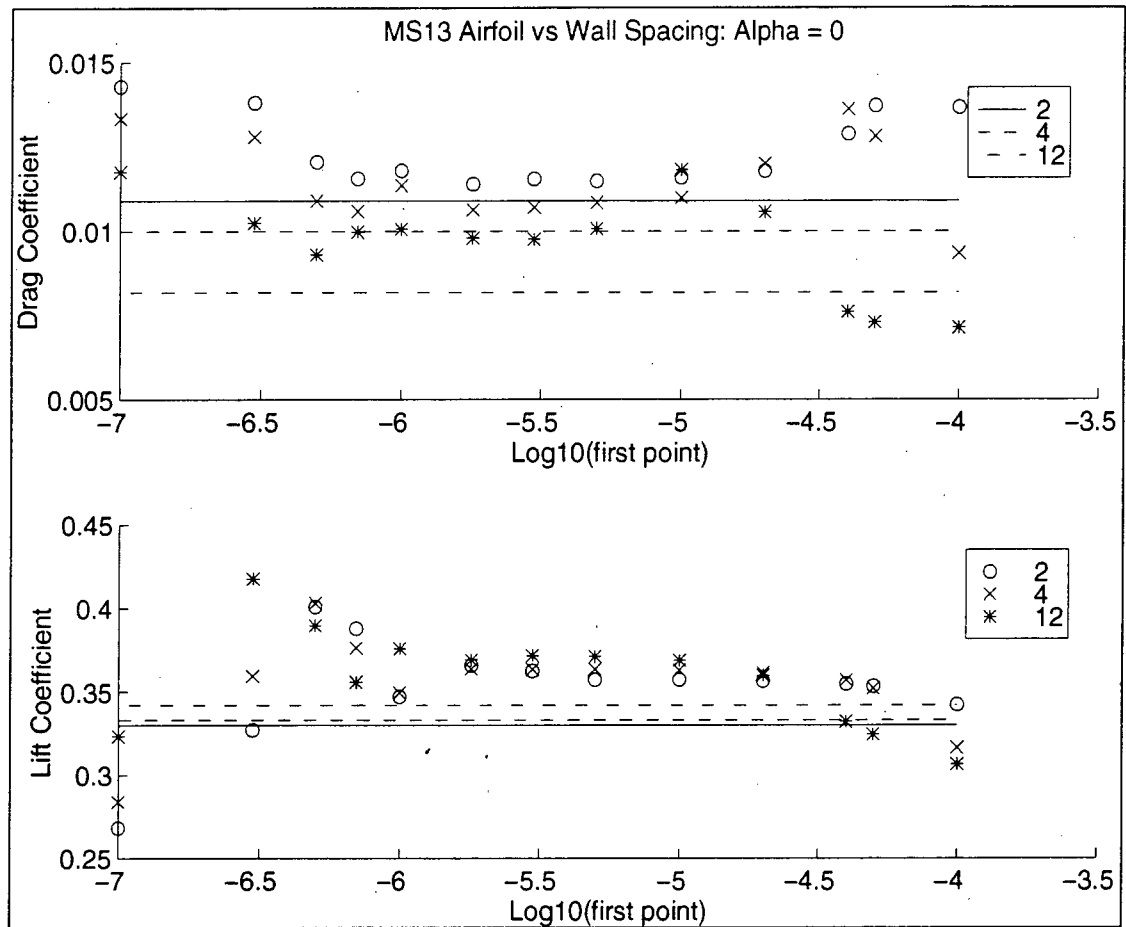
Fig. 3-14   MS13 Airfoil Lift and Drag vs. Wall Spacing (SPT Model, 0° AOA)

Fig. 3-14 plots the CFD solution using the SPT turbulence model for Reynolds numbers of 2, 4, and 12 x 10^6 against the baseline (wind tunnel) data which is plotted as straight lines. This is the first look at multiple Reynolds numbers for a single airfoil. At zero degrees, very few of the lift or drag values across the grid spacing values and Reynolds number values actually cross the true solution. In other words, the CFD solution is seldom absolutely correct, but again, if it is *incorrect consistently* across Reynolds number then trends can possibly be established. Notice the scattering in performance at the lowest and highest spacings. This is most likely due to the amount of resolution in the gradients of the boundary layer. At very low spacings, more grid points are pulled into the boundary

layer by the grid stretching algorithm. This gives good resolution in the lower regions of the boundary layer but poorer resolution at the edge of the boundary layer. The opposite is true at the larger spacings. In the mid-spacings from about 10^{-6} to 10^{-5} there is a relatively large region where the actual drag value is incorrect in an absolute sense but stays relatively constant. However, there is no obviously consistent relationship across Reynolds numbers. Notice also that the wall spacings for a constant lift trend are not all the same as those for a constant drag trend, although there is some overlap centered at about 3.0 x 10^{-6}. Evidently, there is some "right" amount of gradient resolution spread over the boundary layer which decreases the sensitivity of the solver in the lift and drag calculation. It is not possible to compute this "right" spacing ahead of time from studies of the turbulence model/flow solver combination because there are so many variables interacting during the solution. At this point we are only looking for consistent relationships and are trying to find ways of using the data to find them.

Fig. 3-15 plots the same information but now at 15° angle of attack. Again the drag shows a similar behavior although this time there is not much variance at the lowest spacings. Lift is much different than the previous figure. The grids and grid spacings have not changed between Fig. 3-14 and Fig. 3-15. Certainly the physics of the flow is quite different at this very high angle of attack, which is the stall angle of attack for the 2 x 10^6 Reynolds number case. In neither of the two cases, 0° or 15°, are the flow physics correctly modeled by the solver/turbulence model combination yet the behavior with wall spacing is similar. This variation of C_d and C_l with wall spacing is a "signature" of the turbulence model. Each model behaves differently (see Chapter 4) across this regime. It is possible that with the larger amount of separated flow at 15°, the flow solver/turbulence model has little sensitivity to gradients over a larger distribution of boundary layer grid points. The lift, being a more pressure driven phenomenon, is more affected by the separated flow.

Fig. 3-16 is a similar plot at 18°, which is past the stall angle of attack for all of the lower Reynolds number cases and is the stall angle of attack for a Reynolds number of 12

x 10^6. If a trend can be based upon some parameter perhaps it can then be used to predict the stalling angle of attack at higher Reynolds numbers. The baseline values in this and subsequent chapters has been taken from charts and figures in the literature rather than the raw wind tunnel data. The accuracy should be sufficient to illustrate the current conclusions.
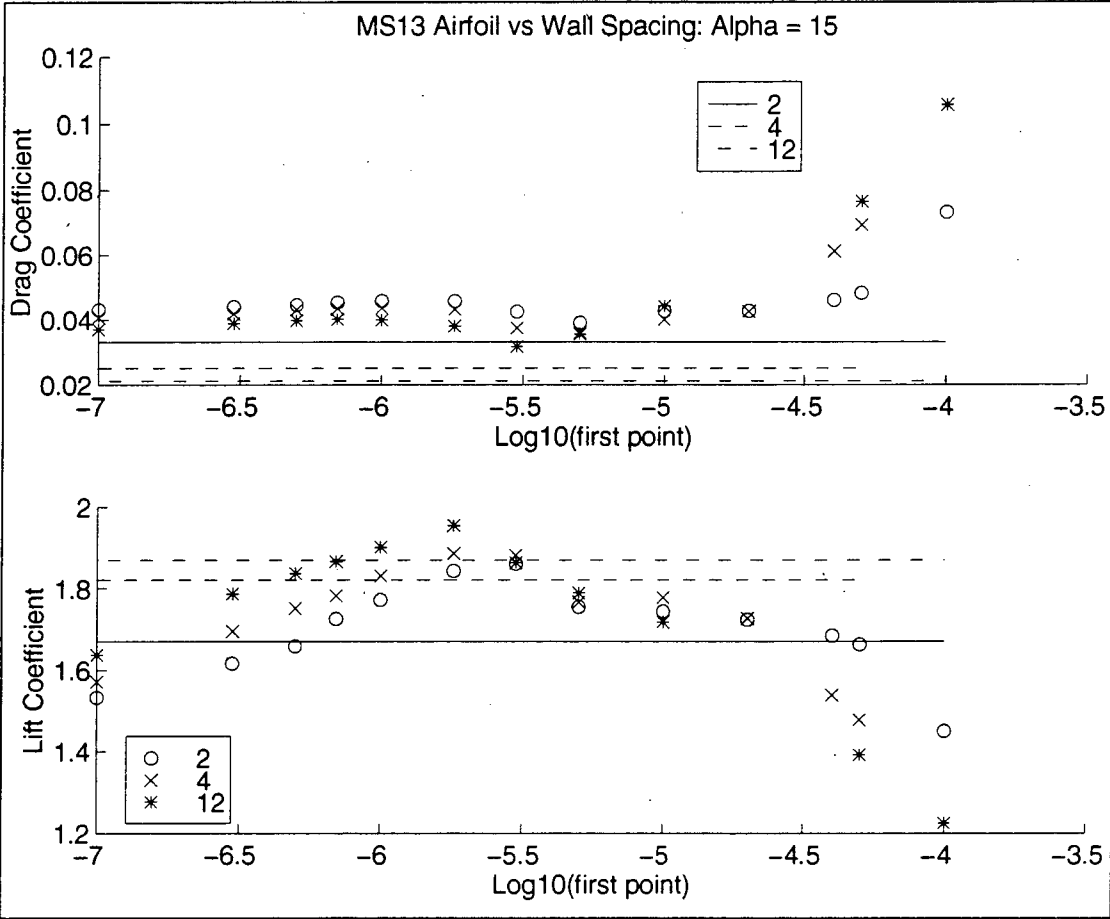
Fig. 3-15   MS13 Lift and Drag vs. Wall Spacing (SPT Model, 15° AOA)
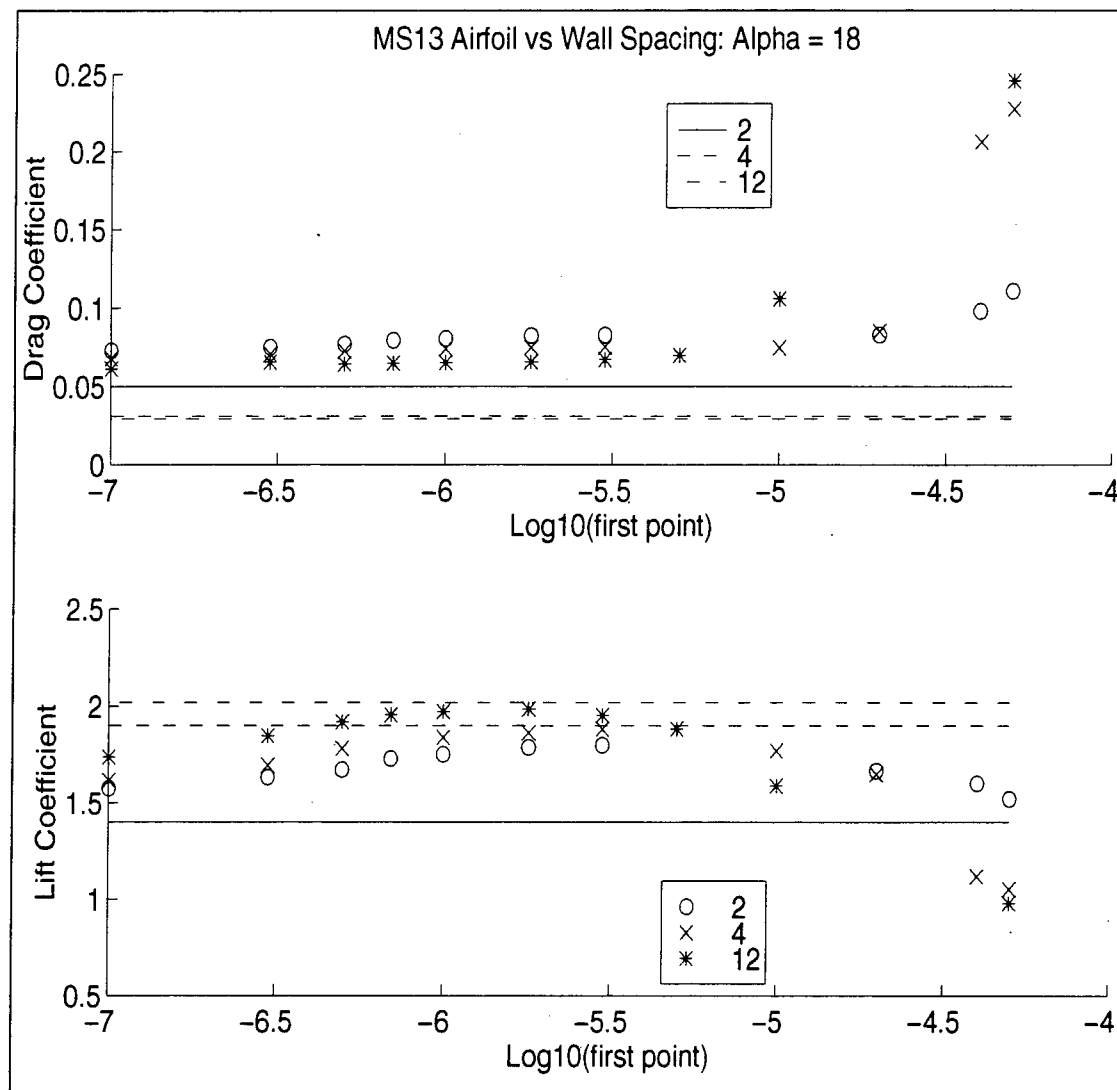
Fig. 3-16   MS13 Lift and Drag vs. Wall Spacing (SPT Model, 18° AOA)

These figures have been examples of the raw data as received from the solver. There are many ways to try to determine consistent ties between Reynolds number. Using Figure 3-14, for example, and the C_f data for that angle of attack, we find that optimum drag occurs at y^+ values of approximately 0.4, 0.8, and 2.3 for the three Reynolds numbers, respectively. The optimum lift y^+ values are even more widely spaced because opti-

mum lift is more widely spaced. The next series of figures merely illustrates some of the possible examples.
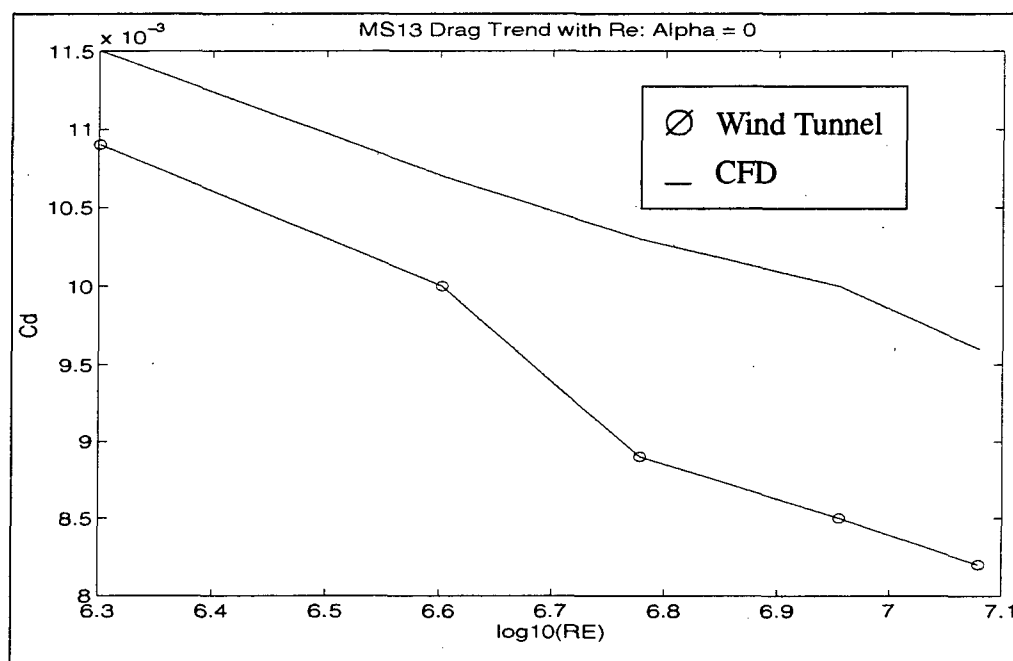
Fig. 3-17   Direct Trend of Drag with Reynolds number, MS13, SPT Model, 0° AoA

Both Fig. 3-17 and Fig. 3-18 show the initial trend of drag coefficient with Reynolds number. They seem to indicate that the CFD and tunnel solutions diverge slightly for these cases. Direct extrapolation might not give predictions of lift and drag within 5%. Fig. 3-19 and Fig. 3-20 show general lift and drag data at 0° and 12° angle of attack plotted versus y^+, but nothing consistent is evident. Fig. 3-21 and Fig. 3-22 show some improvement. Here the error (see Equ 3.4) is plotted versus wall spacing. Some values seem to be consistent across all five Reynolds numbers, which is just what was desired. Notice that both lift and drag do not show consistent behavior at the same time and at the same angle of attack.
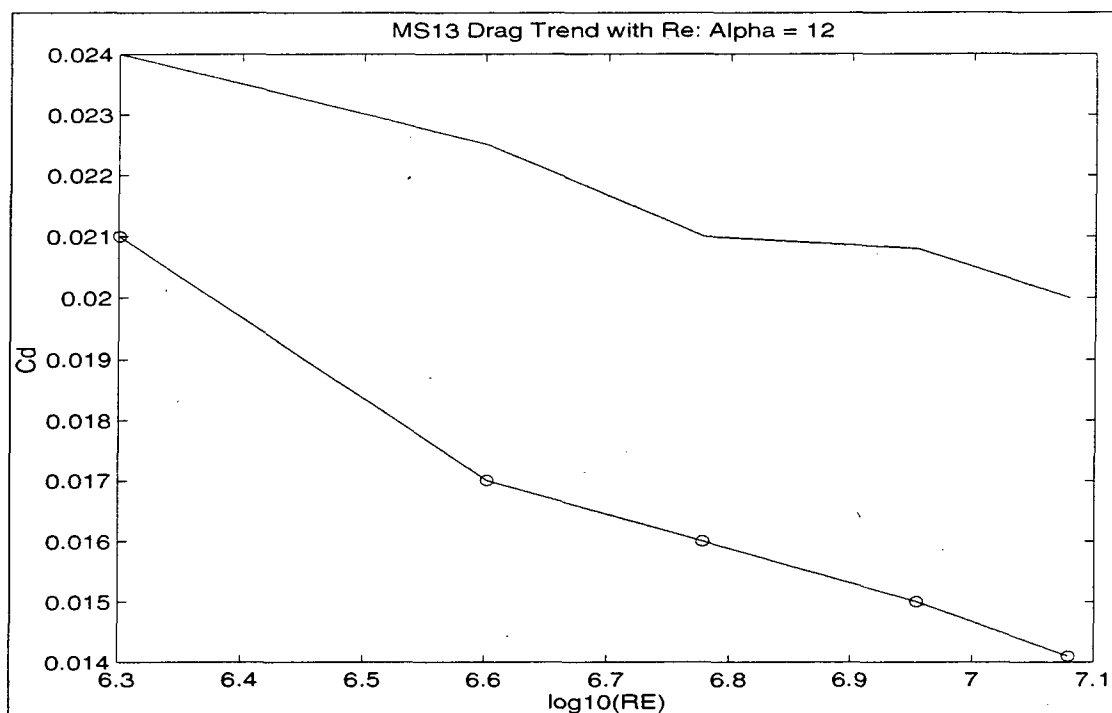
Fig. 3-18   Direct Trend of Drag with Reynolds number, 12°, SPT Model
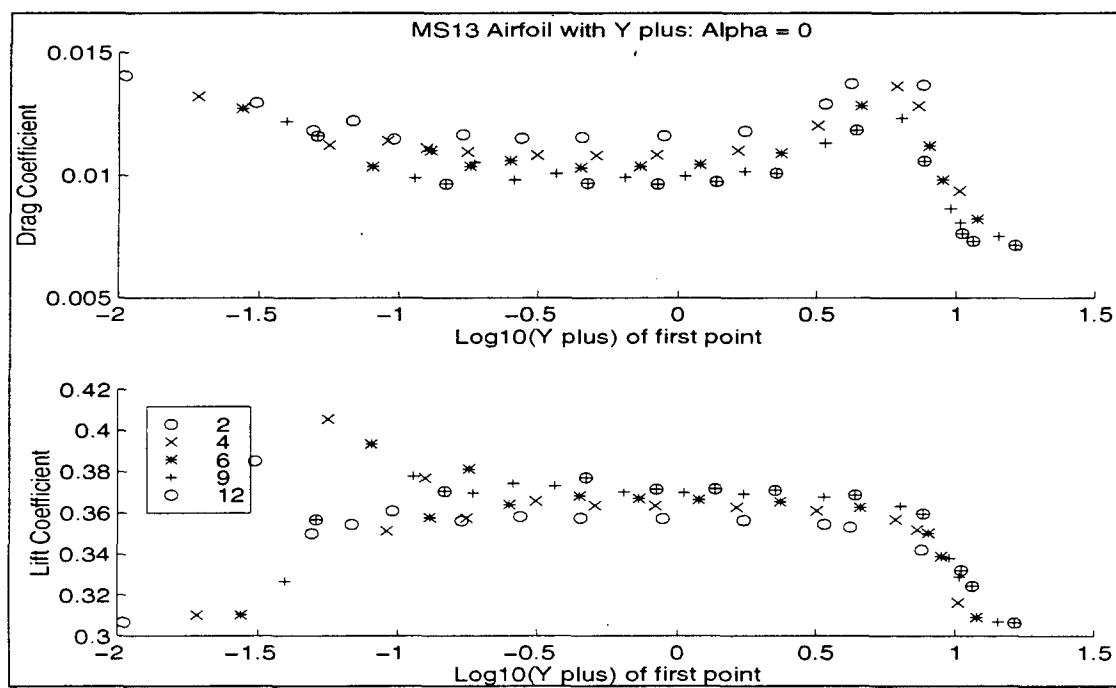
Fig. 3-19   Drag and Lift vs. Log(y⁺), MS13, SPT Model, 0° Angle of Attack
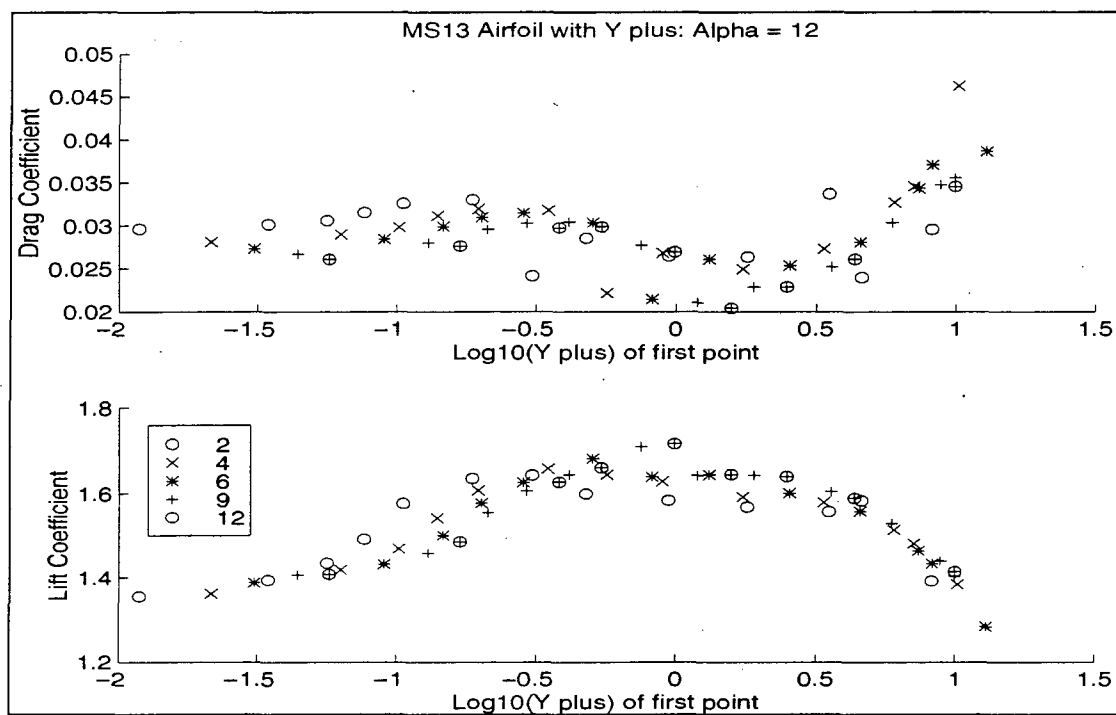
Fig. 3-20   Drag and Lift vs. Log(y^+), MS13, SPT Model, 12°
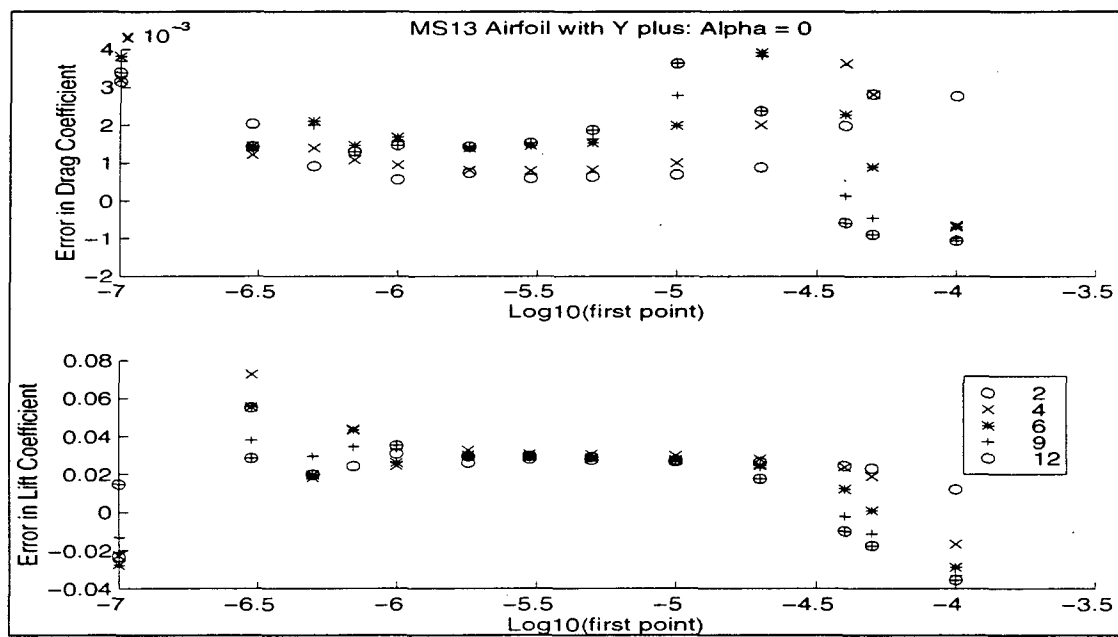
Fig. 3-21   Lift and Drag Error vs. Log(Wall Spacing), MS13, SPT, 0°
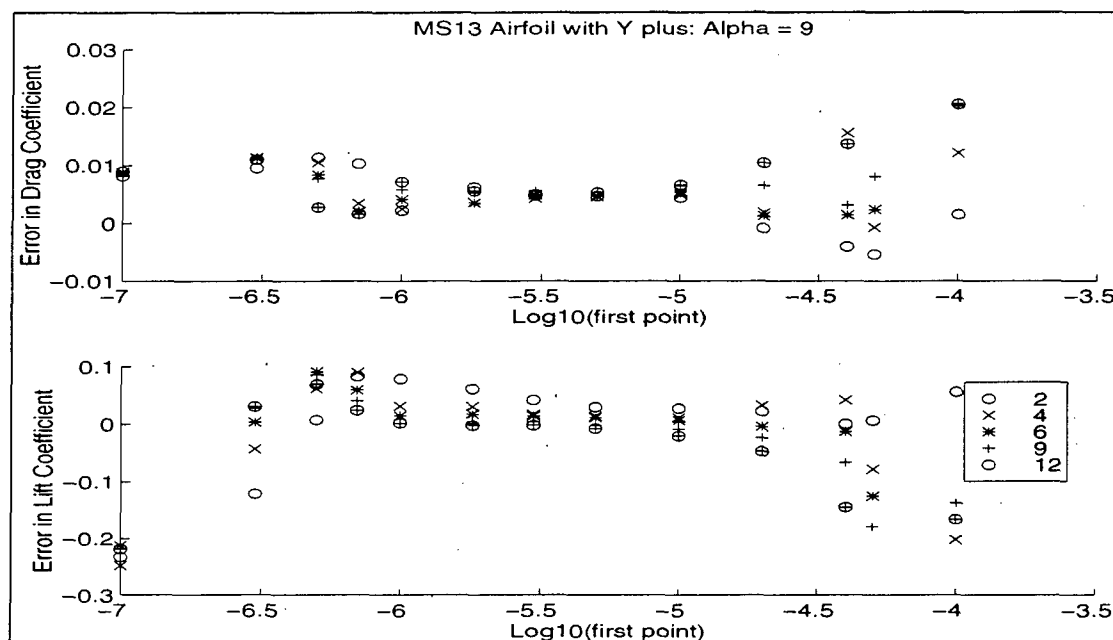
Fig. 3-22   Lift and Drag Error vs. Log(Wall Spacing), MS13, SPT, 9°

As discussed in Chapter 2, wall spacing by itself is not physically tied to the problem of interest. It seems that y^+, or some function of it, would again be a better measure of trends versus Reynolds number. Fig. 3-23 and Fig. 3-24 show the 0° and 15° plots again, but this time plotted against y^+. Instead of using a Reynolds number of 4 x 10^6 in these plots, 9 x 10^6 is used instead to show the relative behavior at higher Reynolds numbers. All five wind tunnel Reynolds numbers are not shown to avoid confusion with overly crowded plots.

The next series of plots seeks to determine if there is a parameter which provides consistent lift and drag data over all the Reynolds numbers at once.
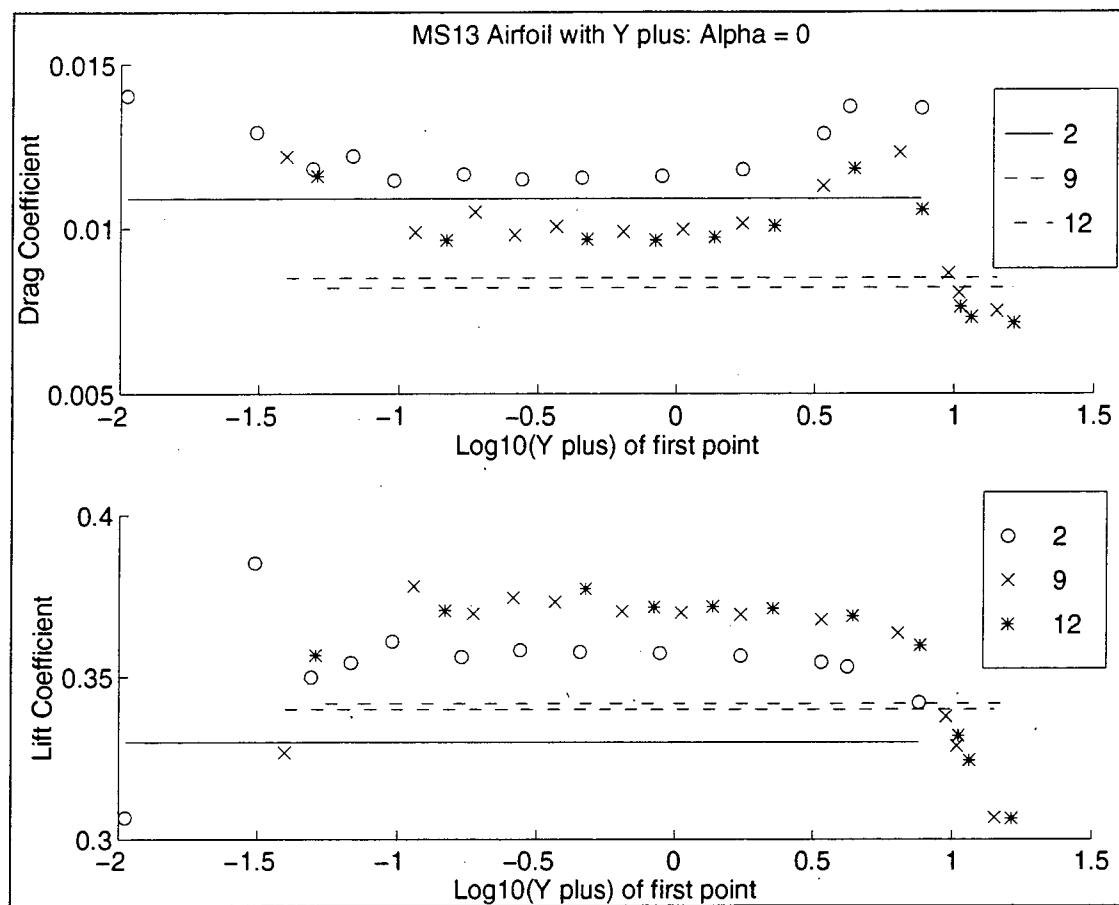
Fig. 3-23   MS13 Airfoil vs. y⁺ (AoA 0° SPT model)
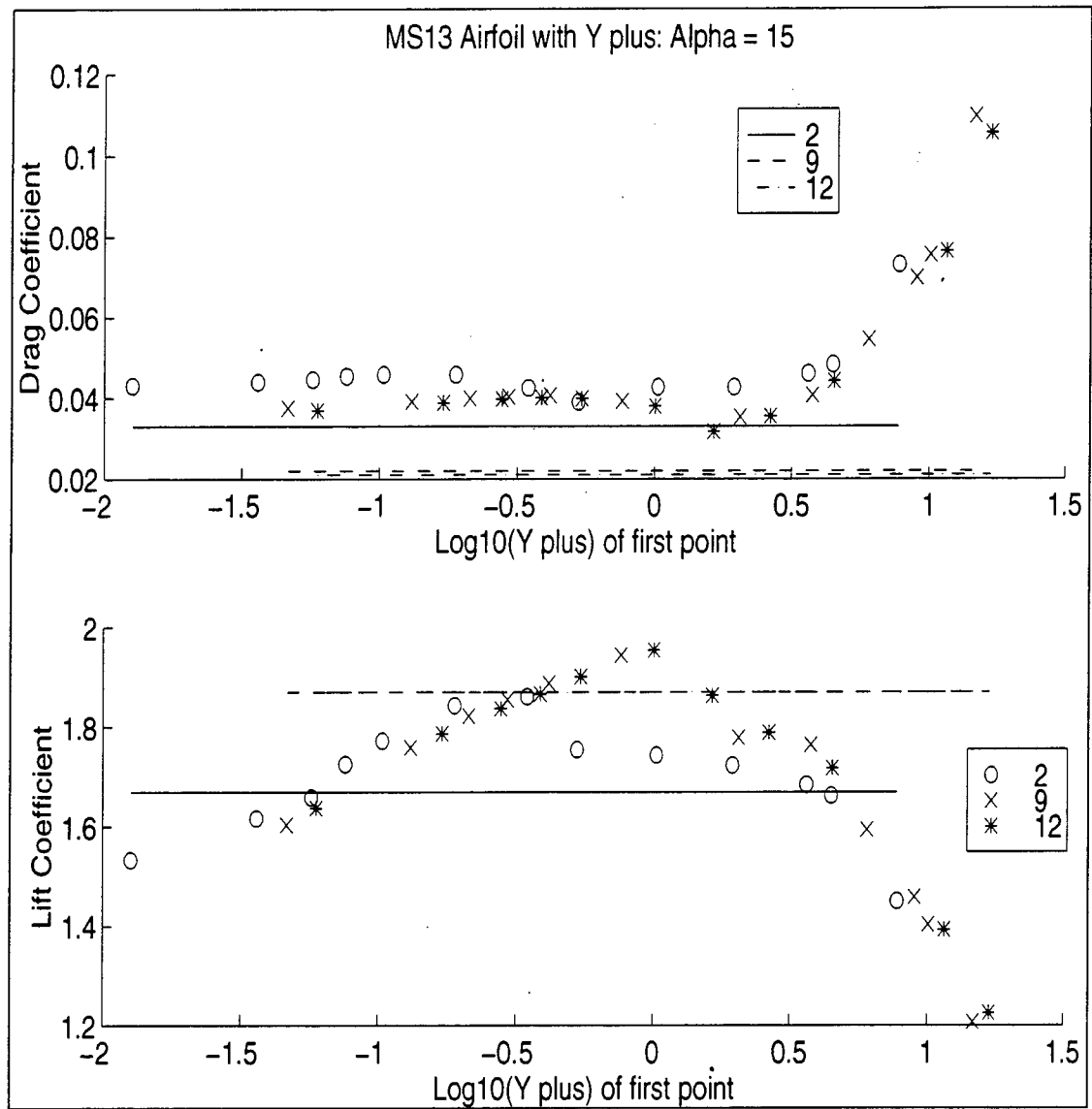
Fig. 3-24   MS13 Airfoil with y^+ (AOA 15° SPT model)

From Fig. 3-23 and Fig. 3-24 we can see that there may be several places in the y^+ range that may supply predictable drag data on the 15° plot, i.e. where the values from all Reynolds numbers lie on one curve but not on the 0° plot. Compare this with the lift data in each of the plots (the straight lines, remember, are the wind tunnel data). Researchers correctly claim that lift is more accurately predicted by CFD solvers; however, for this

study predictability and consistency are even more important than accuracy. At high angle of attack the problem seems actually to be improved as shown in Fig. 3-24; when the lift coefficient is plotted versus y^+ more of the data collapses toward one curve, although not a straight line. A better illustration of this behavior is given when the *error* between CFD and wind tunnel is plotted instead of the absolute lift or drag coefficient.

$$\Delta C_d = C_{d_{CFD}} - C_{d_{truth}} \tag{3.4}$$

This information is plotted versus y^+ in Fig. 3-25 and shows the result at 0° angle of attack for the MS13 airfoil and the SPT turbulence model.
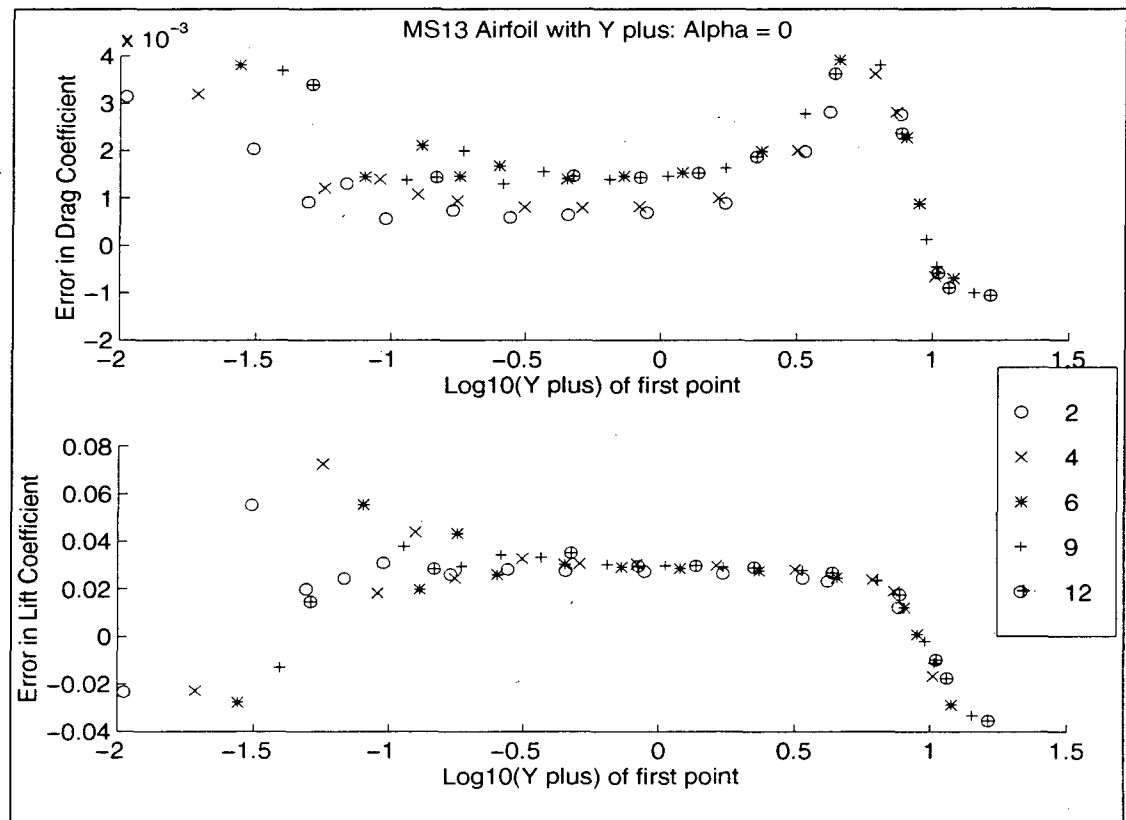
Fig. 3-25   MS13 Airfoil Error versus y^+ (SPT model 0° AoA)

Compare Fig. 3-25 with Fig. 3-26 which plots drag and lift error versus the logarithm of $(y^+ / \sqrt{Re})$. Consistency is good in Fig. 3-25 at the wider spacing side of the curve for both lift and drag where y^+ is on the order of 10. Interestingly, changing the x-scale by $1/\sqrt{Re}$ in Fig. 3-26 tightens up the opposite end of the curve where wall spacing is tighter.
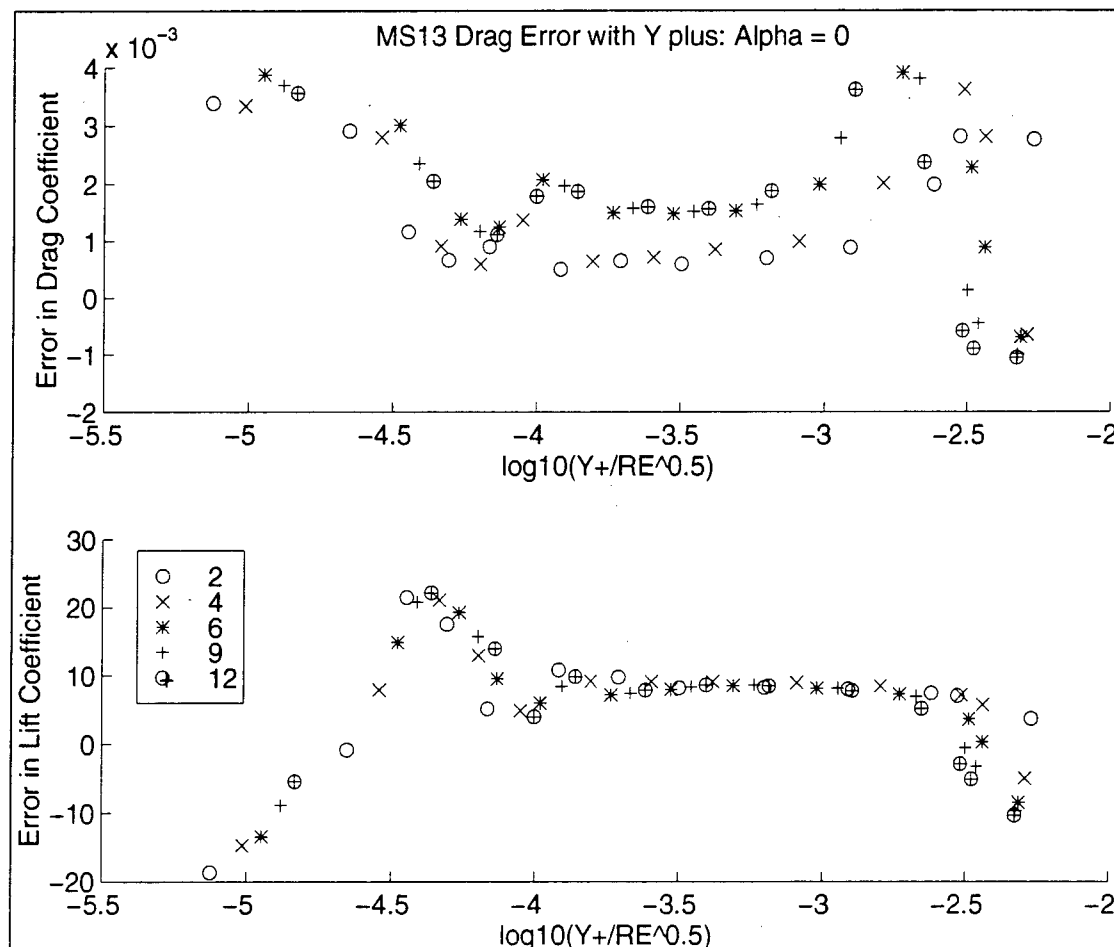
Fig. 3-26   MS13 Airfoils Error versus $y^+/\sqrt{RE}$

The lift (scaled in %error), but not drag, has collapsed extremely well to one curve for all Reynolds numbers from 2×10^6 to 12×10^6. The lower spacing end of the drag plot is more washed out. The "dip" in the data at an x-axis value of -4 is also evident in this scaling over that of the previous plot. The factor $1/\sqrt{Re}$ is the length scale of a laminar bound-

ary layer[54]. It may highlight the tighter spacings because this remains an area of laminar flow. This gives an excellent indicator of a trend of C_l with Reynolds number for this airfoil at 0° angle of attack. The lift coefficient in Fig. 3-26 is plotted as a percentage error from the wind tunnel value to give some idea of scale to the deltas.

$$\Delta C_d\% = \frac{C_{d_{CFD}} - C_{d_{truth}}}{C_{d_{truth}}} x100 \qquad (3.5)$$

One would expect the drag to be noisier and that is observed, and only the three highest Reynolds numbers give an excellent trend indicator. Apparently, the drag trend is best taken with one parameter (y^+) and lift with either (y^+ or $y^+/\sqrt{Re}$) at this angle of attack with the SPT turbulence model. Fig. 3-27 shows the drag information from Fig. 3-26 but without the lowest two Reynolds numbers. This time the drag is plotted as a percentage error. By the time the mid-level Reynolds numbers are reached, but still nowhere near the flight Reynolds numbers of interest, the CFD solvers are already about 20% in error even at this cruise angle of attack. But they are 20% wrong consistently with Reynolds number, or nearly so. Without a group of data such as presented here there would be no hope of correcting the drag data using the CFD solver alone.

MS13 Drag Error with Y plus: Alpha = 0

(%) 60

Error in Drag Coefficient

40

20

0

-20

o 6
x 9
* 12

-5   -4.5   -4   -3.5   -3   -2.5   -2

log10(Y+/RE^0.5)
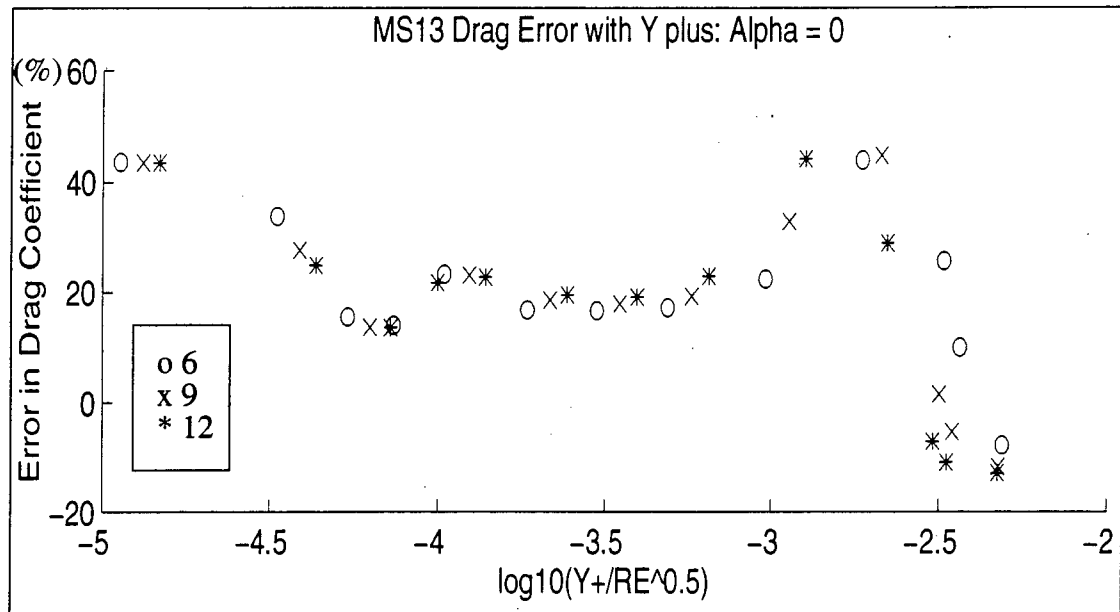
Fig. 3-27   MS13 Airfoil Drag Error; 3 Highest Reynolds numbers

To continue, the lift and drag error at $15°$ angle of attack are plotted in Fig. 3-28. Excellent convergence is seen across only 4 of 5 Reynolds numbers plotted. The lower Reynolds number appears noisier because the separated flow at this angle of attack can have much more variance in a lower energy flow. Higher Reynolds number flows will stay attached longer, and having more energy will behave much more predictably after separation. This may be a function somewhat of the turbulence model because even the plot for $0°$ angle of attack showed some variance at the lower Reynolds numbers (2 and 4 x 10^6). The following two figures show the results with x-axis scalings of $Re^{-3/4}$ and $1/Re$. The ratio of smallest to largest turbulent eddy size is $Re^{-3/4}$ and this may in fact be the best scaling at this high angle of attack. It is difficult to tell if $(y^+)Re^{-1/2}$ or $(y^+)Re^{-3/4}$ is the better parameter but it is clear that y^+ alone is not sufficient as the flow becomes more complicated. The parameter $(y^+)Re^{-1/2}$ will be chosen for the present, with the knowledge that some kind of turbulent scaling parameter is required in addition to y^+ at the higher values of angle of attack.
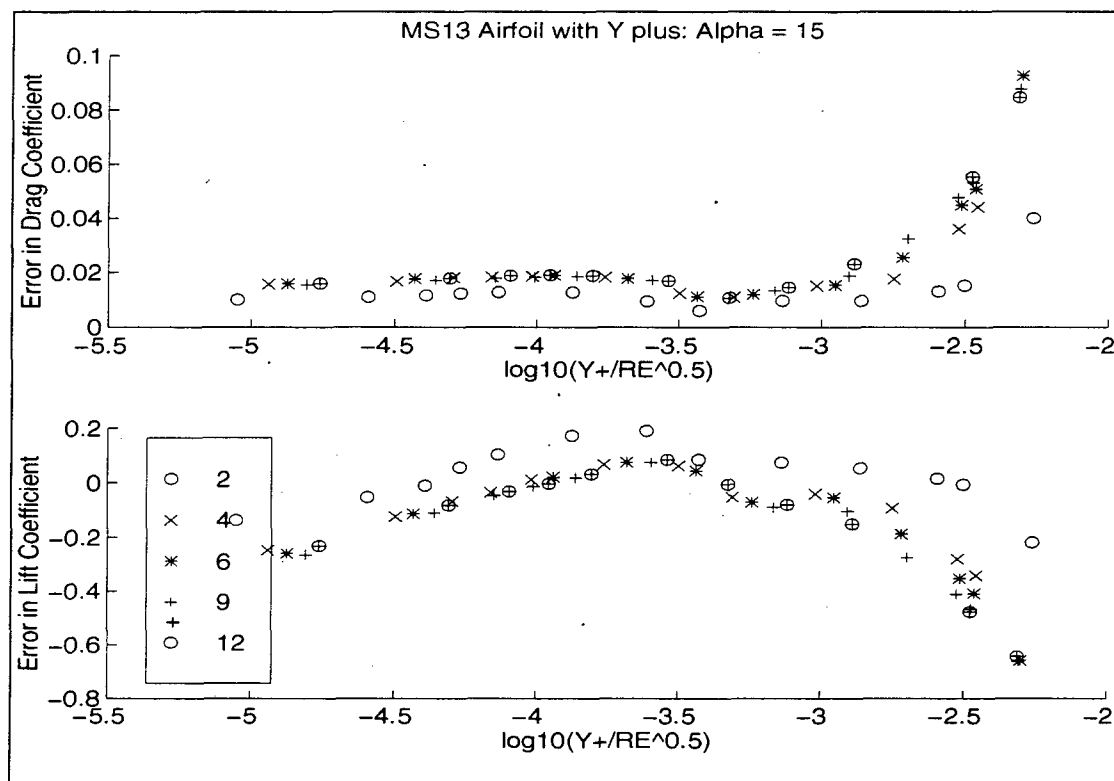
Fig. 3-28   MS13 Airfoil Lift and Drag Errors at 15° Angle of Attack (SPT Model)
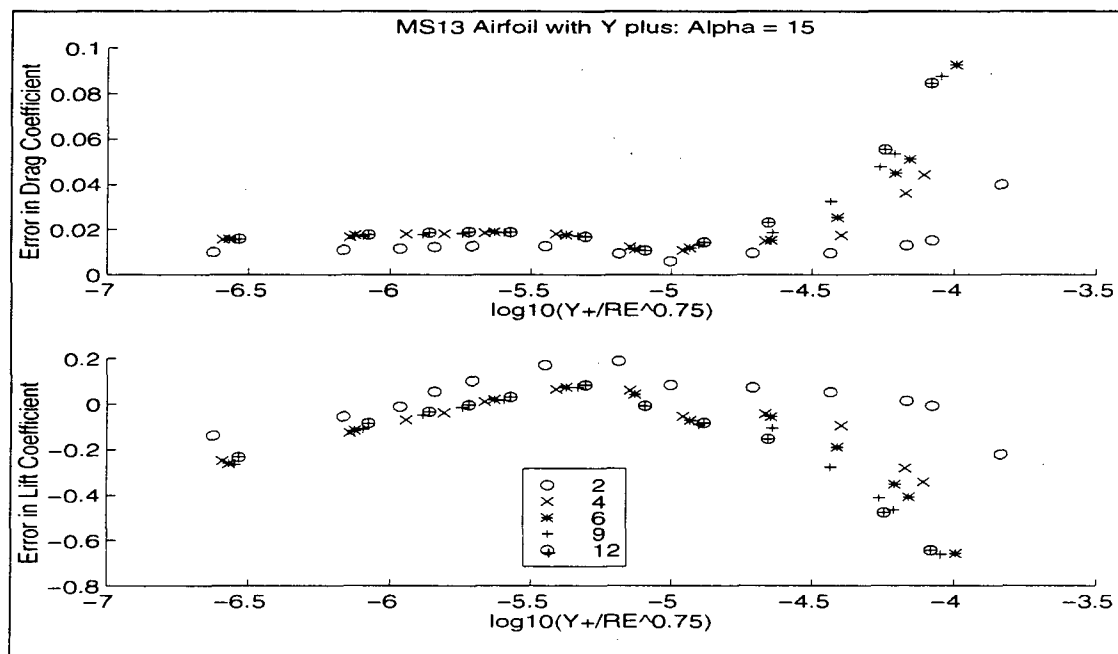
Fig. 3-29   MS13 Scaled with $Re^{-3/4}$, 15° Angle of Attack
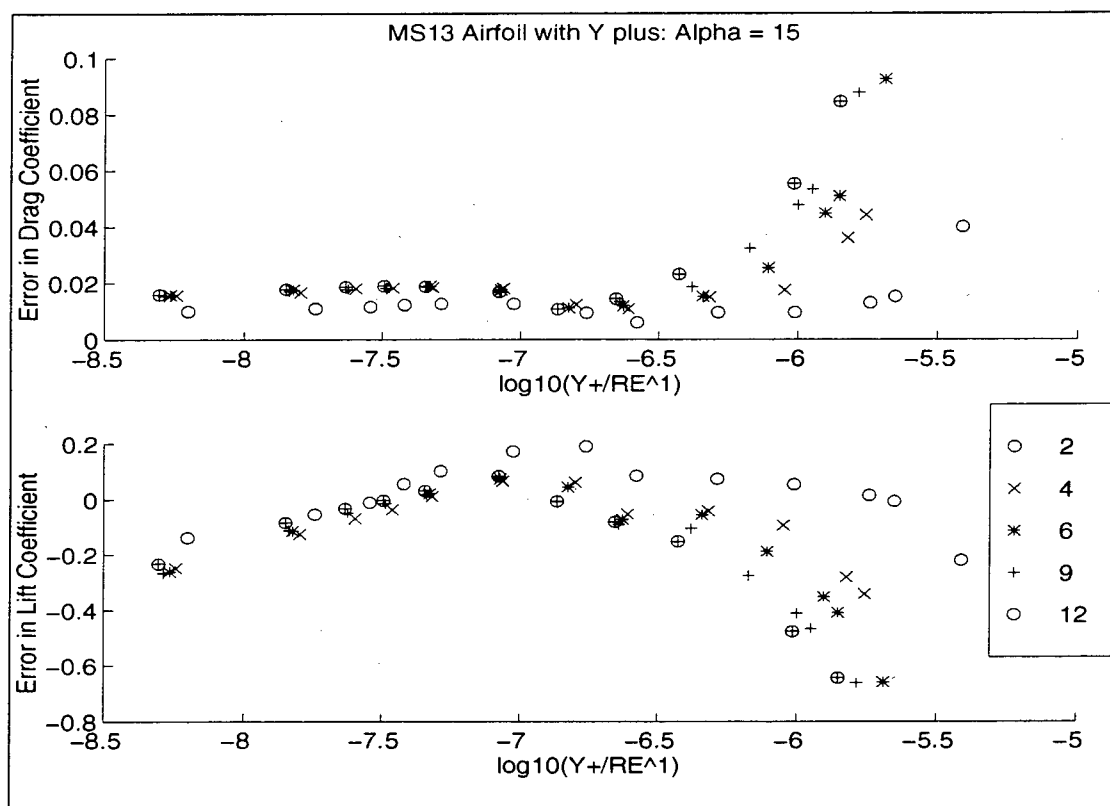
Fig. 3-30   MS13 Scaled with 1/Re, 15° Angle of Attack
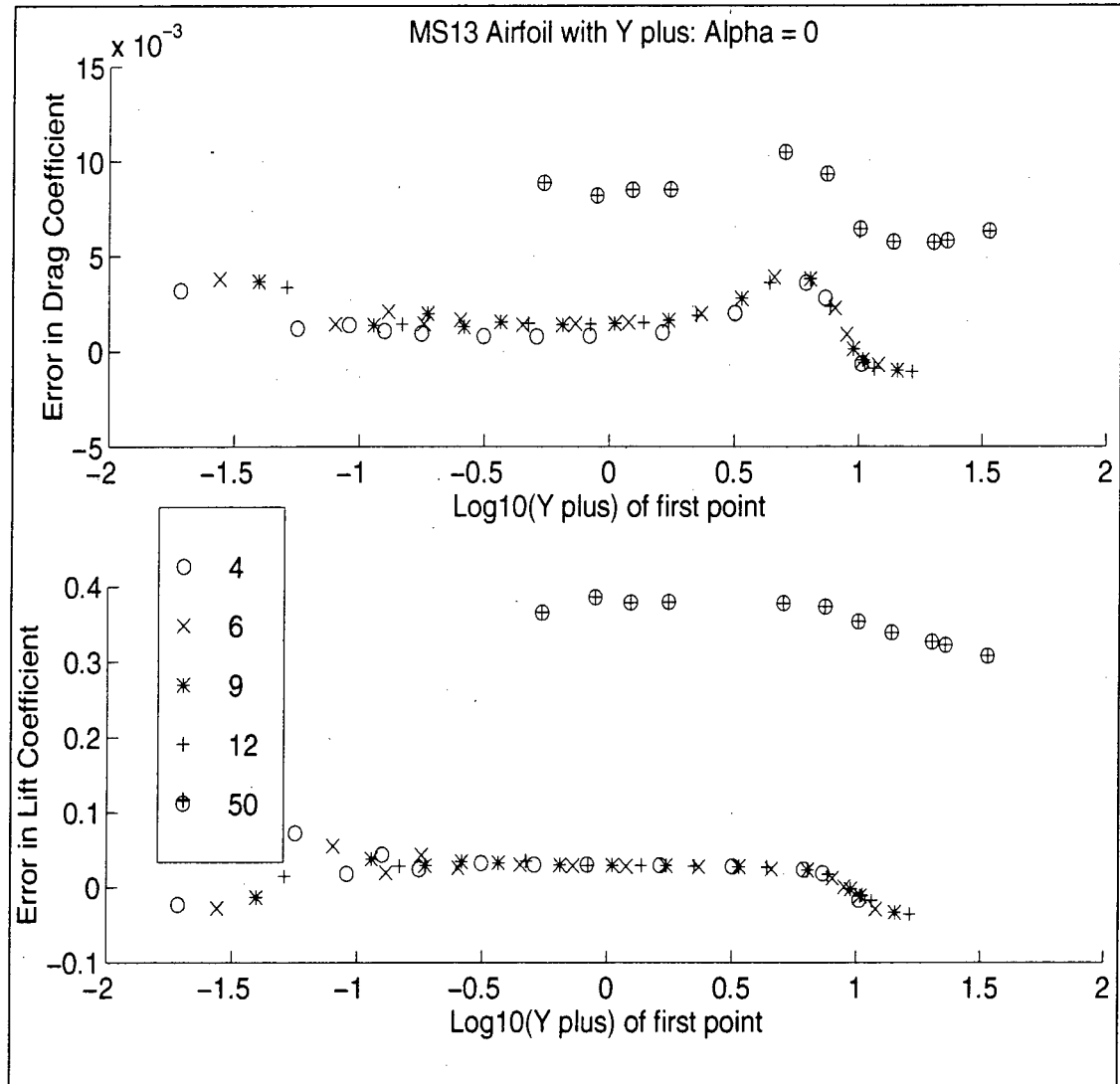
Fig. 3-31   MS13 Airfoil with Flight Reynolds Number Lift and Drag

To illustrate one of the uses of the information from these plots we first run the MS13 airfoil at 50×10^6 which is much more representative of a flight Reynolds number. The result is shown in Fig. 3-31. The highest Reynolds number data is uncorrected because no baseline data is known about this Reynolds number value. To correct the new data we must subtract the value of error that the other Reynolds number runs converged to. At a y^+ value of approximately 10 (no Reynolds number scaling at this low angle of

attack) the value of the drag error (K_d) is read or graphically calculated from the converged curve and is subtracted from the value of the uncorrected drag. The corrected drag is calculated as follows for this drag example:

$$C_{d_{CFD}} - C_{d_{truth}} = K_d \quad \text{(from plot)} \tag{3.6}$$

$$C_{d_{NEW}} = C_{d_{CFD}} - K_d \quad \text{(for new value)} \tag{3.7}$$

$$= 0.0068 \tag{3.8}$$

The value for lift coefficient is approximately 0.348 following the same procedure. Both of these values can be added to the known lift and drag trend data created by plotting the known C_d and C_l versus the $\log_{10}$ of Reynolds number.

The next figure shows the lift and drag trends after the new values are added.
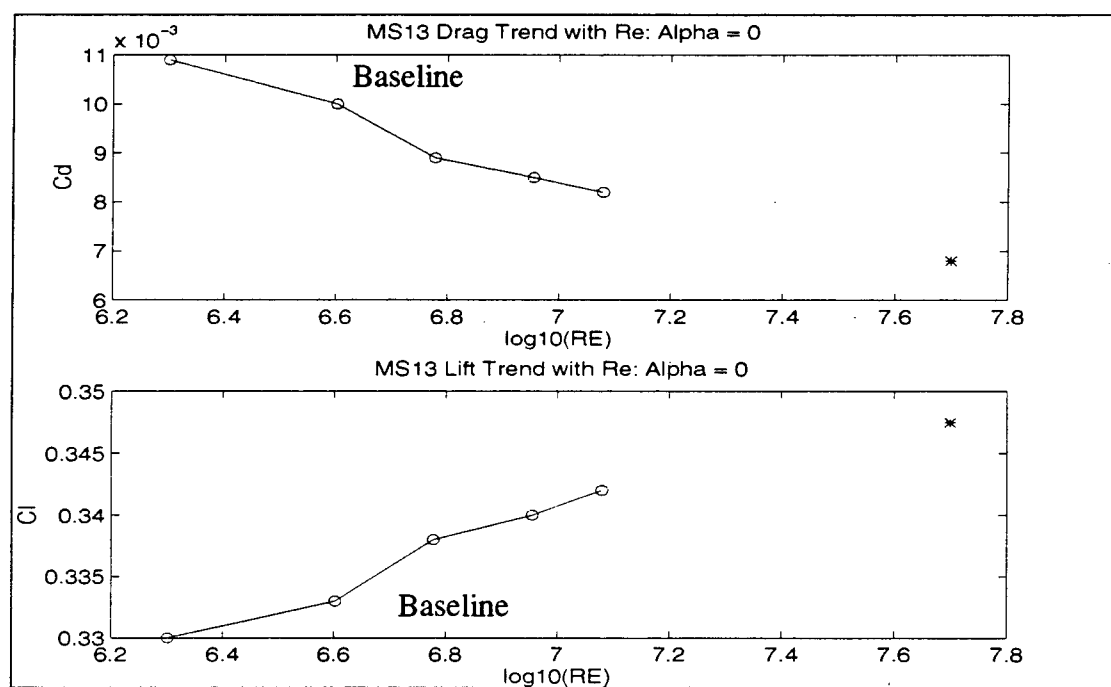
Fig. 3-32   Updated MS13 Lift and Drag Trend Data at AoA = 0.0°.

It is true that no known true solution exists for these two new data points. They certainly appear reasonable and could not have been computed with the use of CFD or wind tunnel alone. Both lift and drag show some evidence of asymptoting (drag is very slight), as they should with increasing Reynolds number (Figure 2-1). To sum up the procedure to this point:

1. Select solver/turbulence model combination and grid generator.

2. Gather data in the wind tunnel over a series of Reynolds numbers.

3. Generate grids at spacings from $y^+ = 0.2$ - 20.0 (modify based on experience) and run airfoil cases at correct Reynolds numbers and boundary layer trip conditions.

4. Plot low angle of attack C_d and C_l error versus $\log_{10}(y^+)$ and mid-to-high angle of attack versus $\log_{10}(y^+ / \sqrt{Re}\ )$

5. As Reynolds number increases, the data should converge to a constant (K_d and K_l) over some portion of the curve. Note that this constant value does not need to be taken at a straight line point on the curve - anywhere where the trend data and the new CFD data are similar.

6. Calculate new C_d and C_l as required (Equation 3-6, 3-7)

These steps can of course be modified as new information becomes available, new turbulence and/or transition models are created, etc. The x-scaling may be better at the laminar boundary layer length scale or the turbulent eddy length scale.
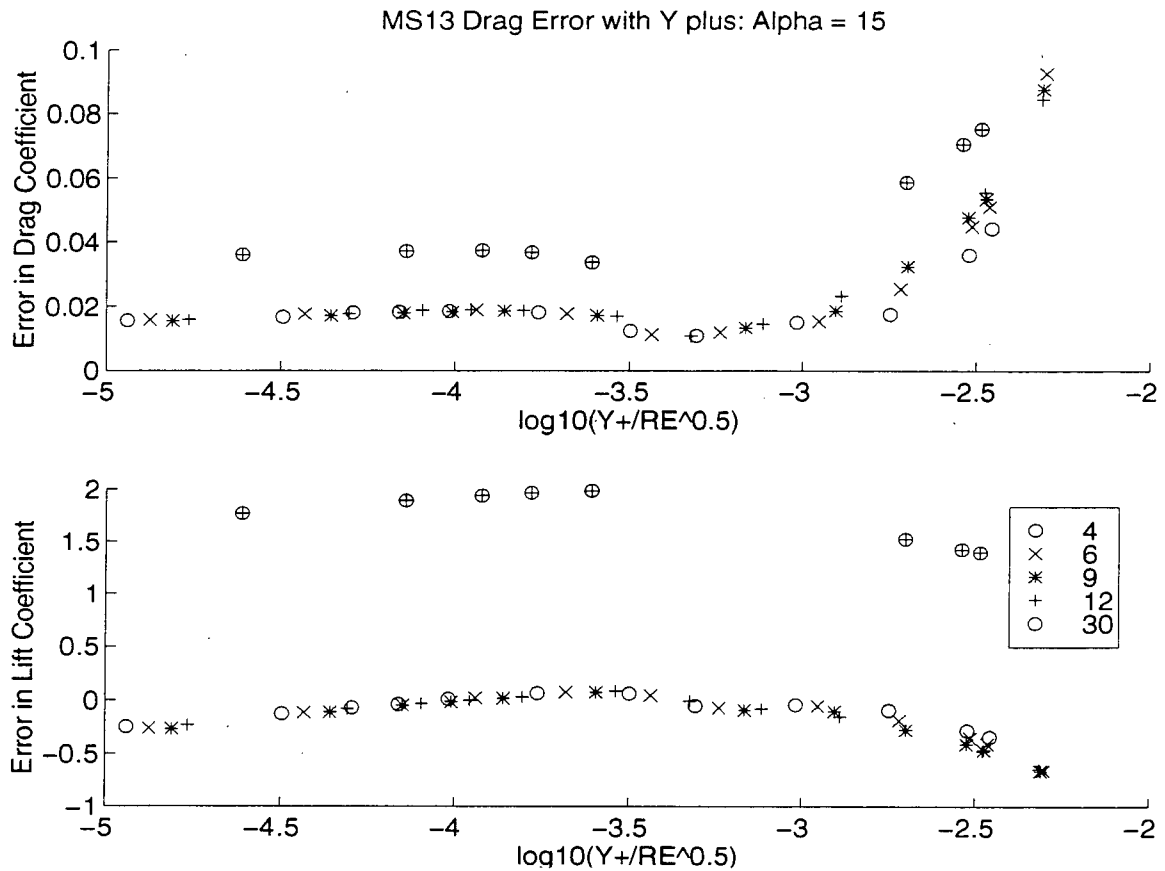
Fig. 3-33   MS13 Airfoil with 30 x 10^6 Reynolds Number Curve at AOA = 15°

Applying the same corrective procedure as before at 15° (except using the tight spacing end of the curve) with Fig. 3-33 results in the trend diagram of Fig. 3-34. Notice in Fig. 3-33 how a range of data at the highest Reynolds number of 30 x 10^6 between x-axis values of -2.75 to -3.5 is not plotted. This is because the CFD runs did not complete here. Certain grid/gradient combinations are more sensitive to others numerically within the solver. If required to determine the trend data, cases such as this may need to decrease the grid cell aspect ratio by increasing the number of points circumferentially around the airfoil in the manner of Jameson[37].
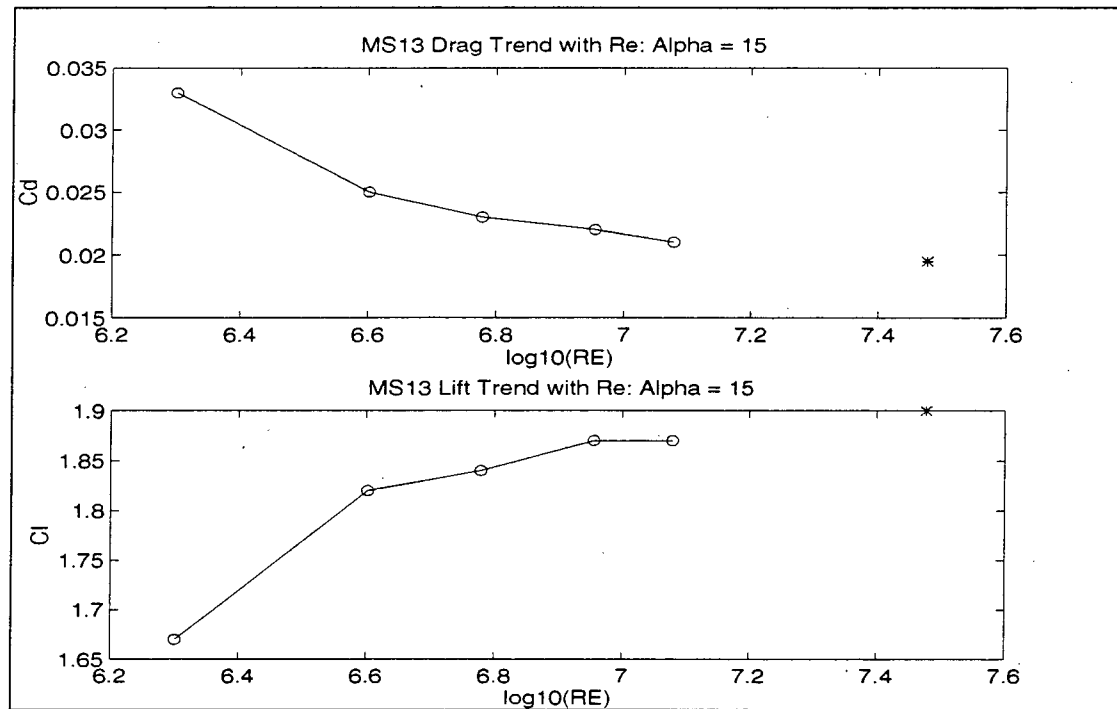
Fig. 3-34   MS13 Airfoil 15° Lift and Drag Trend

The drag continues its asymptotic behavior as with the previous trend plot. In both cases the drag continues to flatten out with increased Reynolds number. Although this would be expected, without the sort of analysis presented here for the first time, there would be no way to place the drag value at 30 x 10^6. This value of Reynolds number is a bit lower than the flight Reynolds number used for the 0° angle of attack case because in order to fly at 15°, the aircraft would have to slow down. 50 x 10^6 would not be realistic for this angle of attack case. The lift curve is more interesting for this case because experimental scatter at the last known point (12 x 10^6) would lead one to believe the curve was flattening out early. In reality, it seems that the curvature is actually more gradual at the higher Reynolds numbers. Unfortunately, there are no airfoil wind tunnel tests of *incompressible* airfoils that go to a Reynolds number of 30 x 10^6 or higher. And those that are tested at higher Reynolds numbers are at a low angle of attack. A method of this type may be the only way

to get data for this phase of flight which might occur during slow-flight testing or if the high-lift systems fail.

The behavior of intermediate angles of attack are interesting for this turbulence model. At intermediate angles of attack, the flow is more unsettled. Areas of different flow regimes may all coexist together. Plots at these conditions show more noise in the CFD solutions but an identifiable trend is still present. Fig. 3-35 shows the solutions at 5° for this airfoil and Fig. 3-36 shows the results at 9°. Even though 5° seems like a low angle of attack, it requires the turbulent scaling of the x-axis.
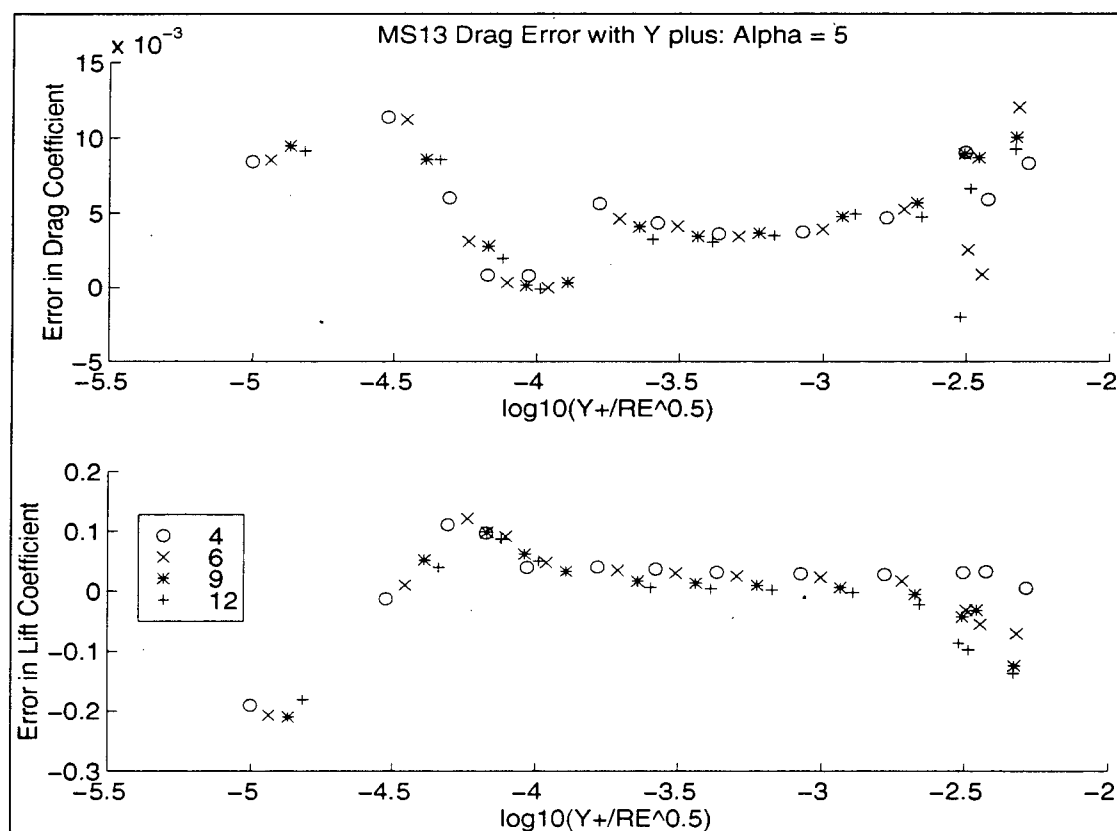
Fig. 3-35   MS13 Airfoil at 5° (SPT Model)
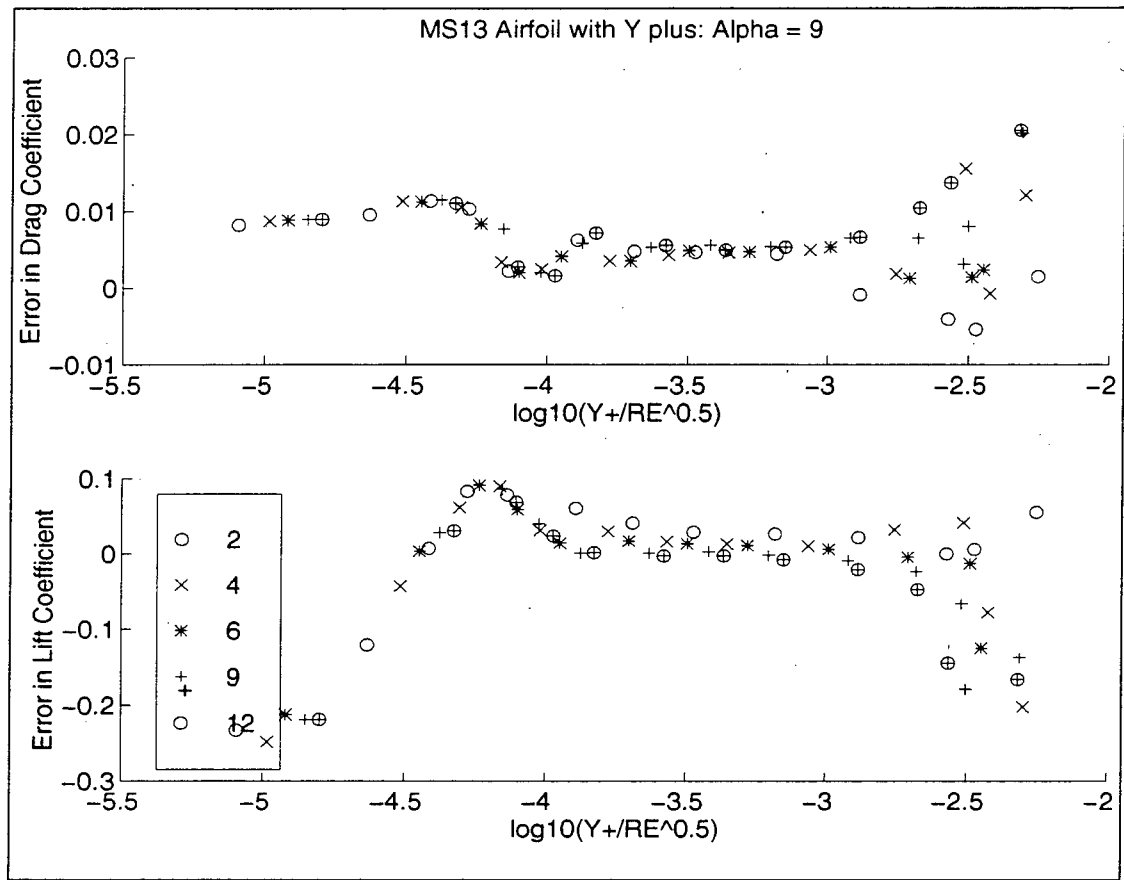
Fig. 3-36   MS13 Airfoil at 9° (SPT Model)

This angle of attack in Fig. 3-36 is significant because of the Reynolds number reversal present in the drag (see Fig. 3-38). Usually we expect drag to decrease with Reynolds number but every so often it will increase. This makes it especially difficult to draw conclusions about the drag trend at angles of attack that exhibit this behavior. However, experience with other similar airfoils and high lift airfoils[20] shows that the drag can be very erratic under certain conditions, Fig. 3-37. This figure is difficult to read but the highly convoluted drag polar is quite evident. This drag polar is the result of configuration changes on a high lift airfoil. Assuming this is not from wind tunnel error, today's CFD algorithms could not absolutely match this behavior. However, it appears to follow an identifiable trend.
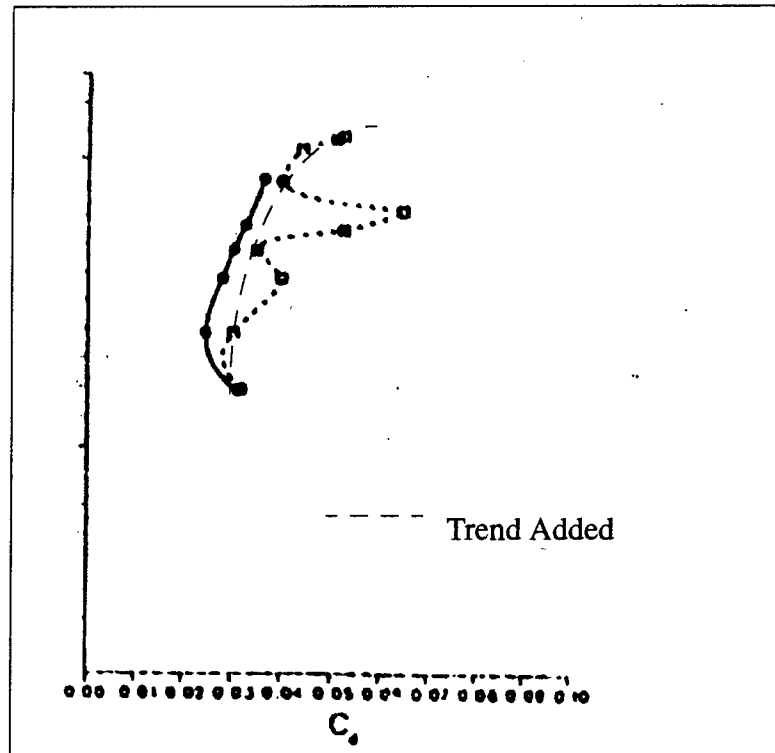
Fig. 3-37   Severe Example of Highly Convoluted Drag. Trend is still Present.

Because of this there is reason to believe that the method of the present section might create a valid trend even with Reynolds number reversal because the present method is more concerned with the performance over a large body of data than at one point. The subject of Reynolds number reversal does not seem to present a major stumbling block to this method at this point, especially in light of Fig. 3-36 which shows satisfactory convergence for the Reynolds numbers leading up to the 30×10^6 value.
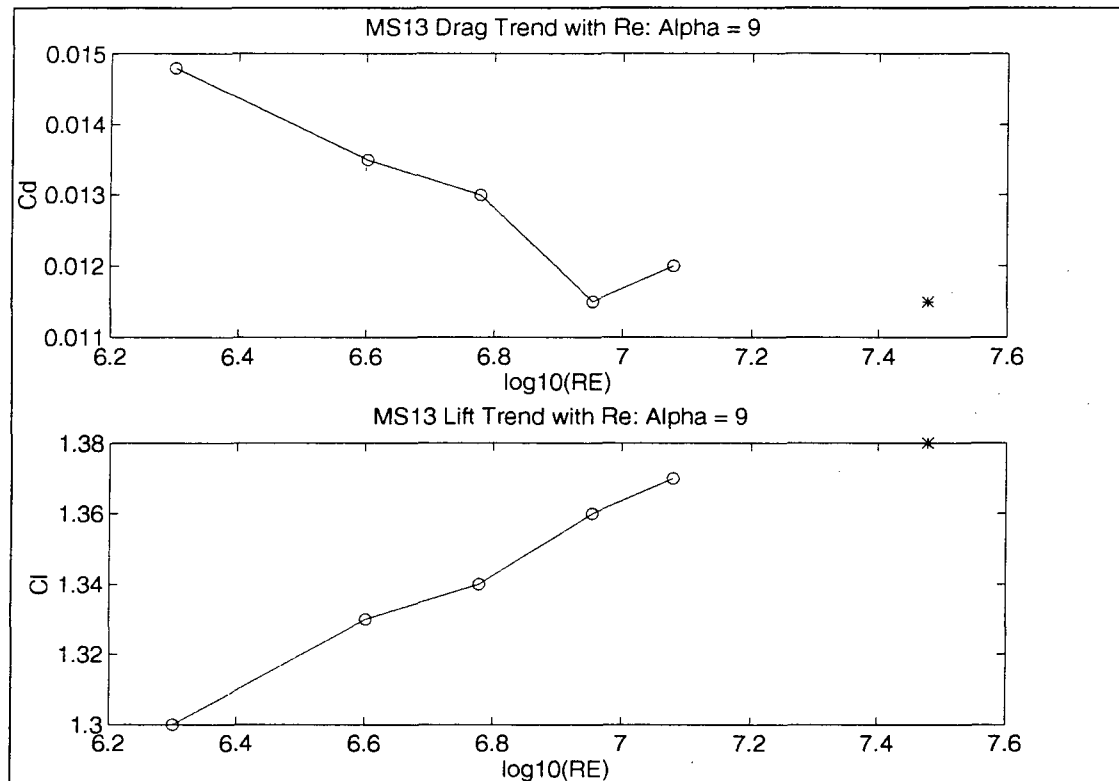
Fig. 3-38   MS13 Airfoil Lift and Drag Trend at 9° (SPT Model)

3.5 MS13 Observations

These figures show several features of interest besides the trend information. Three obvious ones are the curved data on each end of the plot and the small dip in the drag curve. This dip seems to move with angle of attack. In Fig. 3-35, the 5° plot, this dip is centered at an x-axis value of -4. On the 9° plot the dip remains at about the same location on the x-axis. In Fig. 3-33 for 15°, it has grown smaller and moved to approximately -3.5 on the x-axis. A similar but smaller behavior is seen in the lift plots. Since the common denominator between lift and drag is the pressure, the pressure drag may show evidence of this jump. Fig. 3-39 below shows another view at 5° angle of attack that exhibits the skin friction coefficient and the pressure drag coefficient. It appears that at least with this turbu-

lence model there is a pressure jump of some kind that depends upon the gradients in the boundary layer and the angle of attack. As angle of attack increases, this pressure discontinuity occurs at smaller absolute values of $\log_{10}(y^+/\sqrt{Re})$. This corresponds to larger values of y^+, which in general means the gradients in the boundary layer have moved out into the flow more. It may mean that the SPT model is tracking the same flow phenomenon as it flows further away from the airfoil at elevated angle of attack or it may be an artificial creation of the turbulence model.
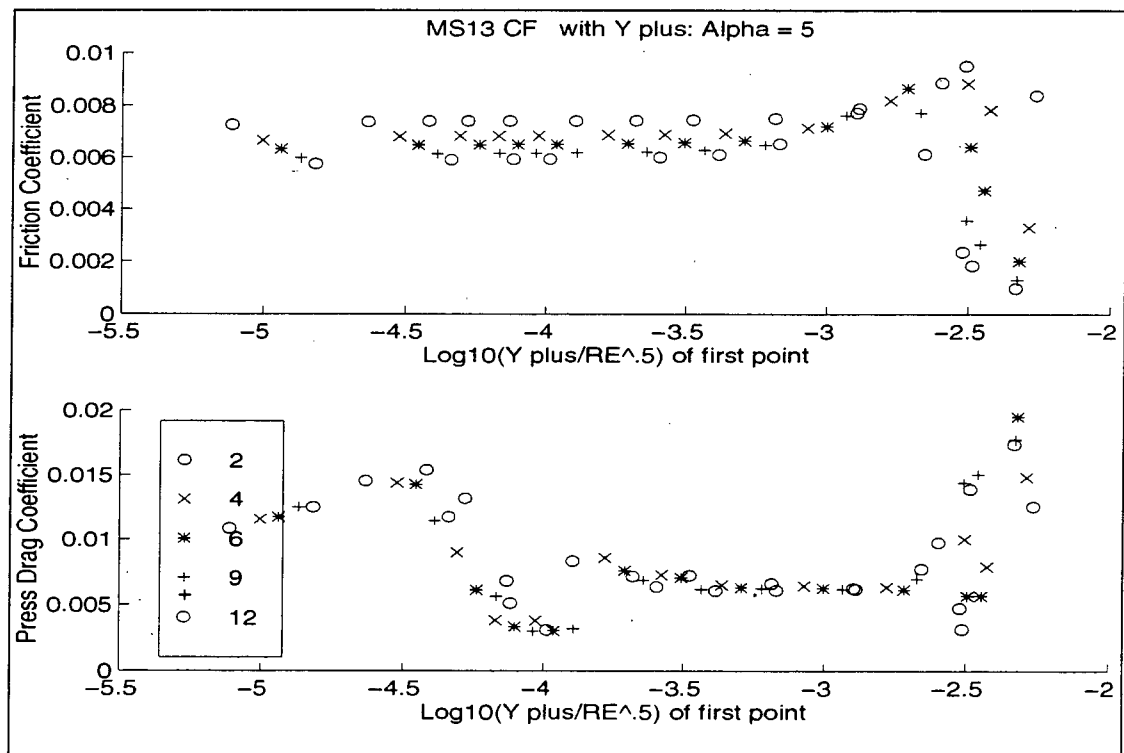
Fig. 3-39   MS13 Airfoil 12° Angle of Attack (SPT Model)

It is also interesting to see that the pressure drag collapses much better to a single curve when graphed versus $y^+/\sqrt{Re}$. Friction drag is of course much more dependent upon Reynolds number and y^+ than pressure and this may account for the difference. There may also be a particular feature of the turbulence model that produces this behavior.

The remaining two turbulence models as well as other effects will be investigated in the next chapter. This chapter has introduced and investigated an entirely new way of combining and comparing wind tunnel data and CFD data. Drag and Lift trends with Reynolds number have been extended using a combination of wind tunnel and CFD. The complementary nature of the two methods is a new way of using their respective contributions.

The effect of blunt trailing edge airfoils on the interaction of y^+ and force coefficients has been noted and possible explanations given for this combination of airfoil, solver, and turbulence model. Lift and drag error, rather than simply lift and drag coefficients, seem to be a key parameter in finding consistencies across Reynolds number. At even moderate angles of attack the y^+ value must be scaled by $1/\sqrt{Re}$ to capture information contained in the tight spacing data. Only at angles of attack less than at least 5° can y^+ alone be used and then the consistency in the lift and drag errors fall at about $y^+ \sim 10$.

Chapter 4   Further Investigation

4.1 Introduction

Now that a possible trend method is somewhat familiar perturbations can be investigated around the established guidelines. There are two additional turbulence models to try, the Baldwin-Barth and Baldwin-Lomax models. In addition to these models we can investigate the behavior of the method when using more grid points in the direction along the airfoil surface as well as more points normal to the surface. We can also look at the effect of the rounded (as opposed to blunt) trailing edge on the airfoil.

4.2 Remaining MS13 Performance

4.2.1 Baldwin Lomax Model

There remains the question of how the Baldwin-Barth and Baldwin-Lomax models perform as well as how the SPT model interacts with the remaining three airfoils. Baldwin-Lomax (BLO) was the turbulence model used on the initial NACA0012 investigations. However, this model was also the most suspect in trials involving the evaluation of y^+ as a consistent grid spacing parameter. The MS13 is a blunt airfoil and BLO seemed to have some trouble with the pressure field generated by these airfoils. Fig. 4-1 shows the plot from a run with this model at $0°$ and Fig. 4-2 shows the plot at $15°$. Fig. 4-1 shows some trend information, but not nearly so sharp as the SPT model data of Chapter 3 (Fig 3-25). Evidently this model does not respond consistently to changes in Reynolds number. Fig. 4-2 shows a complete breakdown in drag trend data, which can be compared with Figure 3-28.
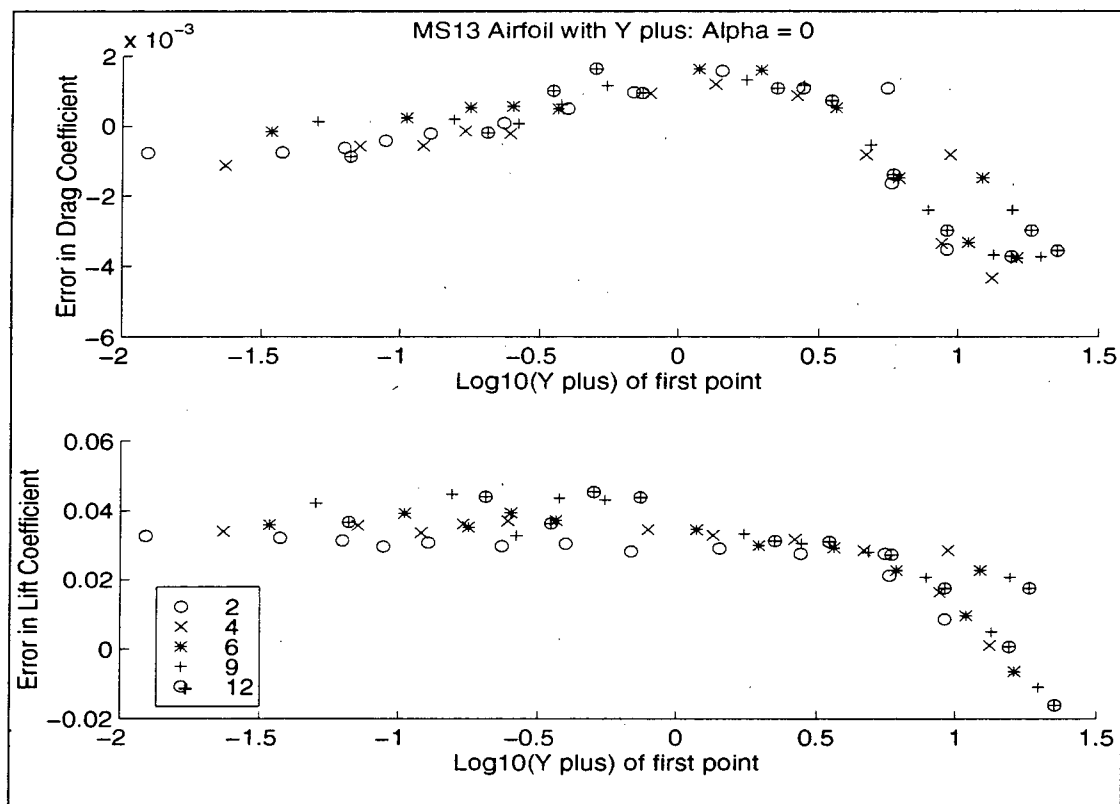
Fig. 4-1   MS13 0° Angle of Attack (BLO Model)
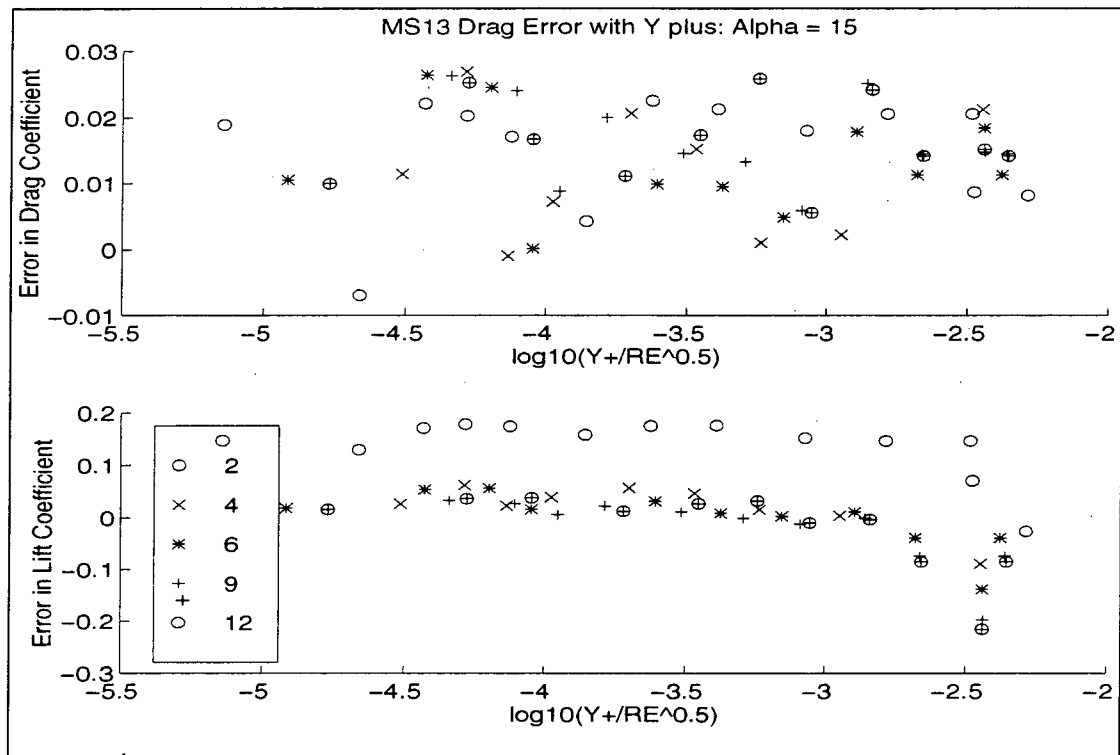
Fig. 4-2   MS13 15° Angle of Attack (BLO Model)

Certainly there is nothing to be gained from this model as far as trend information goes. The fact that this model does much better in lift seems to indicate that viscous effects (shear) are modeled less precisely. If the BLO turbulence model used in this study is non-dimensionalized, the following form results:

$$\mu_\tau = Re * \text{[Non-Dimensional Turbulence Model]} \qquad (4.1)$$

for both the inner and outer forms of the BLO model. This seems to indicate that certain turbulence effects will be increased with Reynolds number and may help to explain why this model does not converge to a trend line at higher Reynolds numbers, especially the drag, which responds much more to Reynolds number changes. The other two models are in production form:

$$\frac{D(\nu_\tau)}{Dt} = S + \frac{1}{Re}(remaining\ terms) \tag{4.2}$$

Where S is a source term proportional to the norm of the strain rate tensor, giving natural convective growth of ν_τ with increased Reynolds number while the remaining terms such as diffusion and destruction are inversely proportional to the Reynolds number.

The Baldwin-Lomax turbulence model is obviously not satisfactory for this study. It cannot consistently compute the effects of highly viscous flow. Note that it *does not* have to be absolutely correct, it only needs to be able to compute drag in a consistent manner across the Reynolds number range selected for this study. Because of its algebraic, uncoupled nature and apparent Reynolds number dependence, it cannot do this. This model will not be used for the remainder of this study.

4.2.2 Baldwin-Barth

Fig. 4-3 shows the lift and drag error plot for this turbulence model at an angle of attack of $0°$. Immediately, the convergence behavior with Reynolds number can be seen as it was with the SPT model. Notice that the data is smoother than the same plot using the SPT model (Figure 3-25) and that the area of the best convergence is still centered at about $y^+ \sim 10$. At least at this angle of attack, spacing changes do not seem to affect this model as much. Also notice there is no "dip" in the data. The $15°$ Baldwin-Barth data is shown in Fig. 4-4 and Fig. 4-5 and a plot of $9°$ is Fig. 4-6.
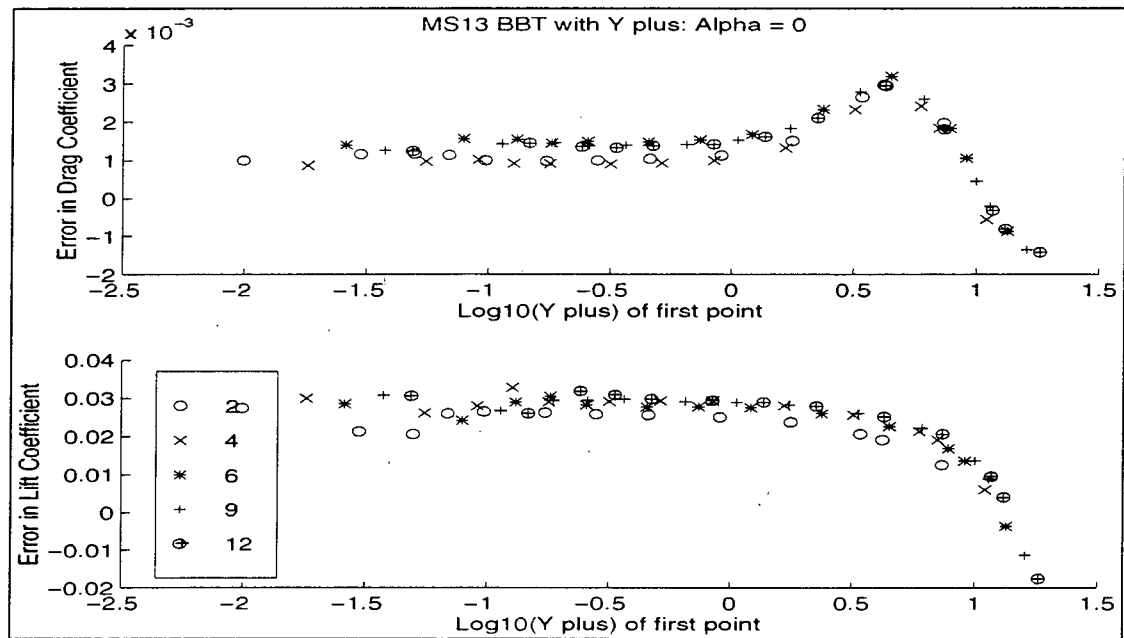
Fig. 4-3   MS13 BBT Model 0° Angle of Attack
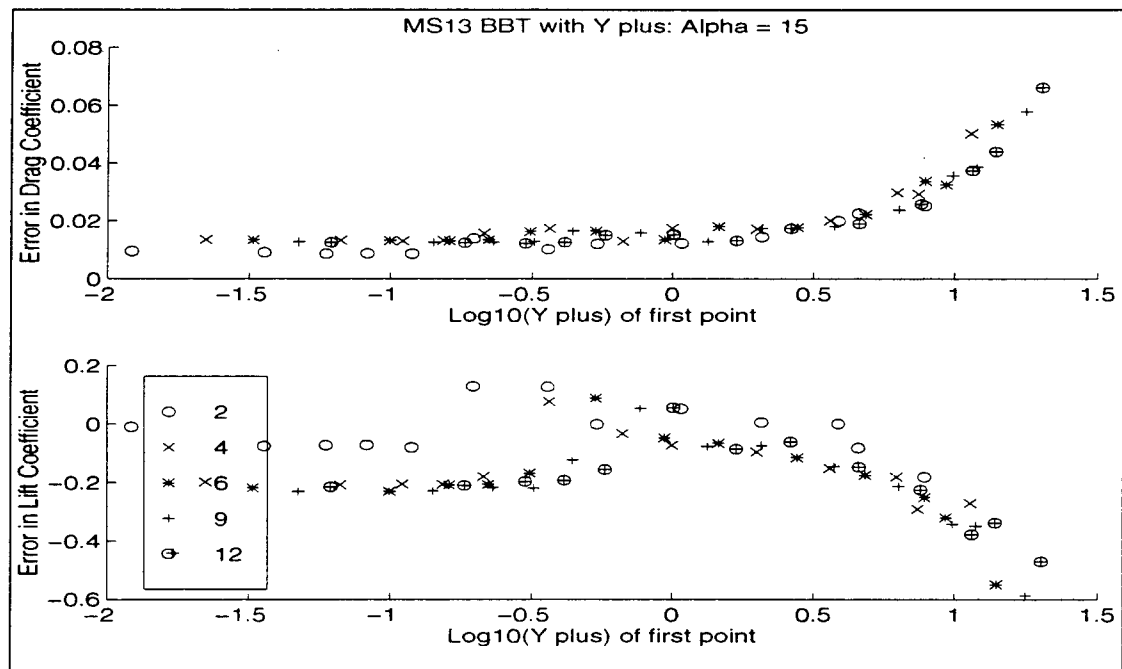
Fig. 4-4   MS13 BBT Model 15° Angle of Attack vs. y^+ Alone
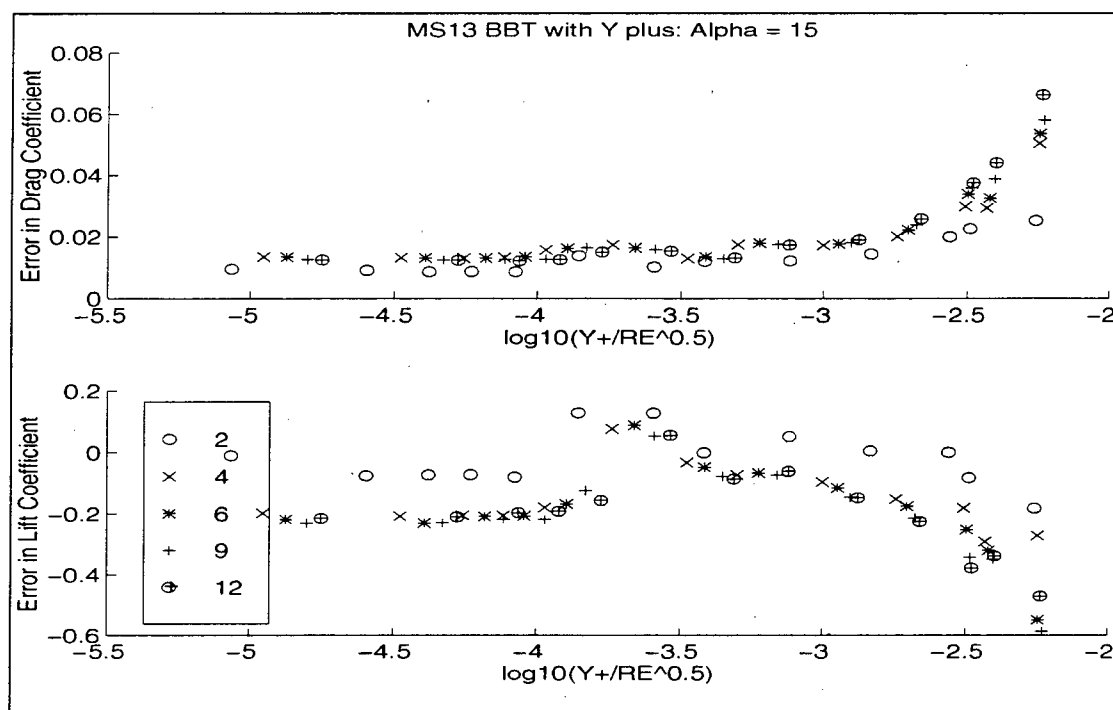
Fig. 4-5   MS13 BBT Model 15° Angle of Attack vs. Scaled y$^+$

The trend information is still evident at this angle of attack in Fig. 4-4 and Fig. 4-5 although not quite as smoothly as the SPT data. This time the data is better presented versus y$^+$ than y$^+$/$\sqrt{Re}$ as it was for the Spalart data (Fig 3-28). It appears that trend information for this model at this angle of attack is better taken against y$^+$ alone. It appears that the 1/$\sqrt{Re}$ factor may correct for some pressure effect. There is a definite hitch in the data around -3.5 on the x-axis, although it is more pronounced than that using the SPT model. It is interesting to note that both turbulence models experience this dip at virtually the same point on the x-axis, which may mean they are responding in similar manner to gradient changes at this high angle of attack. At this angle of attack, the SPT model seems less sensitive to changes in lower Reynolds number over the entire range of wall spacings and seems to be the better candidate for trend information. However, in the next figure, at 9° angle of attack, the behavior is very different than the SPT model (Fig 3-36) at intermediate angles of attack.
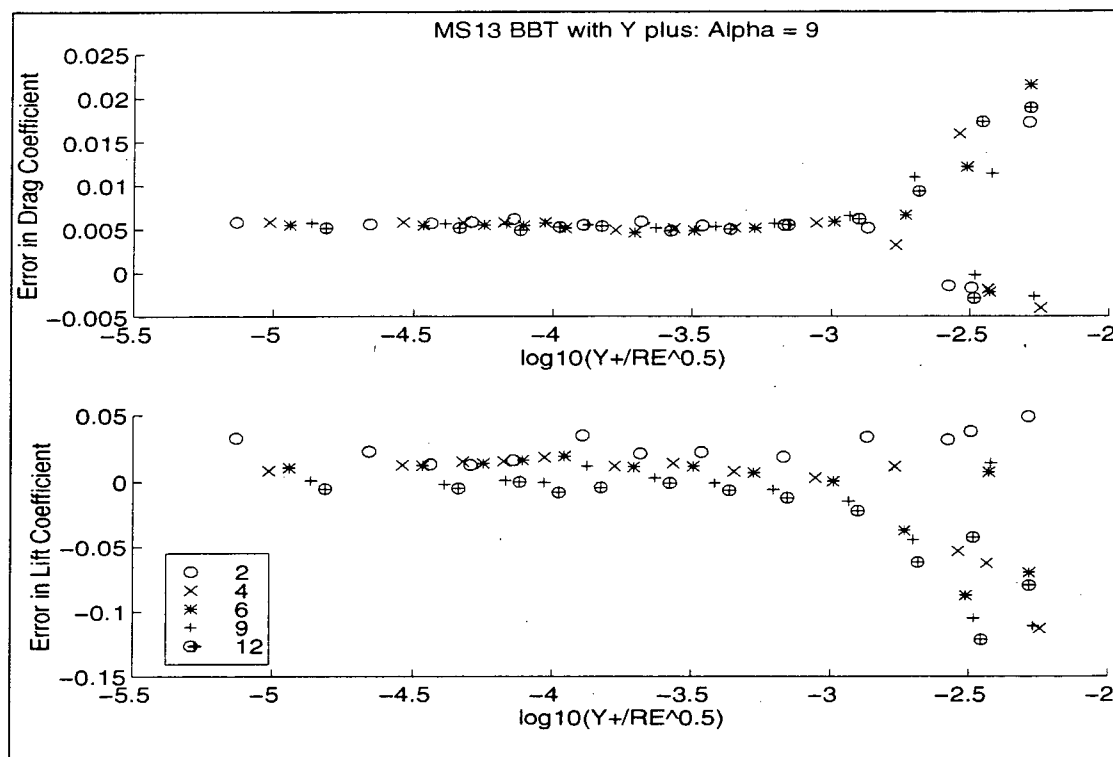
Fig. 4-6   MS13 BBT Model 9° Angle of Attack

Here there is no evidence at all of any dip in the data and the drag convergence is even tighter than the SPT model (this plot appears virtually unchanged if graphed vs. y^+ alone). But the lift is much worse than the SPT model (Fig 3-36) at comparable angles of attack, although the higher Reynolds numbers do converge to some degree. It seems that both of these turbulence models can be used successfully to identify lift and drag data trend and in fact each model appears better in certain areas of the testing regime. At least one researcher[39] who used both of these turbulence models in a study specifically designed to compare them on high lift airfoils found that at different angles of attack either one or the other turbulence model did better at different parts of the airfoil. It should be no surprise then that each of these models might do better or worse than the other depending on the amount of viscous flow present over the airfoil and the y^+ value. Accordingly, the remainder of this study will present the results of only the Spalart model unless something

warrants showing data for both. The SPT model has sharper convergence at more angles of attack and is more consistent in that $y^+/\sqrt{Re}$ is the parameter which works the best to identify trends at mid-to-high angles of attack, whereas in the BBT model y^+ alone is sometimes preferred.

If other turbulence models are chosen to attempt to find this trend information, this study has given examples of some of the comparisons to be made and some of the behaviors to examine.

4.3 Spalart-Allmaras on Remaining Airfoils

It seems that this model does a credible job over a large Reynolds number and angle of attack range. The critical parameter seems to be $y^+/\sqrt{Re}$ at mid-to-high angles of attack and y^+ at the lower ones. A looming question is how this model operates on different airfoils when undergoing the same changes in angle of attack and Reynolds number.

4.3.1 MS17

The MS17 airfoil is a slightly thicker cousin to the MS13 (Figures 3-1 and 3-2). In general, although the general lift and drag values might be slightly higher than the MS13 airfoil at corresponding angles of attack, the behavior should be relatively similar. At high angles of attack with a larger nose radius the turbulent and separation qualities will be different than the MS13. These effects probably cannot be picked up in detail by the turbulence models but would show up as different transition points and different transition Reynolds numbers in the physical airfoil test. To find trend data, however, should be no different for this airfoil if the data is consistent as it was for the MS13. Fig. 4-7 and Fig. 4-8 show the MS17 at $0°$ and $9°$ angle of attack using the SPT turbulence model.
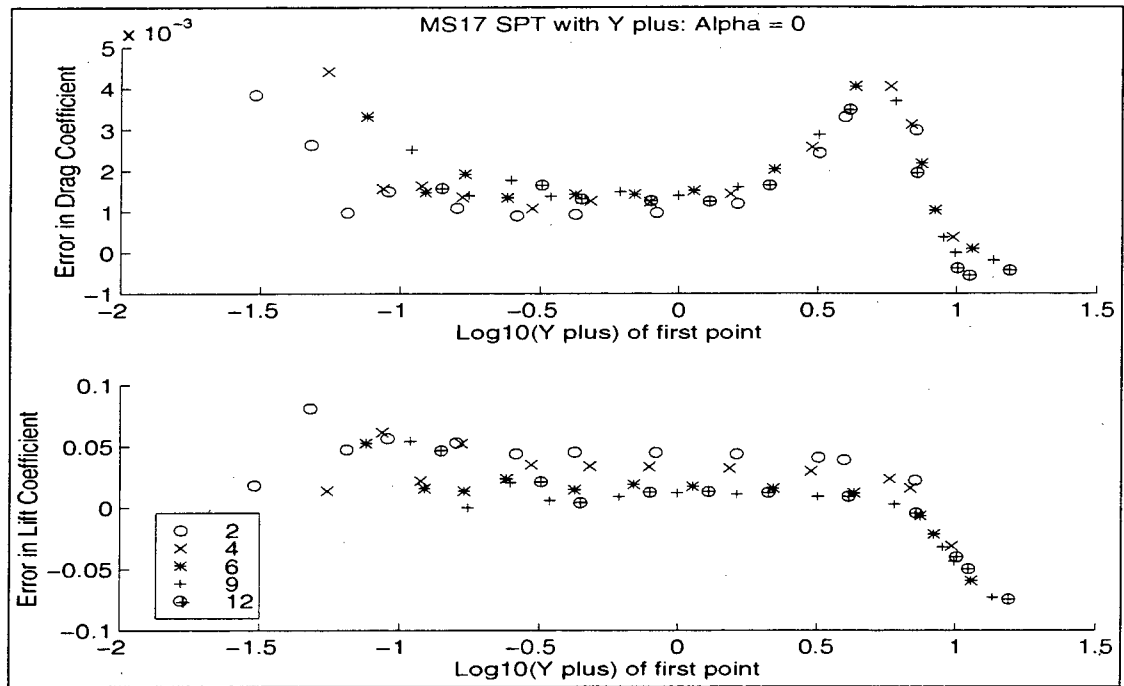
Fig. 4-7   MS17 Airfoil at 0° (SPT Model)
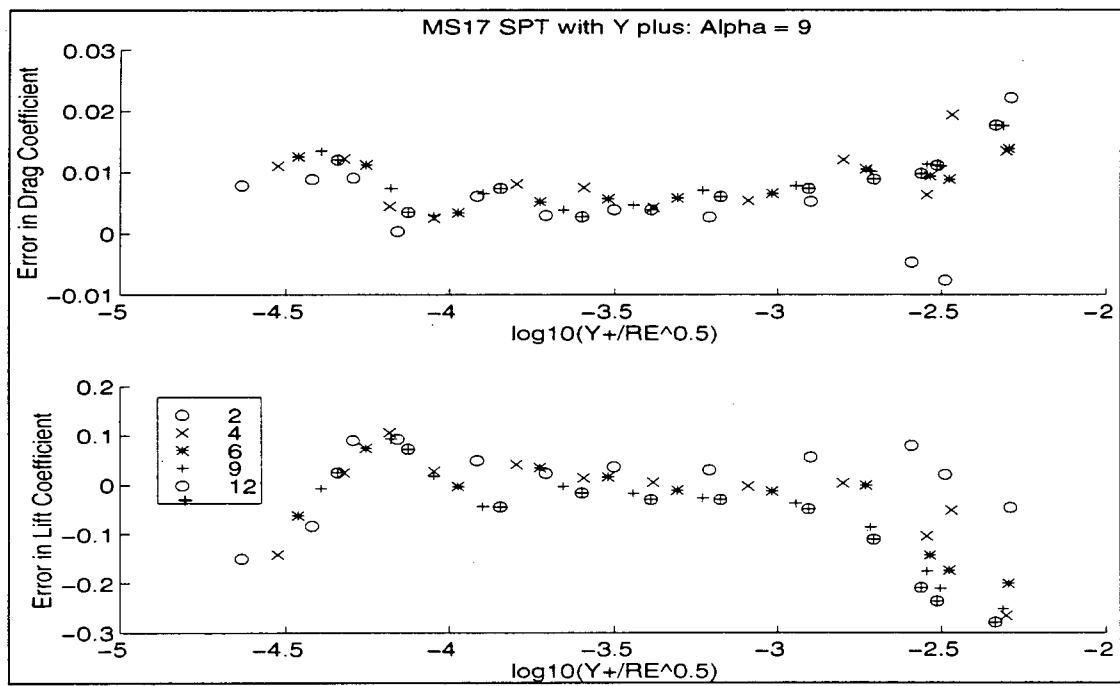
Fig. 4-8   MS17 Airfoil at 9° (SPT Model)

The trend data is not as precise as it was for the MS13 airfoil although the wide spacing end of the curve is still the most consistent for the low angle of attack case and the tight spacing end of the curve is used for the 9° case when plotted versus $y^+/\sqrt{Re}$.

4.3.2 MS21

The MS21 is much thicker than the MS13 and enough thicker than the MS17 to change the flow characteristics significantly over even moderate angles of attack. High speed transport wings will not be this thick. If this method seems to work on this airfoil, however, that would be encouraging for flapped airfoil systems since to some approximation, a flapped airfoil is just a higher thickness and higher camber airfoil. The MS21 does not have much different camber than the others but the thickness will generate different considerations for the solver/turbulence model combination.
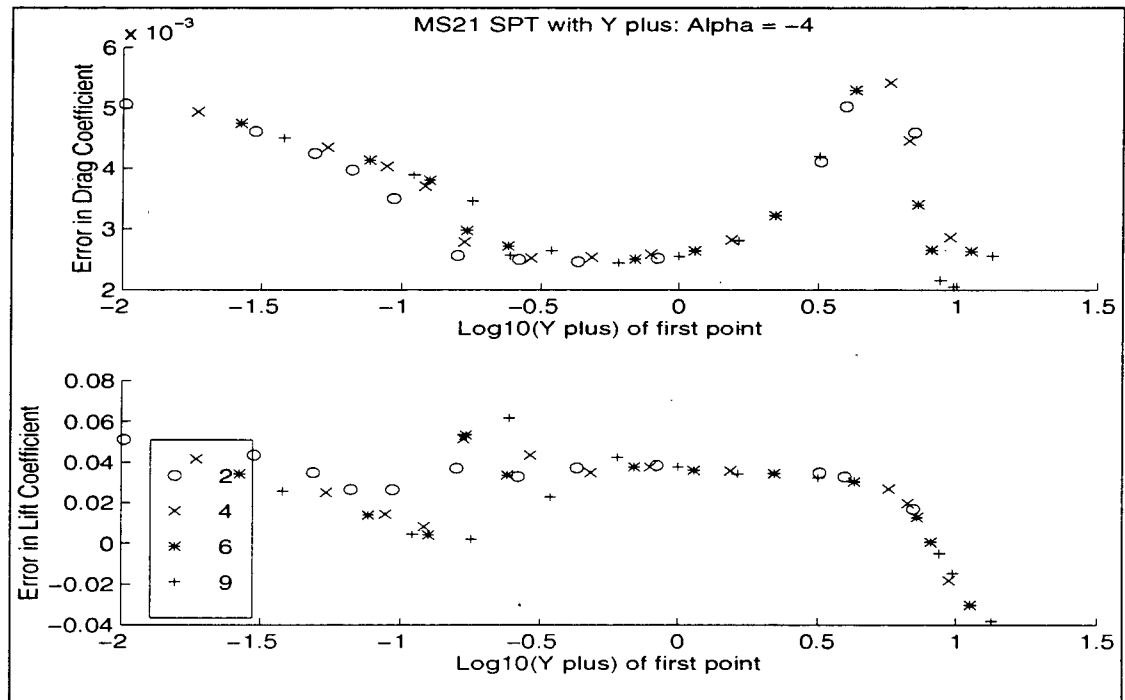
Fig. 4-9   MS21 SPT Model -4° Angle of Attack
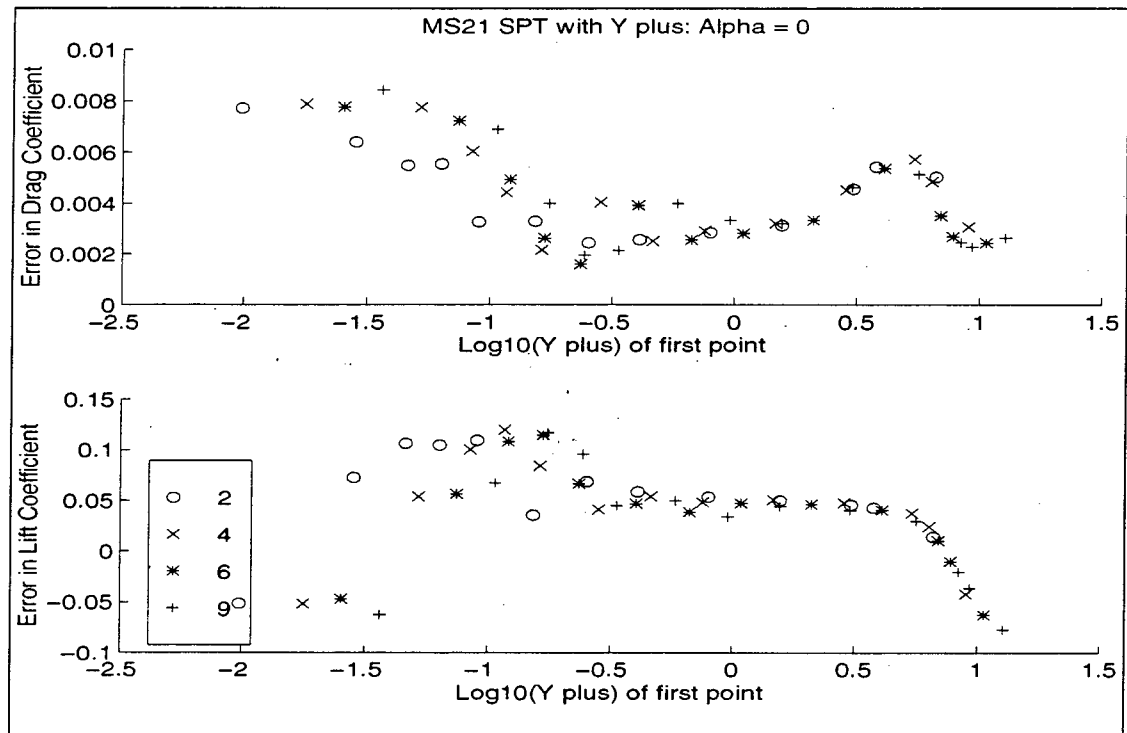
Fig. 4-10   MS21 Airfoil at $0°$ (SPT Model)

From Fig. 4-9 (the zero lift angle) and Fig. 4-10 there seems little change with this airfoil at this angle of attack The preferred y^+ seems to be slightly less than 10 in the low angle of attack case. The wind tunnel test of this airfoil did not include a Reynolds number of 12×10^6. But it appears that just as in Chapter 3, it could be corrected quite accurately because the convergence of the other Reynolds numbers is very good. The tight spacing end of the drag curve behaves somewhat differently than the MS13 or 17. The values have a higher drag error as a percentage of the wide spacing end of the curve, where it remains well behaved. The points are not necessarily more scattered, just more in error.
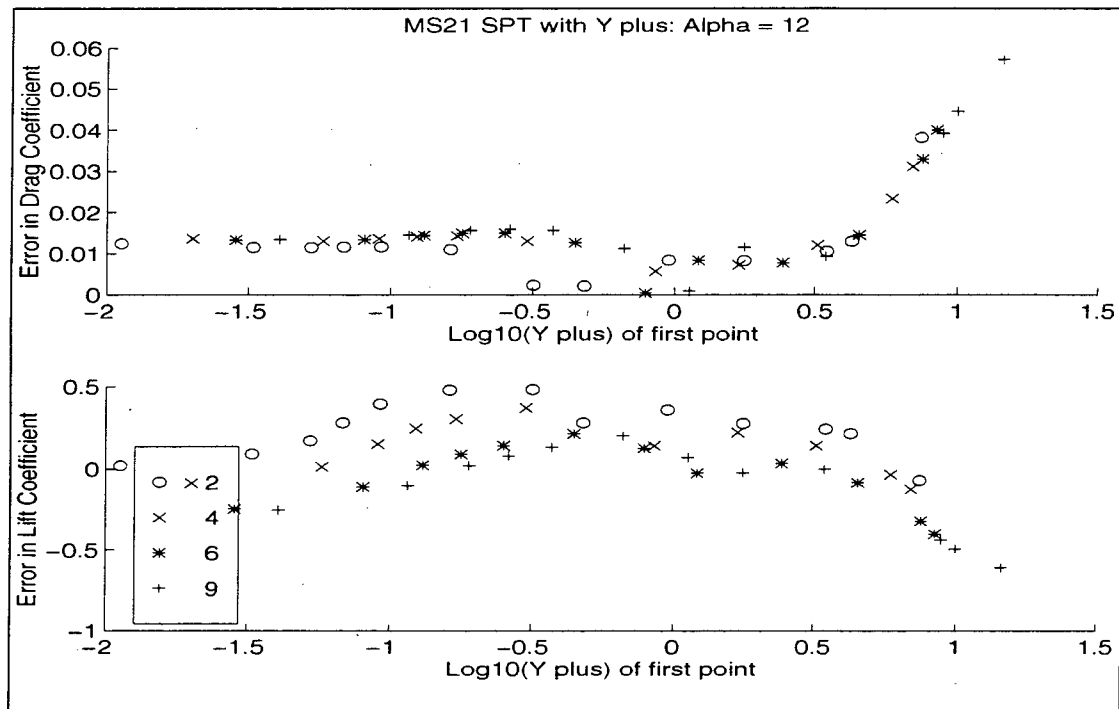
Fig. 4-11   MS21 SPT Model 12° versus y⁺ Alone
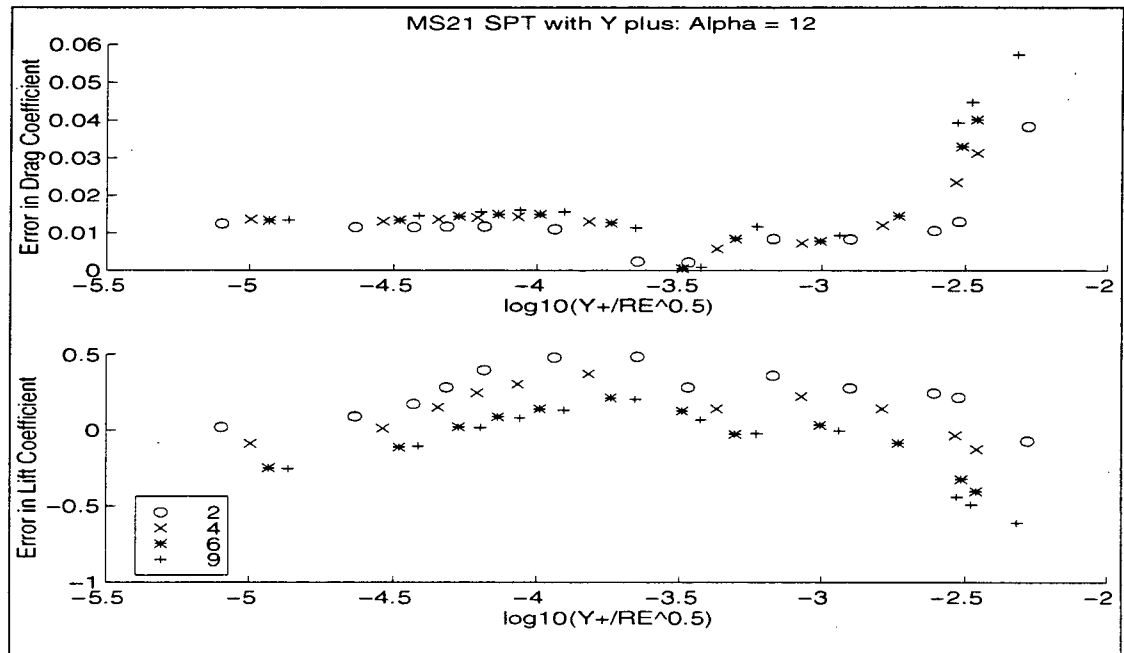
Fig. 4-12   MS21 Airfoil at 12° Angle of Attack (SPT Model) with y⁺ Scaling

At 12°, the data still looks acceptable for the MS21 when plotted versus $y^+/\sqrt{Re}$. This is past the stall angle of attack for both the 2 and 4 x 10^6 Reynolds number cases which may be why they do not converge to the remaining Reynolds numbers in lift. This leads toward the conclusion that perhaps the $\frac{1}{\sqrt{Re}}$ factor is a pressure or pressure gradient driven requirement that somehow corrects the data. Twelve degrees is the stall angle of attack for the 6 million Reynolds number case and yet the drag data to some degree appears quite reasonable. It may be easier to predict drag data past stall or to use post stall drag values in describing the trend data than it is for lift but it seems to correlate very well up until that point. Notice that the "Spalart Dip" is still present on this thicker airfoil, which is perhaps even more evidence that it is a gradient induced, non-physical phenomenon. This dip in the pressure drag has proved very consistent over all angles of attack and Reynolds numbers and now airfoils, too.

4.3.3 MS93

This thin, supercritical airfoil is perhaps more representative of the jet class of airfoils than any of the others. Good cruise performance at high speed is the design point for long range transports and a supercritical wing is usually called for. With a narrow nose and a small nose radius its stall characteristics should be very abrupt compared to the other airfoils and there should be several turbulent modes during its angle of angle of attack travel such as transition and relaminarization, separation and reattachment, bubbles, and full turbulence and separation. It is very unrealistic to assume any turbulence model can get all of this correct, especially at lower energy flows with thicker boundary layers. However, the method remains the same because we want to make no special allowances for any flow or solver phenomenon and we should take the data "as is".

Fig. 4-13 shows generally good results at the Reynolds numbers 29, 59, and 116x10^5. The drag converges rather well but perhaps not as precisely in lift. This is a good example of using more limited Reynolds number data from the wind tunnel. Only half as many points were available from the wind tunnel tests of this airfoil but if past indications

are correct, any other runs would fall on the same curve. If using data from $y^+ \sim 10$ gives good results (at this angle of attack) for predicting lift and drag then perhaps less Reynolds number data will be called for. The preferred y^+ value has returned to approximately 10 again from slightly less than 10 as it was with the MS21.
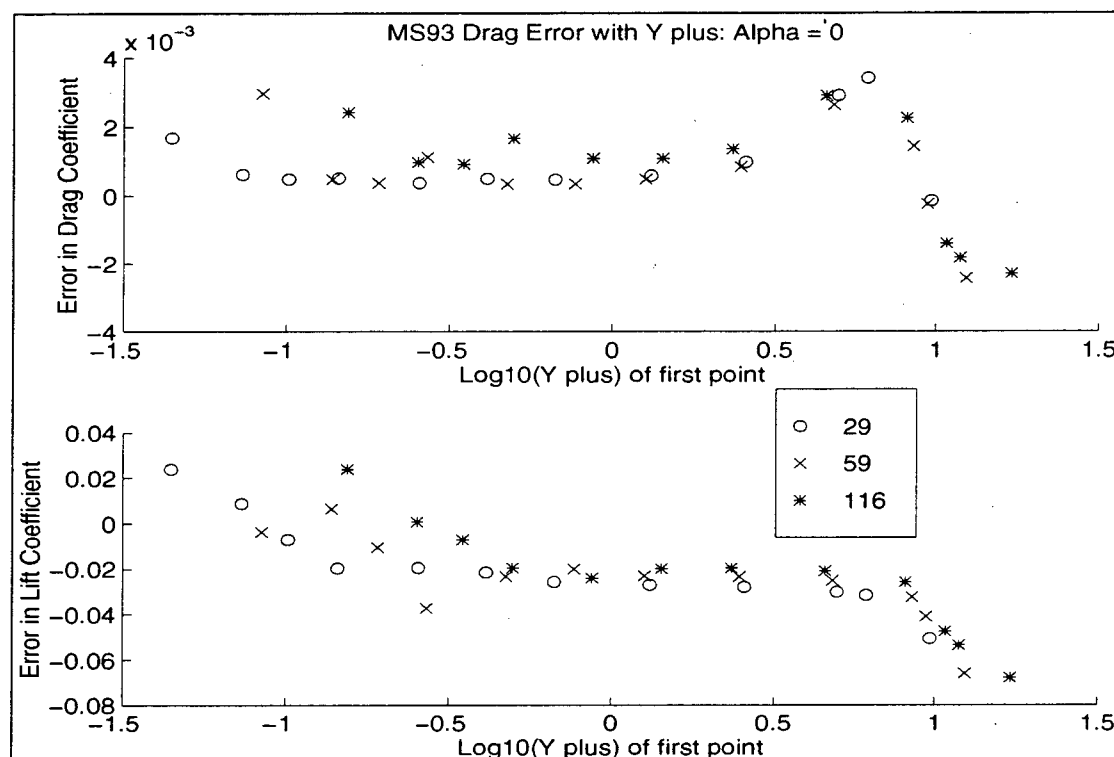
Fig. 4-13   MS93 Airfoil $0°$ Plotted Vs. y^+ (SPT Model)

In this plot, the y^+ values between 3 and 10 seem to have converged satisfactorily for all Reynolds numbers. Conventional literature recommends that y^+ never exceed 3.5 or the solver will not be able to properly compute C_p and C_f. But if these errors are consistent across a wide Reynolds number range the drag trend data can be obtained here. This behavior has been seen on the other airfoils and with both valid turbulence models but only at angles of attack equal to or less than about zero. As the flow changes with angle of attack, the y^+ value must be scaled again as shown in the next plot.
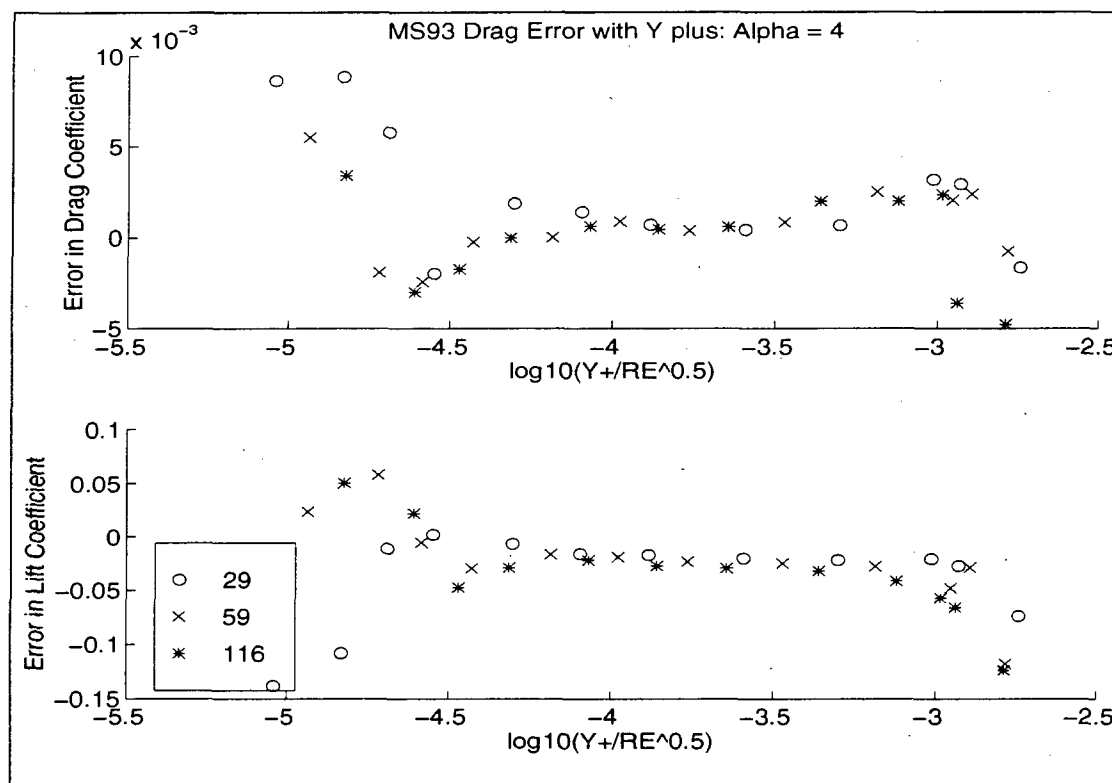
Fig. 4-14   MS93 Airfoil 4° (SPT Model)

Figure 4-14 shows generally good results at 4° angle of attack, (the Reynolds numbers listed in the legend are multiplied by 10^5) which is probably a degree or two higher than the cruise angle of attack for an airfoil like this. Four degrees is a moderate angle of attack for this thin airfoil. Good trend estimation should be possible under these conditions using the middle of the curves. This airfoil does not do quite as well on either end of the curve no matter how the data is plotted. The thinness of this airfoil presumably provides quite a challenging pressure gradient which may be harder to correct for, both within the turbulence model and in correcting the data. Figure 4-15 shows a plot of the friction drag coefficient and the pressure drag coefficient. Note that the pressure drag is not converged on either end of the curve. Plotting versus y^+ alone collapses the friction drag on

the wide spacing end of the curve onto one line. Plotting as shown collapses only a portion of the tight spacing part of the pressure drag onto a line.
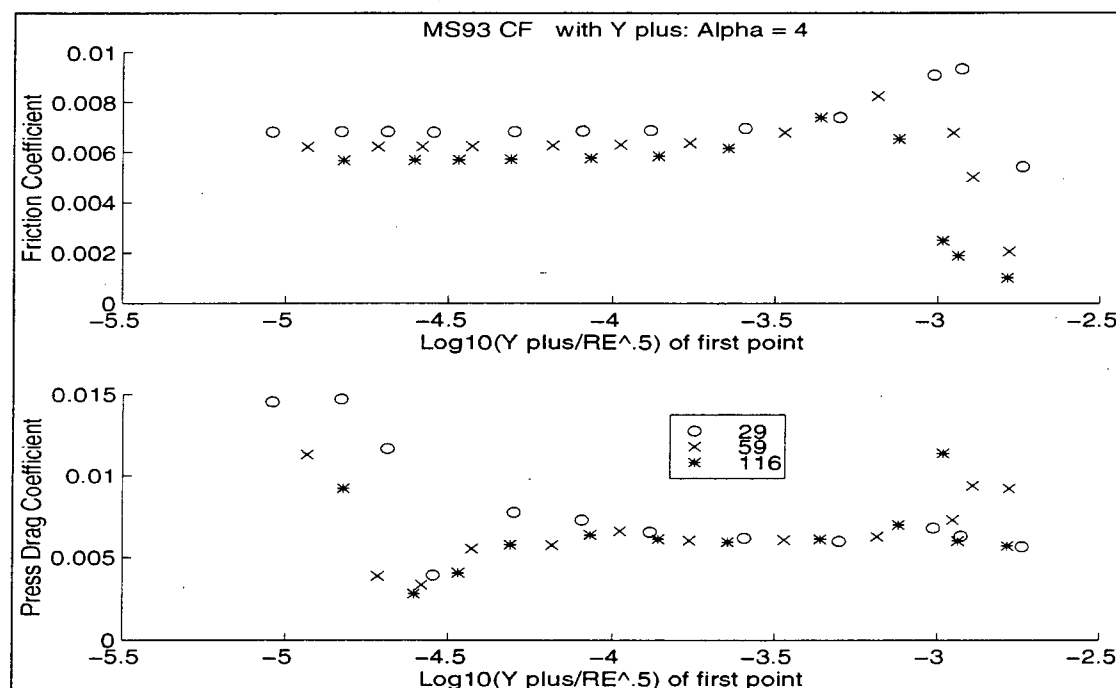
Fig. 4-15   MS93 Friction and Pressure Drag Coefficients, 4° Angle of Attack

4.3.4 A Final Note on Turbulence Models

The SPT model was more completely tested and/or reported for many combinations of airfoil/Reynolds number/angle of attack. The BBT model is generally comparable for all conditions tested with the exceptions we have noted previously. Also, the Taguchi statistical techniques in the next chapter will provide a new way of determining information about the chosen turbulence model. The point is not to evaluate the "goodness" of these turbulence models but to assess their relative importance to this trend process and to determine which, if any, are superior *in this process*. It is much different to see whether or not a turbulence model correctly models the size and location of a separation bubble than it is to find its relative worth for obtaining aerodynamic solutions over a large selection of flow conditions, some of which the turbulence models may not necessarily be best at. It is therefore probably erroneous to try to point to one "best" turbulence model, especially

when discussing such varying areas as detailed flow physics or widely changing trend data. It is important to realize that this method relies on performance over ranges: ranges of spacing, Reynolds number, and angle of attack. The point to point behavior of turbulence model may not be the best indicator of its performance in determining trend information with Reynolds number. It is more important to realize the importance of the turbulence model to the success of obtaining the trend information. Both Spalart-Allmaras and Baldwin-Barth seem sufficient but as the models become better, so will the Reynolds number extension.

4.4 Other Factors

One could perform many excursions on the main body of this research and only a few of these were chosen for inclusion in this study. All of them use only the MS13 airfoil to illustrate their performance. Since the performance of the initial body of research was mostly consistent over all four test airfoils it is supposed that the behavior of the excursion testing would remain consistent also. More detailed studies of these excursions would be an excellent area for future research.

4.4.1 Rounded Trailing Edge

Figure 3-6 shows the rounded trailing edge. As remarked previously, other researchers have used this non-physical trailing edge to allow the CFD solution to approach a more accurate answer for lift and drag. This occurs because current turbulence models have difficulty resolving the forces created by the shedding vortices from the more physical blunt trailing edge. With this trailing edge, the vortices and their affects are weaker and the turbulence models can get better approximations for the viscous effects.
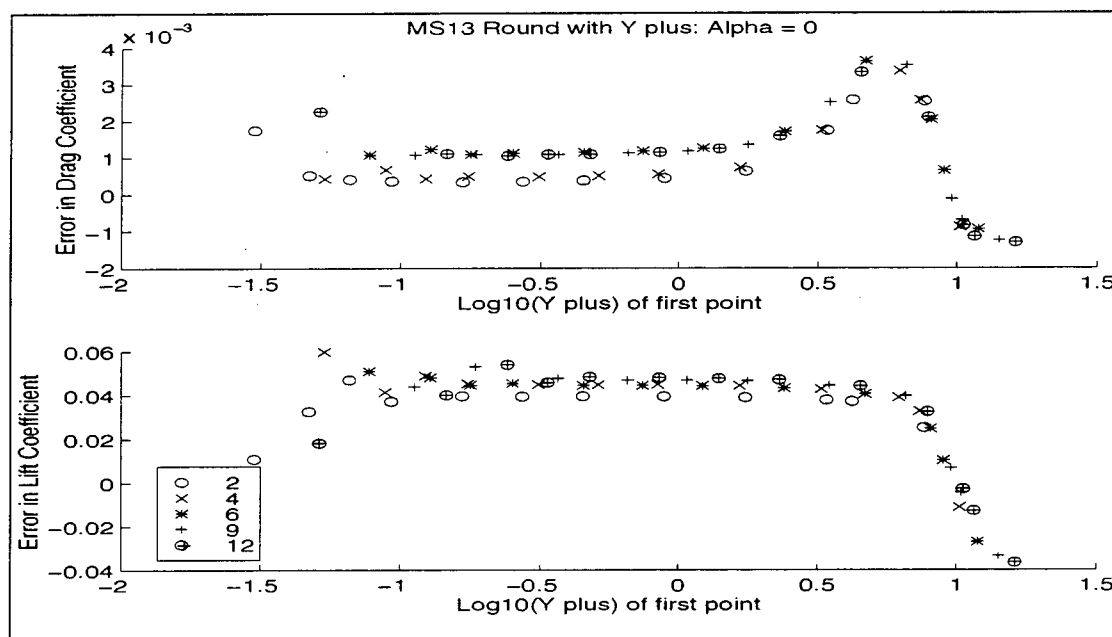
Fig. 4-16   MS13 Round Trailing Edge SPT Model, 0° Angle of Attack

The round end airfoil behaves very similarly to the blunt end. The absolute drag and lift errors are actually a bit smaller at higher angles of attack. All else remaining the same, it may be good practice to use the round ends when determining trend data, although it may not be necessary. Further research may show that with other airfoil/Reynolds number/turbulence model combinations, the round end adds enough improvement to universally recommend it.

4.4.2 299 x 62 Grid

This modification increases the number of grid points circumferentially around the body of the airfoil and in the wake. The increased resolution should better resolve the flow gradients and improve the performance of the CFD solution. As with the round end case, the actual errors have improved but not the convergence to trend consistency. Since adding grid points will increase computer time, there is no need to run these cases unless the trend convergence is better for some cases. An exception to this would be to decrease the aspect

ratios of the smallest grid cells near the surface of the airfoil. Some of the CFD runs for this study halted due to floating point overflows - not a great many but enough to lose a data point here and there. If a decrease in aspect ratio through increased grid density solves this problem, it may be worthwhile, but a very large grid on the order of 500 x 100 does not appear to be required. If the trend data is available with the current grid however, there should be no reason to increase this density. The next figure shows the $9°$ case, which is very similar to the initial grid case. The dip in the data remains.
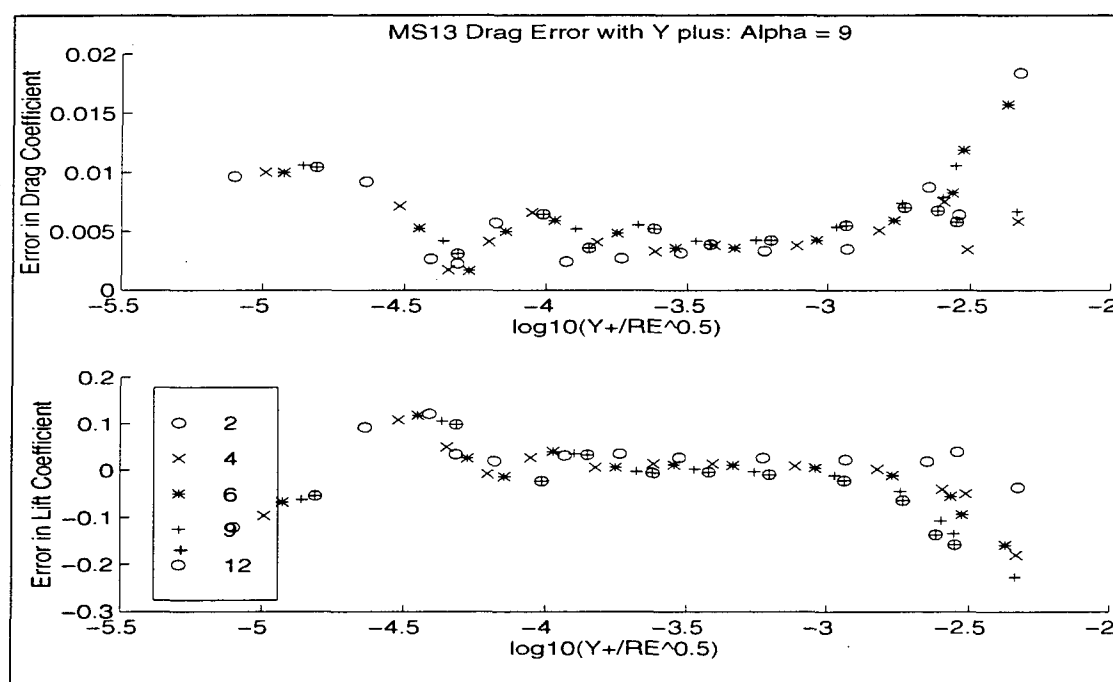
Fig. 4-17   MS13 Result on 299 x 62 Grid, $9°$ Angle of Attack

4.4.3 199 x 82 Grid

In contrast to the previous section, these results are reported from grids with increased resolution in the normal direction. As shown in the main body of research and from well known behavior of viscous Navier-Stokes behavior, the normal direction through the boundary layer should have a greater impact than increasing the grid in the circumferential direction. Although this direction has a more pronounced effect than the

other grid direction, it really does not change anything observable in the plots. The lift convergence is actually a little worse here, although the magnitude of the error is lower.
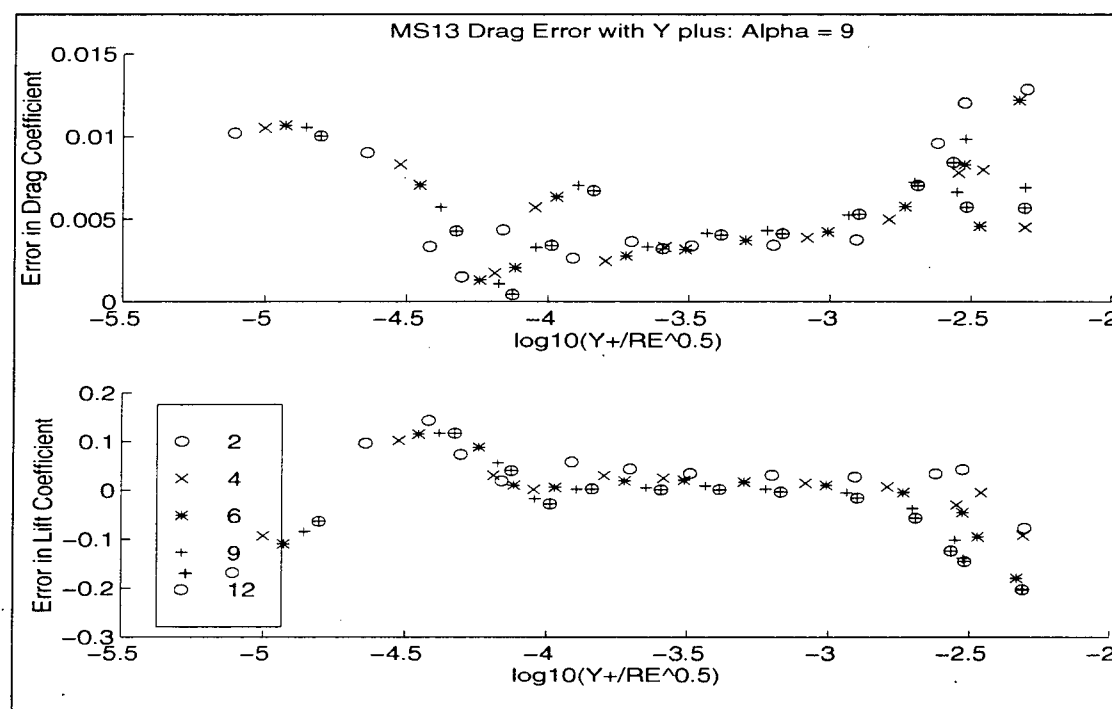
Fig. 4-18   MS13 199x82 Grid, SPT Model, 9° Angle of Attack

The data is very similar between the two different grid excursions (Fig. 4-17 and Fig. 4-18). The 199 x 82 grid has more scatter in drag near the mid range but is otherwise similar. The maximum errors are reduced somewhat on this grid but the trend data on the tight spacing end of the curve has not really improved. The original 199 x 62 grid appears sufficient for this effort.

4.4.4 Grid Stretching

If you happen to hit the "right" grid that the turbulence model really "likes" (best gradient resolution for a given problem or set of problems) you can greatly affect the performance but it may not be worth looking for the right grid. The next figure shows a plot of trend data on a grid that was stretched by 2 on each cell level. In other words, the wall

spacing remained the same and each level of grid cells above the surface was stretched by a constant factor from the original spacing. This can be done from within the grid generator or after the fact as was done here. Since the gradients are so important to the final solution it is no surprise that the figure shows vast changes over the previous cases. The error values are only slightly larger, but the trend consistency is better. There is no guarantee which grid will do this for a given problem although it seems that relaxing the gradients as opposed to tightening them performs better.
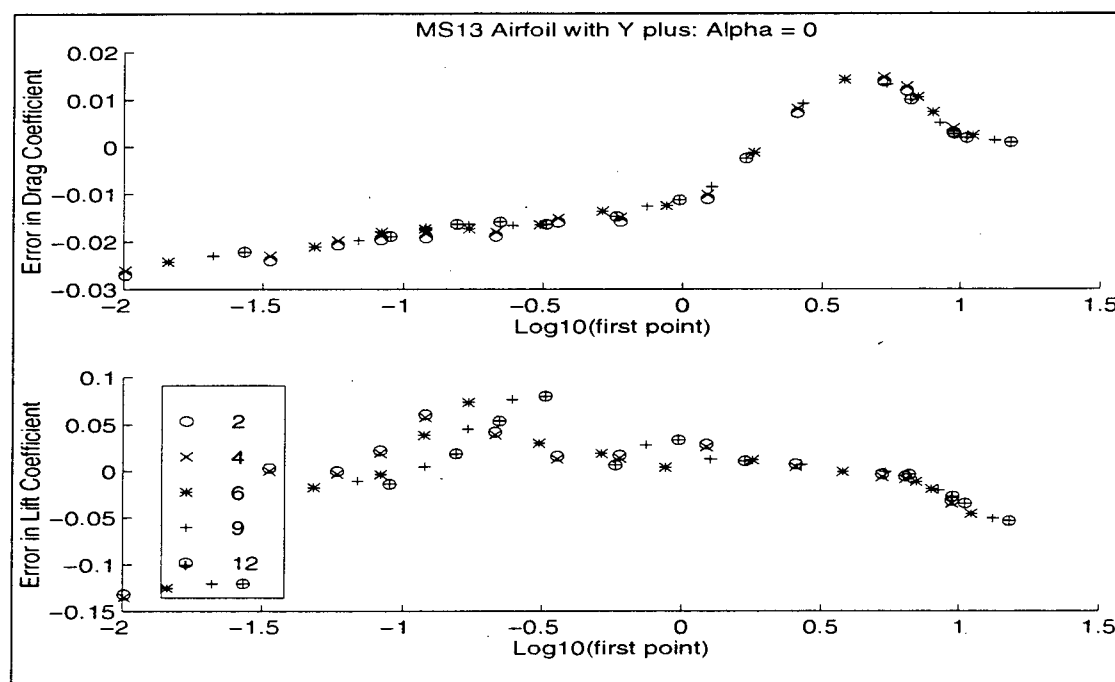
Fig. 4-19   MS13 Trend Data on a Stretched Normal Grid, $0°$, SPT Model

4.4.5 Across Angle of Attack

The main body of research has been concerned with the behavior of lift and drag with Reynolds number and the plots to illustrate this behavior concentrated on the behavior of this error with respect to Reynolds number and functions of y^+. It may also be of interest to investigate this behavior with respect to angle of attack. Fig. 4-20 shows the behavior of lift and drag errors versus y^+ but this time the different curves represent angle

of attack including 0°, 5°, 9°, 12° and 15°. Drag does not converge to any predictive trend curve but there is one lift value that all curves intersect. This can help predict lift values only but is an interesting effect in its on right. On the MS17 plot of Fig. 4-21 the point where all the values cross seems associated with the pressure dip effect that has been seen on all of the airfoils.
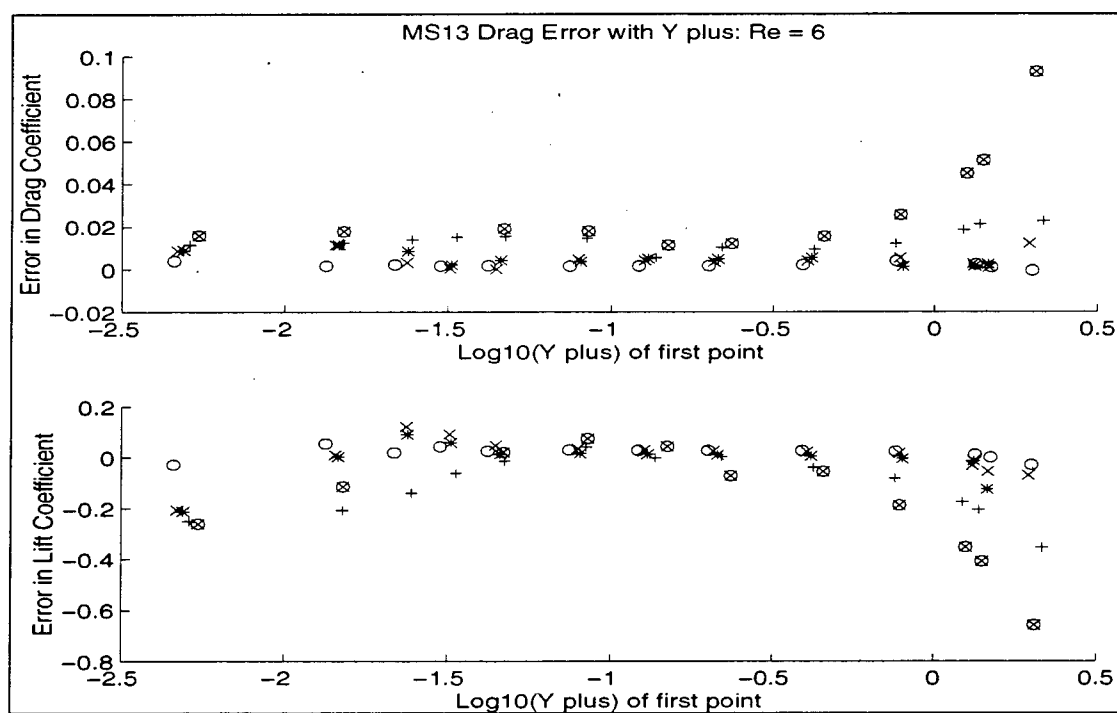
Fig. 4-20   MS13 Across Angles of attack at Reynolds number of 6 x 10^6
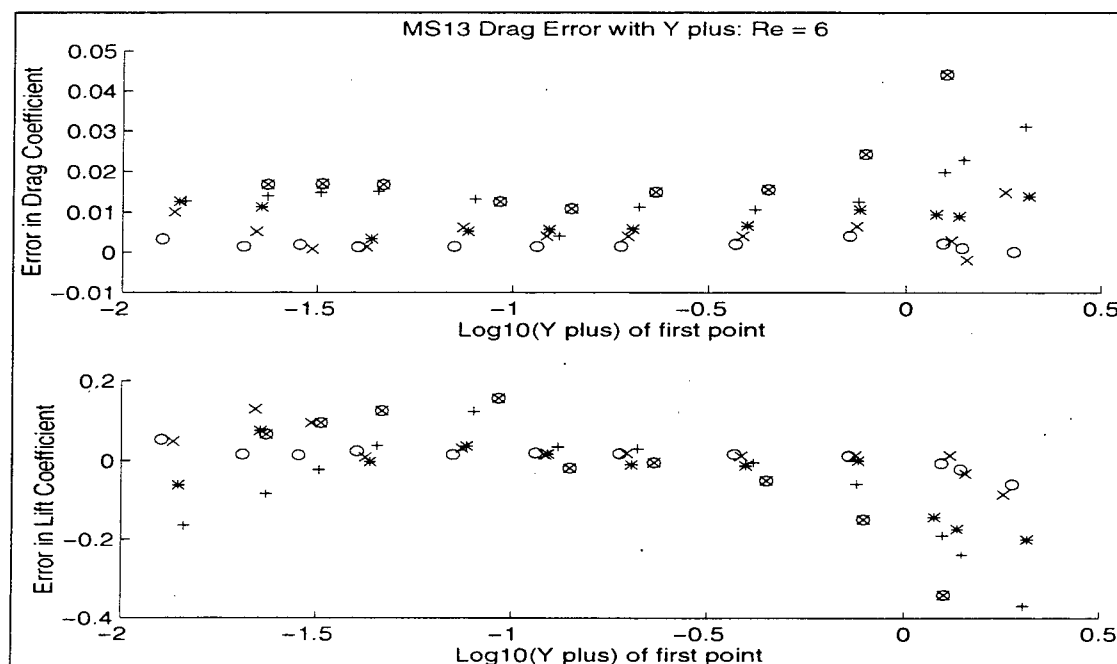
Fig. 4-21   MS17 Across Angles of attack at Reynolds number of 6 x 10^6

4.4.6 Three Dimensional Wing

If the behavior of lift and drag errors is consistent over Reynolds numbers on air-foils, might it also be consistent over 3-dimensional wings? This would be another excellent research topic although computational requirements would be challenging. Although this research is not equipped to evaluate the CFD performance of wings it can investigate the possible correlation of the CFD solution over an airfoil to the wind tunnel data from a 3-D test of the same airfoil. The University of Washington's Kirsten wind tunnel performed NACA0015 3-D wing tests at Reynolds numbers of 96, 148, and 193 x 10^4. This is not a large Reynolds number range and the trend information computed from this data may be incomplete; however, it still may be possible to relate the CFD solution over the 2-D 0015 to that of the 3-D wing and at least show initial performance. Shown here are two figures to illustrate. Notice the trend data is only good at the tighter spacings (not at all like the 2-D airfoil). Neither are best plotted vs. y^+ alone. This may be due to the pressure field being much different over the 3-D wind tunnel model at all angles of attack. The same y^+

scaling parameter still seems to work but the lift is better than the drag. The performance at mid-range angles of attack was not as consistent as the airfoils. An angle of attack of 1.0 degrees is very close to zero lift so it may be no surprise that lift is quite noisy at this angle of attack. The remainder of the data seems to show some consistent behavior however and further research may be warranted. If 3-D lift and drag could be accurately predicted from a 2-D source it would save time and resources.
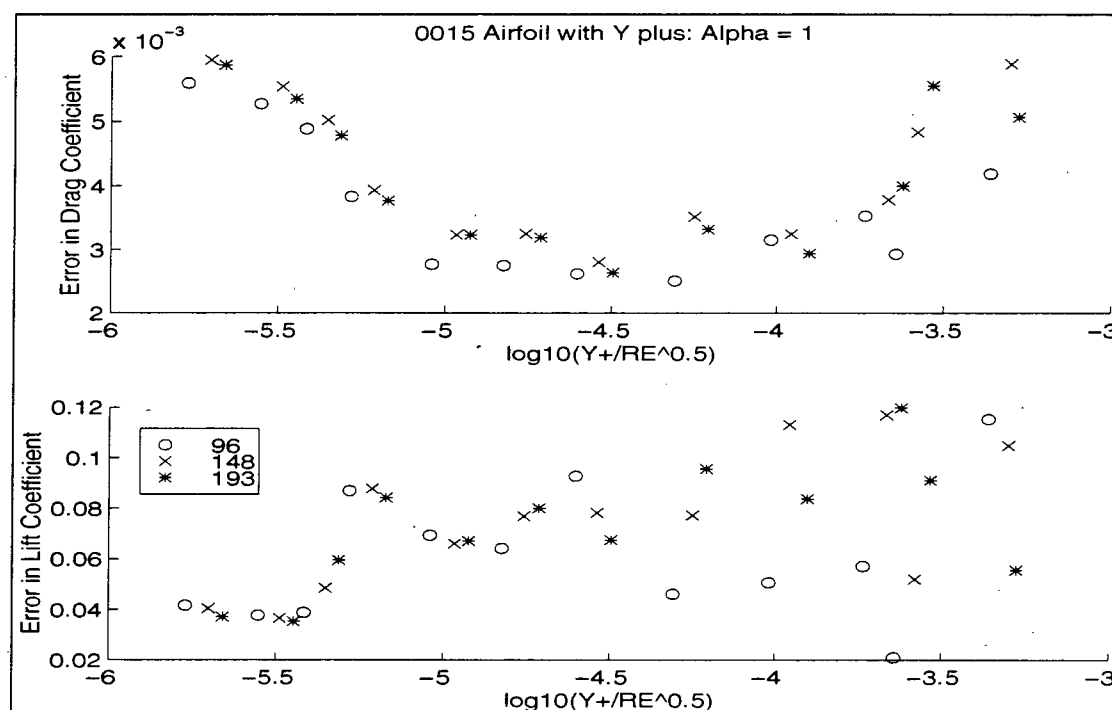
Fig. 4-22   Comparison of 2-D CFD to 3-D Wind Tunnel Tests, NACA0015, 1°
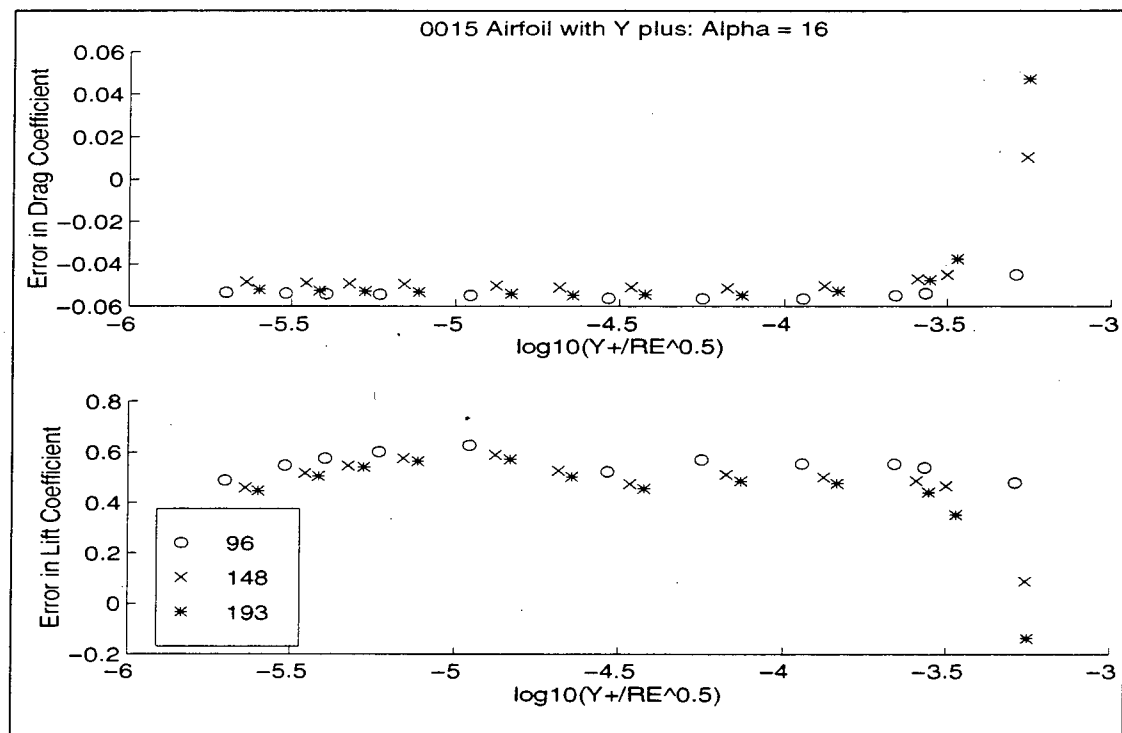
Fig. 4-23   Comparison of 2-D CFD to 3-D Wind Tunnel Tests, NACA0015, 16°

Chapter 5   Taguchi Techniques

5.1 Introduction[55,56]

This study involves a large number of experimental data points created at different Reynolds numbers, angles of attack and wall spacings using different turbulence models and airfoils. Looking at plots is certainly one way of seeing how the lift and drag (or any other parameter's) trend data are developed but they cannot always display the relative effect between the important factors which impact lift and drag calculations in order to improve lift and drag predictions in the future. To examine each effect against the others would require either an inordinate amount of figures and an accurate eye or would be simply impossible since the relative importance of some factors such as the relationship between the turbulence model and the angle of attack cannot readily be observed and characterized on a plot. In such a case a statistical picture is perhaps a better way to see the relationships between the factors of the CFD runs, which are actually just a series of numerical experiments. In these numerical experiments all independent factors are *external* to the solver itself since no code variables were changed other than the chosen turbulence model.

Such a statistical approach is provided by the methods of Taguchi. They are normally used to optimize quality on an industrial scale by determining the significant factors in experimentation and then changing those factors which will have the most effect on the outcome. One example might be testing a leaky water pump by varying the parameters that might cause it to leak. The goal would be to determine which one or two main factors cause the leak without too many experiments. The current study is somewhat different in that we are not trying to design hardware, yet it is still beneficial to determine the parameters that are most important to determining lift and drag as well as the level of their importance. Taguchi Techniques have been used only infrequently in the aerospace community with CFD to optimize hardware design results.[46,47] The current application is the first known attempt to use Taguchi Techniques to investigate the statistical performance of the CFD solver itself and its interactions.

Had the Taguchi Technique been a familiar CFD evaluation tool beforehand, it conceivably could have cut down the required number of computer runs while identifying those parameters which might be important in deriving trend information. As just one example, Rogers[33] reports on a series of 98 runs on high-lift airfoils. If a method such as the Taguchi Technique could cut this number down, it would be quite significant. Once these important factors are identified, more detailed testing could concentrate on those areas without as much wasted effort. This assumes that the engineers are knowledgeable enough to identify likely candidates as important factors in the experiment and constructs the experiments accordingly. If not, then the Taguchi Technique would show that few or none of the chosen factors are important to the result and the process would have to begin anew. In effect, the data taken as part of this research for Chapters 3 and 4 will become the basis to evaluate the performance of the Taguchi Technique as a method of testing CFD codes.

The method involves setting up an interaction table which determines which factors are measured against the others in a series of experiments. Taguchi has constructed several of these tables depending on the number of factors and how many levels the factor will take during the experiment. In this work for example, the turbulence model is a two level factor because it can be either the Spalart or Baldwin-Barth model. As the number of factors and their interactions increase, these tables can grow quite large and complex. For this study the main factors have been the angle of attack, the turbulence model, the airfoil, the Reynolds number, and the grid spacing. The Taguchi method also allows the computation of the effects of interactions between the factors. Depending on how the experimental factors are assigned to the columns of the interaction table, (called an Orthogonal Array in the Taguchi Technique) we can study not only the relative importance of the factors in each numerical experiment but, say, the importance of the interaction between Reynolds number and turbulence model. It will not indicate how they interact but it will show how important this interaction is to the final answer.

For example, using the five factors listed in the previous paragraph there are 2^5 (or 32) possible ways to arrange them in unique experiments if each only has two levels. The

smallest Orthogonal Array that will handle these relationships is composed of eight experiments using seven possible factors. In other words, the 32 experiments can be statistically analyzed using only eight experiments if the factors are distributed correctly. This array will work for up to seven possible factors which conceivably could replace 128 experiments (2^7) with only eight experiments. This Orthogonal Array is shown in the following table:

TABLE 5. Eight Experiment Orthogonal Array

Trial	A	B	C	D	E	F	G
1	1	1	1	1	1	1	1
2	1	1	1	2	2	2	2
3	1	2	2	1	1	2	2
4	1	2	2	2	2	1	1
5	2	1	2	1	2	1	2
6	2	1	2	2	1	2	1
7	2	2	1	1	2	2	1
8	2	2	1	2	1	1	2

"Trial" refers to the experiment number and the letters A, B, etc. are the factors that vary during the experiment. Since the current experiments do not have seven variable factors, two of the columns will contain interactions between two of the other factors. Which interactions are measured depends upon which columns contain the main factors. If the first two columns contained, or represented, turbulence model and Reynolds number, the third column might be assigned to no specific factor and then it would measure the statistical importance of the interaction between turbulence model and Reynolds number. It is important to note that if the third column *did* contain an experimental factor both its effect and the interaction of column A and B would be contained in column C. All of the columns contain the effect of interactions to some degree - this is the price paid for using so few experiments from the set of all possible ones. It is recommended that to the greatest

extent possible, factors only and not interactions be assigned to as many columns as possible. Later examples will help to illustrate this.

The results of a statistical study of this sort have never been done to evaluate the performance of a CFD code or CFD method by itself but has been used a few times to evaluate the design of air vehicles.[46,47] In a design study, the results of this statistical approach would indicate which factors are important to the particular design. In one transonic CFD study of flow distortion on the F-15 inlet fairing, it was discovered that the most important factor was actually an interaction effect between the length of a certain piece of the aircraft and its radius. This is difficult for engineers to design for but at least they know where to concentrate their efforts. It is also important to remember that Taguchi Methods do not provide "hard engineering" numbers - only the statistical significance of a particular experimental factor or set of factors as well as a guide to help design experiments. For this specific research, we hope to see which factors are most important in predicting the drag and lift trends so that future researchers might know better how to structure numerical experiments and improve codes. It may also be possible to use these techniques to systematically study the performance of the solver and/or the turbulence model itself. In this case the important factors might be items such as the overall scheme (implicit vs. explicit), artificial viscosity coefficient, matrix solver (decomposition, approximate factorization, etc.), and others as appropriate. There are many other possibilities.

Certainly some factors in this research and other possible projects may have more than two levels. Reynolds number has at least five values in this study and grid spacing has 13. However, the experimental complexity increases greatly with the number of different levels so it is recommended[55,56] that some engineering judgement be used both to reduce the number of possible important factors as much as possible and to use no more than two levels until the most important factors are highlighted, at which time more experiments can be run with a lower number of more important factors. But computer experiments (and industrial experiments too, it is supposed) are expensive and time consuming on problems of realistic complexity. In such cases it is best to choose only one factor that may vary with

more than two levels. This way, the number of required experiments can be kept to a minimum and if necessary the multi-level factor can be reassigned and a new set of experiments run. If the engineer selects only one factor out of seven to have 4 levels and the remainder to still have two, the total number of experiments would be $2^4 \times 2^6 = 2^{10} = 1024$ different possible experiments if the number of experimental factors remains seven (one varying four ways and six varying two ways). Fortunately, the statistically required number of experiments can remain at eight (eight out of 1024) if the number of experimental factors is lowered from seven to five - one that varies four ways and four that have only two levels.

In order to avoid having "mixed information" (information about interactions and main factors becoming mixed together) it is best to keep the resolution of the experiment high. In the Orthogonal Array of Table 5, if only three main factors can be used, the remaining information will be only interaction effects and the two will not mix. If there are more factors that are important to the experiment, the engineer must realize that the effects may be mixed and that additional experimentation may be required to sort out the magnitudes of the effects. As a first guess, it is usually assumed that any important effects are due first to the main factors if any and secondly to any interactions.

If engineering judgement says that the number of factors cannot be lowered and that at least one factor must have more than two levels the required statistical number of experiments may grow larger than eight (perhaps much larger) but will still be far lower than 1024, or whatever the maximum number of independent experiments would be. In this research, either the Reynolds number or grid spacing (but not both at the same time) will be allowed to take on four values in one Taguchi experiment. The remaining factors would remain the same (turbulence model, angle of attack, geometry, and either spacing or Reynolds number) with two levels. Or one column could be left open to study a possible interaction effect. The Orthogonal Array for this situation looks like Table 6, where again the letters represent the factors. Factor "A" would be spacing or Reynolds number in this study with the others arranged as required to study a possibly significant or interesting interaction. Later examples will illustrate this. In Table 6, only one factor in addition to the

four level factor is allowed for the highest resolution testing. The current work uses more factors than that so the four level tests will accept a lower resolution and possible mixed information.

TABLE 6. Four Level Factor Orthogonal Array

Trial	A	B	C	D	E
1	1	1	1	1	1
2	1	2	2	2	2
3	2	1	1	2	2
4	2	2	2	1	1
5	3	1	2	1	2
6	3	2	1	2	1
7	4	1	2	2	1
8	4	2	1	1	2

Tables 5 and 6 explain how to arrange the factors in each experiment to obtain a statistically significant sample of all possible experiments but they do not tell the engineer what to measure in the experiment. In the leaky water pump example, the answer is relatively straight-forward, it either leaks or it does not. The F-15 example required a determination of just what is flow distortion, how do you measure it, where do you measure it, and how much is "good", "bad", or "acceptable". To use a Taguchi Method to aid in evaluating a CFD code would require sound engineering judgement since so very many measurements can be made. What output does the engineer measure so that the conclusions drawn will really be what was intended? What do you measure to identify a lift or a drag trend? The user should be aware that the results gained will depend upon what is being used as the experimental "result". Incorrect conclusions could be drawn if the wrong results (what Taguchi calls "quality characteristics") are used. Note that this does not mean the answer is wrong but that a result not reflecting the experimental factors is being reported. In this

experiment the quality characteristic is the drag error or lift error. These were chosen to match the plotted data and not because they are the best statistical measure of any trend information. We may have chosen something completely different if the plots had not been seen first.

In this study, a lift and drag trend is sought. To do so, the important factors have been identified. If an important factor were left out, the statistical results, at least, would appear random with large variances. Likely quality characteristics for the application of the Taguchi Technique to the current experiments are drag error, lift error, or the variance of the drag and lift values. The choice of the quality characteristic is very important for a good experimental result.

The results of this form of a Taguchi experiment are the F factor and the percentage contribution (ρ). The F factor is a measure of how statistically significant a particular factor is to the overall experiment. It is a ratio of variances. The ρ value assigns more of a numerical weight to how important a particular factor is. F value says if a factor is important and ρ tells how much. The F value for each factor from the experiments are compared to existing tables which are generated for different levels of "confidence". For example, if the experimenter wants to be 95% sure that a particular value is statistically significant, its F value must be greater than or equal to the value that appears in the tables for the corresponding conditions of the experiment. The ρ value is a percentage of the total sum of squares.

Besides the Orthogonal Arrays and interactions between factors, one of Taguchi's most important contributions was the analysis of noise. If, for example, a particular experiment was conducted under differing environmental conditions that the experimenter had no control over and which may or may not affect the outcome of the experiment, these environmental factors would be examples of experimental noise. Perhaps the temperature of the gasket affects the results of the leaky pump experiment but the pump manufacturer has no control over how his pump is used so temperature would be an example of noise while the pump is operating. Taguchi showed that by correct application of experimental conditions, an engineer can discover those factors which are not only significant to the

outcome of the experiment but those which are relatively unaffected by noise parameters. By concentrating design efforts on these components, a better product is developed.

Computers and computer codes, given a set of input parameters, are unaffected by noise. The answer for drag should be the same to the 15th decimal place in double precision every time the experiment is run with the same set of parameters on the same solver. Thus, while Taguchi might recommend the pump experiment be run two or three times at different room temperatures to get a noise effect, the computer experiment could be run a hundred times and the answers should be the same. But if noise is defined as something the experimenter has little or no control over, then perhaps an effect of this type can be evaluated in this study. In Chapter 2 there was a discussion about grid variables and their affect on the outcome of a trend method. It was discovered that wall spacing would be one of the main factor to be analyzed. In Chapter 3 it was discovered that certain ranges of y^+ or $y^+/\sqrt{Re}$ can provide a problem-specific guideline to determine trends. If no other information is provided to the engineer, she would be free to select whatever grid density she wanted, for example. This effect was discussed briefly in Chapter 4 as an excursion but the grid size was not stipulated for the trend method. In this manner the grid size or grid density appears as noise to this experiment. The question then becomes "When changing the noise parameter (i.e. grid density [and perhaps others]) do the significant factors remain significant and does their contribution increase or decrease?"

In this manner we can perhaps discover factors which are important no matter what grid is selected. This might also be important, for example, if the product being analyzed were the turbulence model or the solver scheme. It would point out areas to concentrate efforts to improve the model in the presence of any grid (or noise variable). Or it might point out areas of important physics in the flow - an excellent application might be in the determination of turbulence models on wing cove effects in high lift airfoils[26]. This effect will be analyzed using both the rounded trailing edge grid and the tighter 199 x 82 grid as noise variables.

5.2 Taguchi Implementation

A code was written that assigns factors according to the Orthogonal Array and analyzes their contribution. The answer is in the form of a percentage effect (ρ) and F factor. If the percentage is high and/or the F factor is within a 90% confidence, one can be sure the effect is important, as long as the error (factors not included that should have been and random chance) is less than 50% or so. The first example will use the Orthogonal Array of Table 5 arranged as follows (each factor has two levels):

Factor A1: Spalart-Allmaras Turbulence Model

Factor A2: Baldwin-Barth Turbulence Model

Factor B1: Reynolds number (one selected from those available for an airfoil)

Factor B2: A Second Reynolds number

Factor C: Interaction effect between turbulence model and Reynolds number

Factor D1: Wall Spacing

Factor D2: A second wall spacing value

Factor E: Interaction effect between turbulence model and wall spacing

Factor F: Angle of Attack, (if selected) otherwise interaction effect between
Reynolds number and spacing.

Factor G: Airfoil, (if selected) otherwise interaction effect between turbulence
model, Reynolds number, and spacing.

Referring back to Table 5, imagine that the third experiment is being run and that airfoil and angle of attack are not going to vary. It is believed that these two factors (airfoil and angle of attack) have such a large effect on the CFD answer for drag that they would overpower other effects. Angle of attack and airfoil will not be selected as separate factors unless otherwise stated. Factors F and G will measure the interaction effects as delineated - above. The Orthogonal Array of Table 5 directs that this experiment be run with the SPT model (A1), the second of two chosen Reynolds number values (B2), and the first of two chosen wall spacing values (D1).

If a four level experiment were conducted using the Orthogonal Array of Table 6, running the third experiment requires (Table 6) the second of four chosen spacing levels, the first level of Factor B (which is turbulence model in the four level test), the first level of Factor C, and the second level of Factor D and E. In the four level experiment either wall spacing or Reynolds number is chosen as the factor with four levels (Factor A) and the other becomes Factor C. Factor D is the interaction effect between whatever the four level factor is and both the turbulence model and Reynolds number. Actually, both interactions are buried in the same factor (mixing effect) but it is assumed that only the interaction with at least one significant factor is the strongest interaction. Factor E is a confounding, or mixing, interaction between all factors.

The code loads the data files based on the entries of the Orthogonal Array. Once the data is loaded, the math leading to ρ or F value can be performed. The first step in the analysis is to construct a response table which is a comparison of the different average levels of the experimental result using different factors to get a first cut on which ones may be more important. If for some reason a computer run intended to produce one of the eight experimental runs failed (i.e. crashed or did not converge) there will be no entry for one of the experiments. The Orthogonal Array will lose its "orthogonality" in this case and either another computer run must be attempted to get the lost data or the engineer must accept possible statistical errors resulting from the missing data (after accounting for the missing data in the calculations). One example of a response table is shown in Table 7.

Table 7: Response Table

	A	B	C	D	E	F	G
Level 1	$\overline{A_1}$						
Level 2	$\overline{A_2}$						
Difference	$\|\overline{A}_1 - \overline{A}_2\|$						
Rank							

Each factor (at least those that are not interactions) has two levels. All of the experimental results in which Factor A is at level 1 are averaged and put in the first entry. All experimental results where Factor A is at level 2 are averaged and put in the second cell down. These two numbers are differenced and the absolute value of the difference is entered in the third cell down. After this procedure is accomplished for all main factors (A-G), including those for interactions, they can be rank ordered in importance from most to least. The most important is the one factor whose two means are the farthest apart. This will indicate which factors play a large role in changing the absolute value of the average experimental answer but not how much or whether that factor is statistically significant. It is possible to have a relatively large effect in the response table and still be statistically insignificant. This happens, for example, when most or all values have about the same effect and the math cannot guarantee which factors are significant to the experiment, which is shown by the F value.

At this point it is possible to compute a predicted optimum value of the quality characteristic. Using the three or four most important values in the response table it is possible to predict what the optimum experimental result would be, in theory at least, if each of the most important factors were combined in one experiment. The other factors would be immaterial because they do not change the experimental result very much. The formula for predicted optimum average is to add the most significant averages from the response table and subtract one less times the overall experimental average. For example, say that from the response table factors B2, D1, E2 and F2 were the most important. Recall that the current experiment measures drag *error*. This number should be as low as possible, what is termed a "Lower is Better Characteristic". In this case the three or four lowest average values from the response table would be chosen. Taking the four example responses, the predicted optimum result would be:

$$\mu_{predicted} = \overline{B_2} + \overline{D_1} + \overline{E_2} + \overline{F_2} - (3 \cdot \bar{y}) \tag{5.1}$$

where $\bar{y}$ is the overall experimental mean. If only three main factors had been chosen the coefficient of the mean would have been 2 and so on. In general, up to half of the main fac-

tors can now be allowed as "important" in order to account for experimental error. A confirmation experiment can be conducted using all of the most significant factors to determine if, indeed, the predicted value of the quality characteristic (drag error in this case) is reached (±5%) when the correct combinations of factors is chosen. If it is, no further analysis is required because the important factors have been identified and they combine linearly to change the experimental value. If they do not, some kind of interactive effect is acting within the experiment and further analysis is required to determine the most important factors and interactions. This is the situation usually found in CFD experiments because of the complexity of the interacting elements within the solver.

To continue with the Taguchi solution, several calculations are made leading toward the F value and ρ.

1. The total sum of squares: $ST = \sum y_i^2$ where "y" represents one experimental result.

2. The sum of squares due to the mean: $Sm = n \cdot \bar{y}^2$ where n is the number of experimental results and y-bar is the mean of all results.

3. The sum of squares due to each factor: $SA = (n_{A1} \times \overline{A1}^2) + (n_{A2} \times \overline{A2}^2) - Sm$

where this example is for factor A. The "n" values are counts of the number of experimental values where Factor A is at level 1 or level 2, respectively. This calculation is performed for all factors, whether they are interactions or main factors.

4. The sum of squares due to error: Se = ST - Sm - SA - SB -.... - SG. In the current experiments, this value will be zero because there is only one set of experimental results at each combination of factors unless noise is present. To overcome this, the least important factors are pooled into the error. Recall that error in the statistical sense refers to randomness or nonincluded factors. In this way, then, the low importance factors (as represented in the response table) become the randomness in the experiment.

5. Pooled error: $Se = S_1 + S_2 + ... + S_{(n/2)}$ where the S values are the sum of squares of the unimportant factors. The n/2 refers to the fact that it is desirable to pool about half of the factors present in the experiment, or more if there are only one or two highly prominent factors. If factors are selected as unimportant and it is found based on ρ and F that it should have been important, simply rerun the Taguchi Technique and do not pool that factor.

6. Degrees of freedom due to error, ve, is simply a count of the number of pooled items.

7. The error variance, $Ve = Se/ve$.

8. The modified sum of squares: $S_j' = S_j - Ve$. Each factor sum of squares (from step 4) will change due to the pooled error, which now accounts for part of the total sum of squares.

9. Now the F value and ρ (in %) can be calculated for each unpooled factor:

$F = Sq'/Se$

$\rho = Sq' * 100 /(ST - Sm)$

Note that ρ can also be calculated for the error (error has a sum of squares) and indicates the percentage of the total variance due to random or unincluded factors. This number should be less than 50%, or the remaining important factors are really not very important. The values for F must be compared with those from a standard table to see the confidence they represent. It is possible to have experiments where none of the factors are important enough to be statistically significant, which is defined as an F value of 90% or more. The figure below is an excerpt from a 90% confidence F table.[55] Across the top is the numerator degrees of freedom which is always one less than the number of levels of a particular factor. In the current experiments, this is always 1 or 3 depending on whether the factor in question is a 2 or 4 level factor. The vertical axis is the number of pooled factors and the resulting table value shows the number that the F-value result must meet or exceed for the experimenter to be 90% confident that the factor in question is significant.

	ν_1 = 1	2	3	4	5	6	7	8
1	39.9	49.5	53.6	55.8	57.2	58.2	58.9	59.4
2	8.53	9.00	9.16	9.24	9.29	9.33	9.35	9.37
3	5.54	5.46	5.39	5.34	5.31	5.28	5.27	5.25
4	4.54	4.32	4.19	4.11	4.05	4.01	3.98	3.95
5	4.06	3.78	3.62	3.52	3.45	3.40	3.37	3.34
6	3.78	3.46	3.29	3.18	3.11	3.05	3.01	2.98
7	3.59	3.26	3.07	2.96	2.88	2.83	2.78	2.75
8	3.46	3.11	2.92	2.81	2.73	2.67	2.62	2.59
9	3.36	3.01	2.81	2.69	2.61	2.55	2.51	2.47
10	3.28	2.92	2.73	2.61	2.52	2.46	2.41	2.38
11	3.23	2.86	2.66	2.54	2.45	2.39	2.34	2.30
12	3.18	2.81	2.61	2.48	2.39	2.33	2.28	2.24
13	3.14	2.76	2.56	2.43	2.35	2.28	2.23	2.20
14	3.10	2.73	2.52	2.39	2.31	2.24	2.19	2.15
15	3.07	2.70	2.49	2.36	2.27	2.21	2.16	2.12
16	3.05	2.67	2.46	2.33	2.24	2.18	2.13	2.09
17	3.03	2.64	2.44	2.31	2.22	2.15	2.10	2.06
18	3.01	2.62	2.42	2.29	2.20	2.13	2.08	2.04
19	2.99	2.61	2.40	2.27	2.18	2.11	2.06	2.02
20	2.97	2.59	2.38	2.25	2.16	2.09	2.04	2.00
22	2.95	2.56	2.35	2.22	2.13	2.06	2.01	1.97
24	2.93	2.54	2.33	2.19	2.10	2.04	1.98	1.94
26	2.91	2.52	2.31	2.17	2.08	2.01	1.96	1.92
28	2.89	2.50	2.29	2.16	2.06	2.00	1.94	1.90

Table heading: F_{10,ν_1,ν_2} 90% confidence† — Degrees of freedom for the numerator (ν_1); left axis: Degrees of freedom for the denominator (ν_2)

Fig. 5-1   F Table 90% Confidence

For example, say that 3 factors are pooled and that all remaining factors are two-level factors. This means that all F-values greater than or equal to 5.54 represent factors that are statistically significant with 90% confidence.

A test with noise requires slightly different analysis. Without noise, the matrix of results is 1x8 (one run at each of eight experiments using the 2-level Orthogonal Array). With noise, the matrix of results adds columns depending on how many noise parameters exists. In this report only one noise factor is tested at a time so the matrix of results gets no larger than 2x8. The response table, F values, and ρ are computed on these results without regard for noise. Once the important factors are determined, the Signal-to-Noise Ratio (Taguchi borrowed the term from controls theory) is calculated to determine those factors which remain important in the presence of noise. The factors which are significant in the first test will be those that can affect the *average value* of the quality characteristic. Those which are significant in the Signal-to-Noise test can affect the *variance* of the quality characteristic. For example if Reynolds number shows up as being important in the first test, we can assume it affects the average value of drag error for that test. If the turbulence

model is important in the Signal-to-Noise test we can assume it affects the variance, or spread, of drag error among that test group. Signal-to-Noise is calculated as follows for a lower-is-better quality characteristic:

$$S/N = -10\log\left(\frac{1}{r}\sum_{i=1}^{r}y_i^2\right) \qquad (5.2)$$

where r is the number of total runs per trial regardless of noise (r=2 in this research unless a data point is missing) and i is the index of entries in the results matrix. For these experiments, using a two column matrix of results, i will take on values of 1,2 for each factor. Once the Signal-to-Noise calculations are complete, an F test and ρ calculation are performed on them as before to determine the relative importance of factors.

5.3 Taguchi Experimental Results

Many experiments have been performed for this research and only a small subset will be analyzed with the Taguchi Technique. The resulting data should indicate how this technique could be another way of evaluating and improving CFD experiments and CFD code and algorithm development.

To test the implementation of the Taguchi Technique on the current data requires at minimum a 2-level test, a 4-level test, and a test with noise. The 2-level test will be used not only to test the Taguchi Technique in the CFD environment but also to determine which factor to select as the 4-level factor in the 4-level test. The noise tests will be performed on both the 2- and 4-level tests to determine which factors remain dominant under the influences of external factors.The following table shows the matrix of tests to be run:

Table 8: Taguchi Technique Test Matrix

2-Level	4-Level	Noise (2-level only)
MS13 0° Drag	MS13 9° Lift	MS13 0° Drag
MS13 9° Drag	MS13 9° Drag	MS13 0° Lift
MS17 0° Drag	MS17 0° Lift	MS17 9° Lift
MS17 9° Drag	MS17 0° Drag	MS17 0° Drag
MS13 0° Lift		
MS17 0° Lift		

This gives reasonable coverage of some of the possible cases and should allow conclusions about the performance of the Taguchi Technique. In each test from Table 8, the data is taken using the following table which divides the Reynolds number and wall spacing into discrete regions. Low Reynolds numbers are 2 and 4 x 10^6, medium is 4 and 6 x 10^6, and high is 9 and 12 x 10^6. Similarly the 2nd and 4th wall spacing values are low spacing, 6 and 8 are medium spacing and 10 and 12 are high spacing. These become the two-level values for each Taguchi test. Others certainly could equally have been chosen, but this allows a delineation between a L/L (low Reynolds number/low wall spacing) and M/H (medium/high) for example. Each test in Table 8 above consists of the nine subtests in Table 9. The effects of each subtest can then be presented in total.

Table 9: Taguchi Subtest Matrix

0 AoA		RE	lo	2,4	SP	lo	2,4
MS13			med	4,6		med	6,7
2 level			hi	9,12		hi	10,12
TYPE	T	RE	T x RE	SP	T x SP	RE x SP	TxRExSP
L/L							
L/M							
L/H							
M/L							
M/M							
M/H							
H/L							
H/M							
H/H							

The next figure shows an example of the type of data provided by the first 2-level Taguchi test of Table 8.
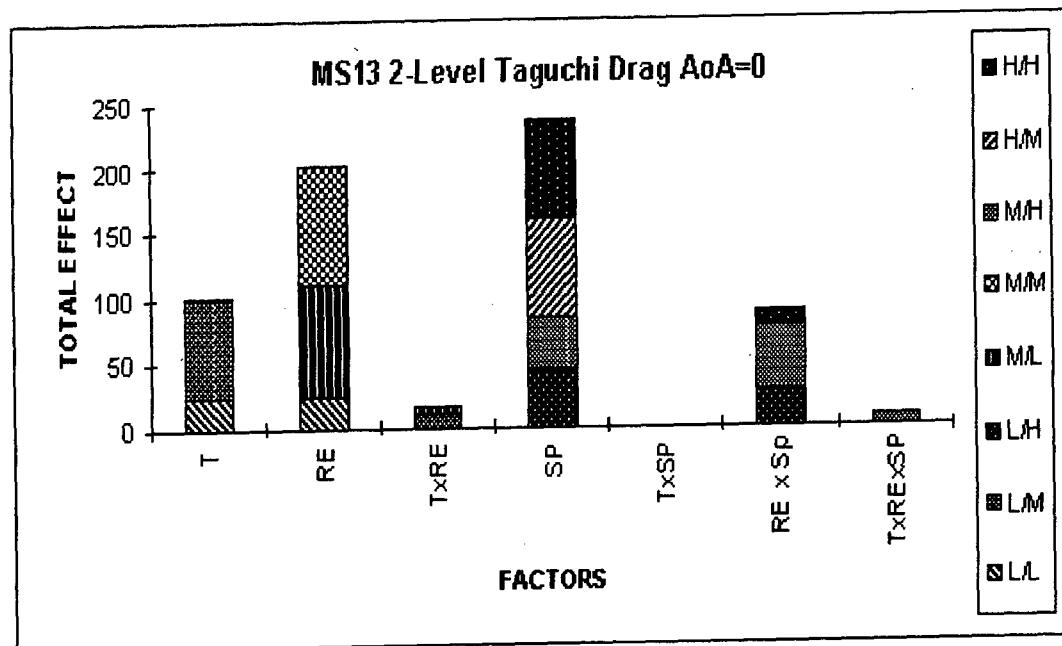
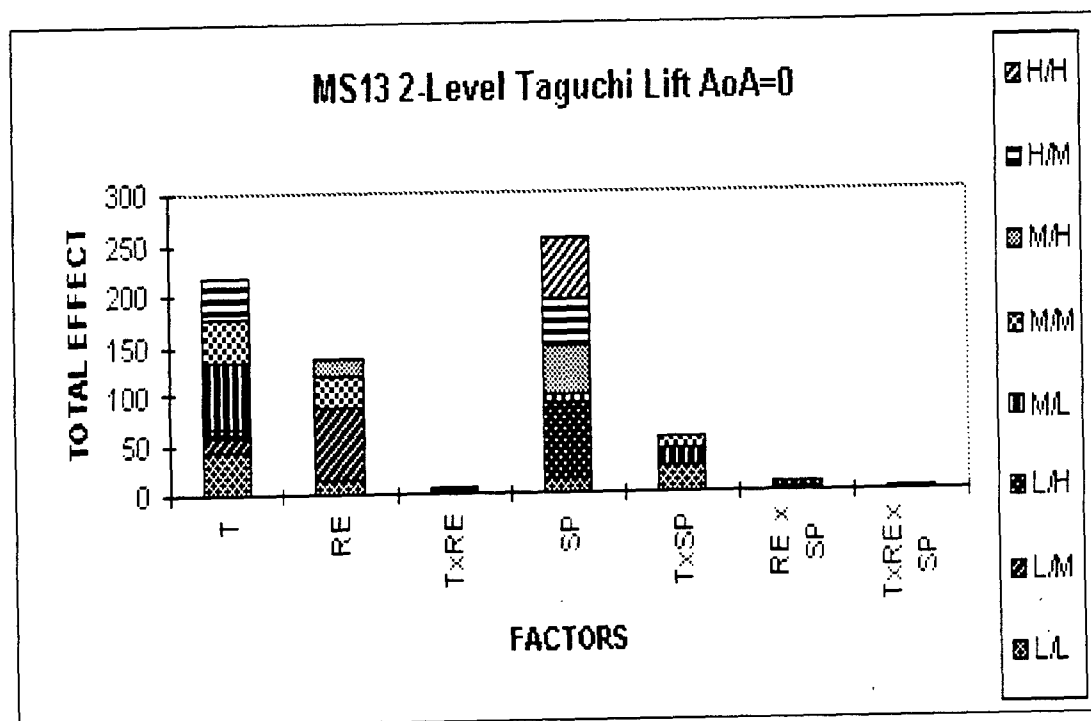Fig. 5-2   Taguchi Test, MS13 0° Angle of Attack, 2-Level Drag Error

Fig. 5-3   Taguchi Test, MS13 0° Angle of Attack, 2-Level Lift Error

Fig. 5-2 and Fig. 5-3 plot the sum total of the ρ values for the 9 subtests in the MS13 0° drag error and lift error tests. Only factors with F values signalling 90% confidence or greater have been retained. This statistical test shows very clearly the importance of wall spacing to the average values of lift and drag error. It was known that wall spacing was an important grid parameter but these plots show that it is the most important factor of all for this airfoil at this angle of attack - more than twice as important as the turbulence model over the entire regime of subtests. It is also very interesting to see that the average lift error depends more upon the turbulence model than the average drag error. In fact not only does turbulence matter more for lift error but it is only third most important for drag error. This reinforces some of the data of Chapters 3 and 4 which showed a high pressure effect in the turbulence model data.

There seems to be less interaction effects in lift than drag. A developer trying to improve his drag result should be aware that changing drag by changing spacing or Reynolds number will have to deal with some interaction between the two also affecting the drag error value. To avoid this, we notice that in Figure 5-2, the RExSp interaction is only important in the H/H, M/H, and L/H results. This indicates that wide wall spacing allows this interaction to occur and the developer might be wise to keep spacings tight. On the other hand, the high spacings are where we found good trend consistency. Possibly the RExSP interaction has something to do with finding these consistencies here. This could not have been seen on the plot. Neither the lift or drag error is affected by much of anything in the H/L test, which is why it does not appear in either legend.

The lift has major contributions from more of the subtest regions - in the turbulence model factor for example, drag error is affected in only two regions, the L/M and L/L, which indicates that the turbulence model isnyt important in most drag calculations for these two turbulence models on this geometry. The lift error, on the other hand, is affected by turbulence model in the H/M, M/M, ML, L/M, and L/L subtests. To avoid the lift error being affected by the turbulence model we should stick to the high spacing regions, much as we found in the plots of Chapter 3. The Taguchi Technique would have indicated where to look before running many tests on the computer.
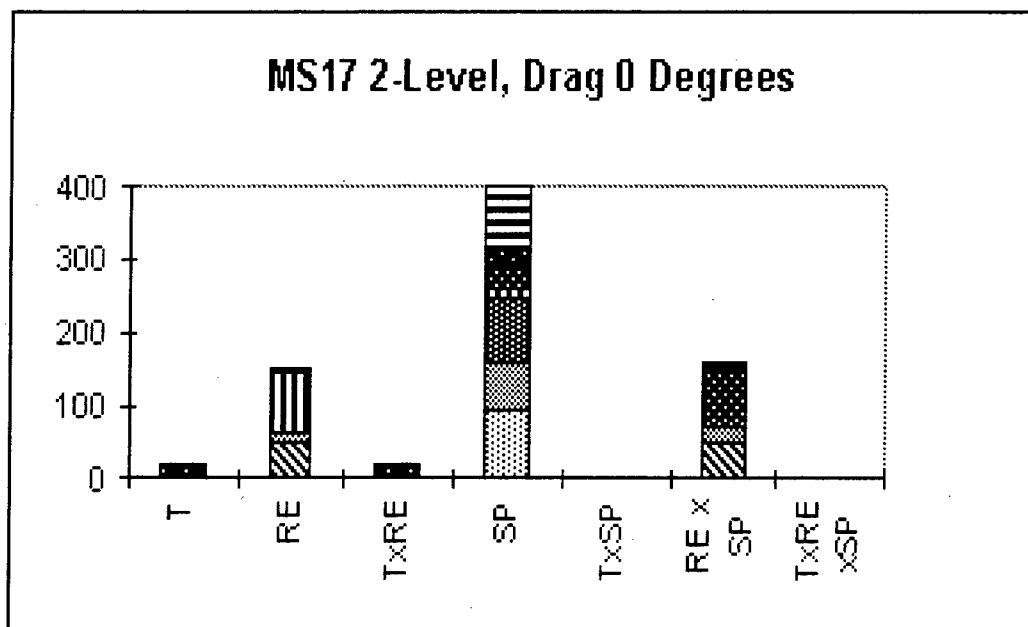
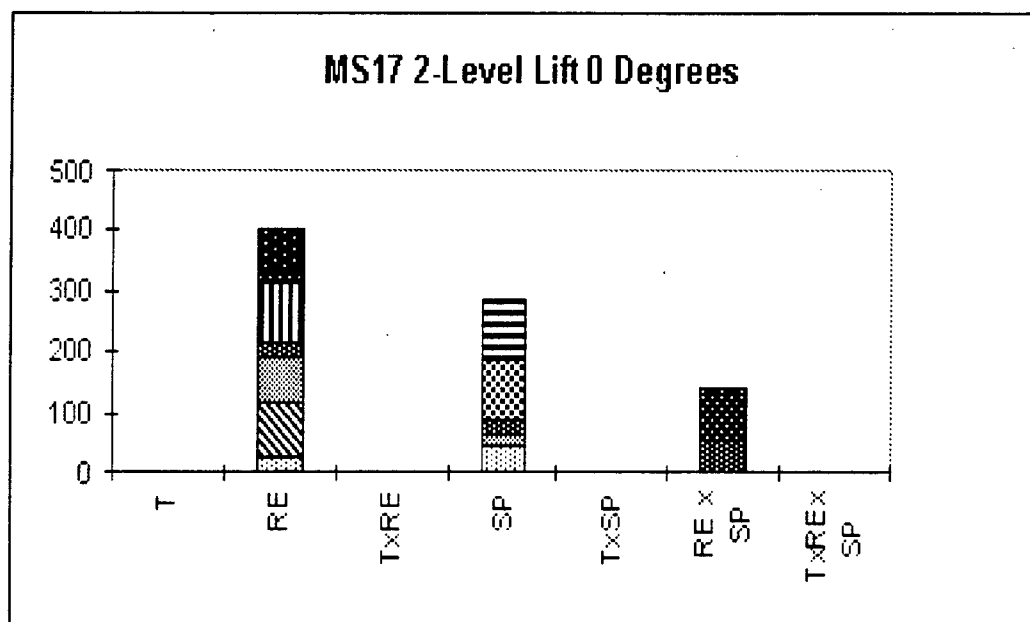Fig. 5-4   MS17 Drag Error 0° Angle of Attack 2-Level Test

Fig. 5-5   MS17 Lift Error 0° Angle of Attack 2-Level Test

Fig. 5-4 and Fig. 5-5 show the same tests as the previous two figures except they were run on the MS17 airfoil. The results are quite different on this slightly thicker airfoil. The legends have been removed to increase readability. The subtest results are still available if the legend is included but the general conclusions can be made without knowing exactly which Reynolds number and wall spacing ranges caused what effects. This type of information would be required to judge which Reynolds numbers are most affected by wall spacing, for example, as was apparent from the discussion of Fig. 5-2 and Fig. 5-3.

Most surprising is that on the thicker airfoil the turbulence model has little or no statistical significance. This conclusion would not have been evident from plots. This does not mean that the turbulence model is immaterial on the MS17 but what it does mean is that the *difference* in turbulence models is insignificant on the MS17. Whether this would be true for other turbulence models would require further computer runs. The Reynolds number is more or less the same in all tests so far except the MS17 lift error, where it more than doubles over the previous tests. Since the body of the work was involved with finding consistencies across the Reynolds number range, this information might indicate that the lift error on the MS17 might be more difficult to predict. This would be a time when the developer might need information keyed to specific Reynolds numbers and spacings so runs could be concentrated in areas that are relatively insensitive to Reynolds number. The MS17 has stronger interaction effects than the MS13. From a practical standpoint this means that a simple change made in Reynolds number or wall spacings could have very different effects on the lift and drag error values because the RE x SP interaction is almost as significant as the Reynolds number itself. Finally, although the wall spacing is still the most significant parameter on the MS17 airfoil, its total effect has doubled over the MS13. No doubt at least some of these effects are due to the thicker geometry and the change in the camber from the MS13 to the MS17. The Taguchi Technique allows the developer to put a relative effect on the experimental factors which are not readily available from a plot or a printout of numbers from the computer runs.

The next series of figures will illustrate the effect of considering noise in the calculations. Recall that in this work noise can come from the choice of grid type after the wall

spacing is set. Many more examples of noise are possible, such as grid density or the distance to the outer boundary.

MS13 Round Noise, Average Drag, 0 Degrees

Fig. 5-6   MS13 Drag Error, 0° Angle of Attack, Round Noise, Average Effect

MS13 Round Noise, Variance Drag, 0 Degrees

Fig. 5-7   MS13 Drag Error, 0° Angle of Attack, Round Noise, Variance Effect
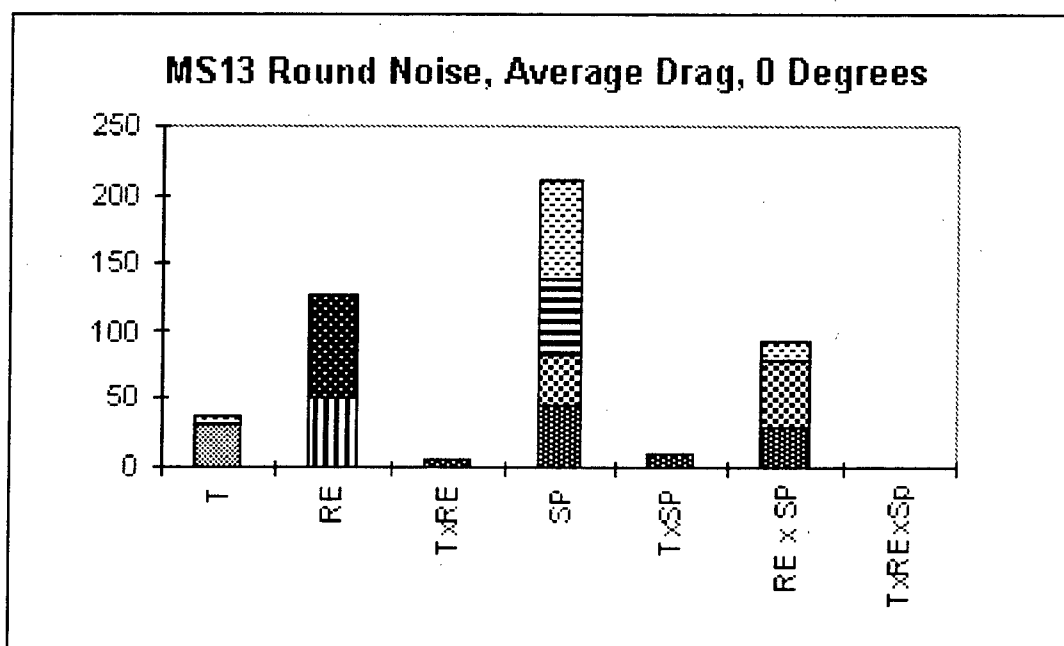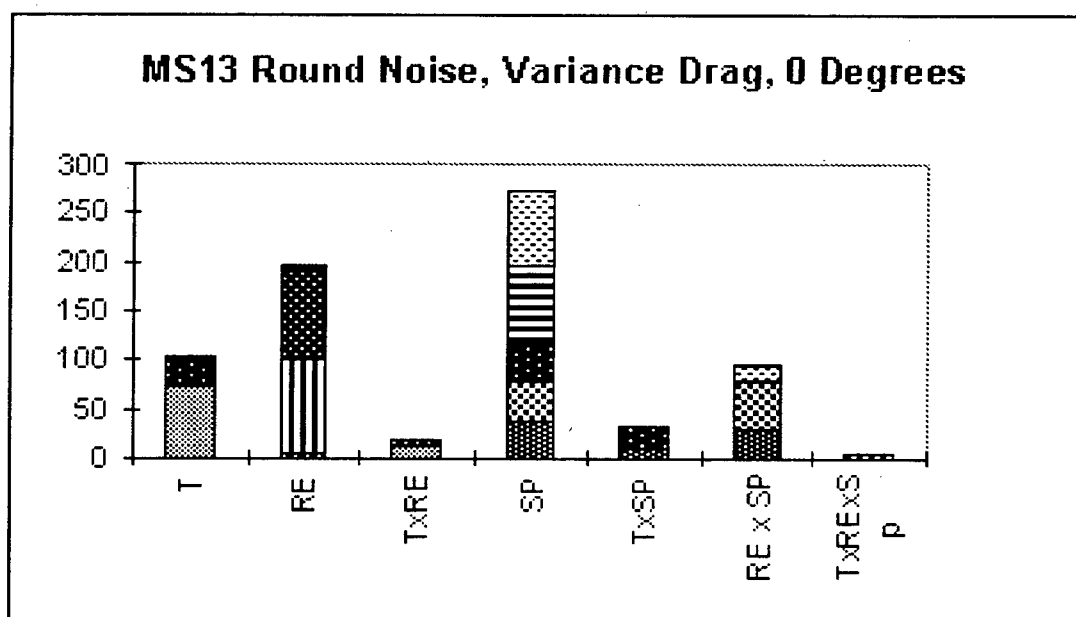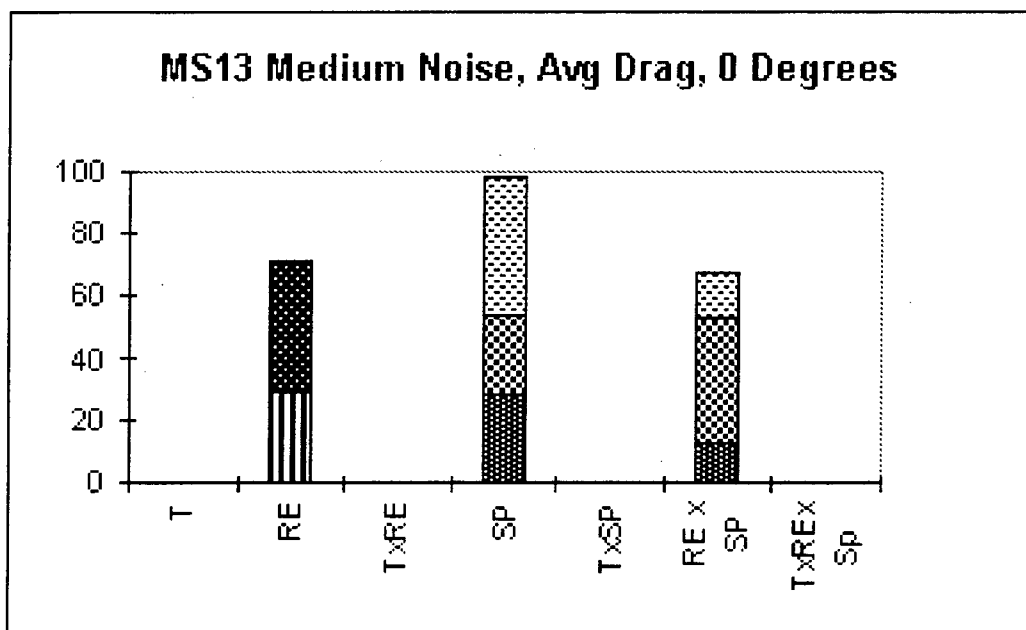
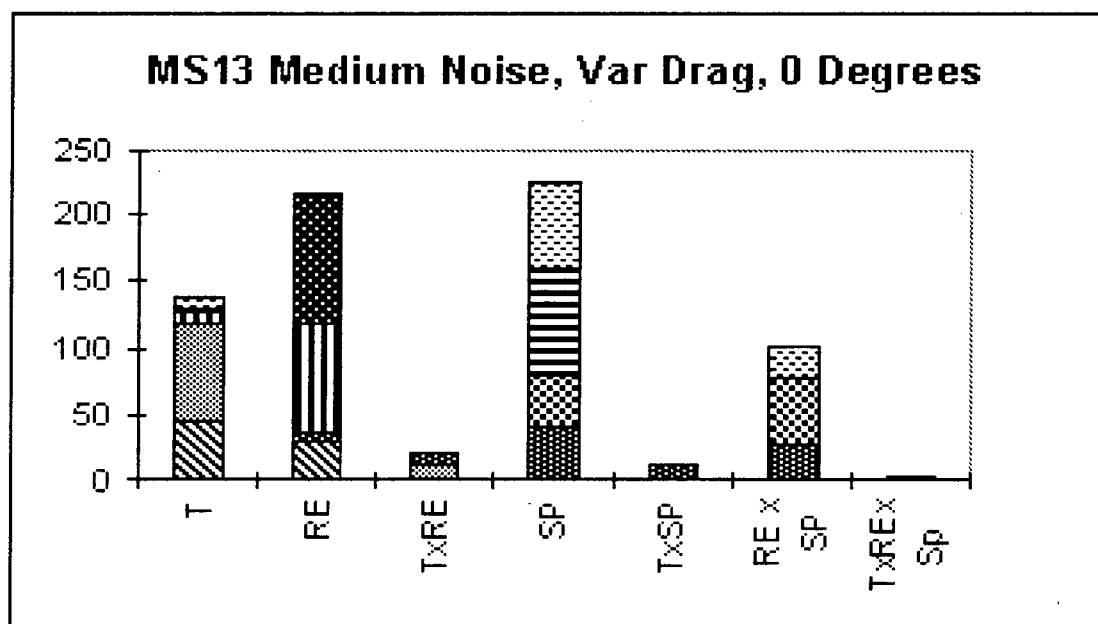Fig. 5-8   MS13 Drag Error, 0° Angle of Attack, Medium Noise, Average Effect

Fig. 5-9   MS13 Drag Error, 0° Angle of Attack, Medium Noise, Variance Effect

Fig. 5-6 and Fig. 5-7 show the result of a test using the MS13 airfoil with both the normal blunt trailing edge and the rounded one as the noise parameter. Fig. 5-6 shows those factors that are significant in changing the *average value* of the drag error. Fig. 5-7 shows those factors which are important in changing the drag error *variance*, or the spread of drag error around the average. This type of information would not be available from the plots and would be beneficial for analyzing the different components of the turbulence model, say, on different grids or different airfoils or some other parameter that can act as noise. Both Fig. 5-6 and Fig. 5-7 look pretty much the same as Fig. 5-2, which was the $0°$ angle of attack test on the same airfoil without the noise. What this tells us is that the round trailing edge airfoil really has no appreciable effect on the calculation and spread of drag error values. An area that gives good results on the normal grid should also give good results on the round grid. Note that we are measuring drag error as the quality characteristic. The noise test doesnyt tell us if the drag error will be better on one grid or another, just which factors to concentrate on if we want to change the average value or variance of the drag errors.

Fig. 5-8 and Fig. 5-9 are the results of a similar noise test using the 199 x 82 grid (what is termed the medium grid, hence medium noise). The first figure shows that the turbulence model has little or no effect on the average value of the drag error when using this grid. In other words, if you use a round trailing edge it matters which turbulence model is used but if the medium grid is used either turbulence model should work the same. There is also a large effect from the interaction between Reynolds number and wall spacing with this grid making it perhaps difficult to predict what changes in Reynolds number or wall spacing would do to the final value of drag error. Fig. 5-9 shows that the selection of either grid doesnyt much matter in the spread of drag error values because this plot is very similar to Fig. 5-7, although the effect of spacing isnyt quite as great on the medium grid, which is a bit of a surprising result considering that the medium grid put more points in the boundary layer. Regardless of this, spacing is the most important factor very consistently across both types of grids in both the calculation of variance and average drag error. The same calculation can of course be applied to lift error (or some other parameter) and other noise parameters.
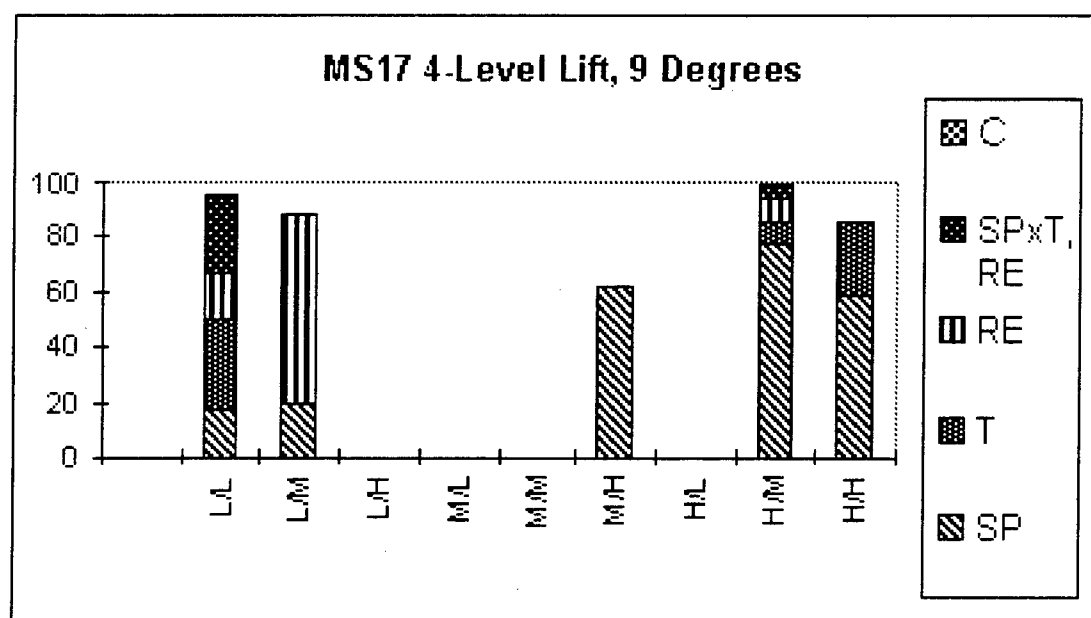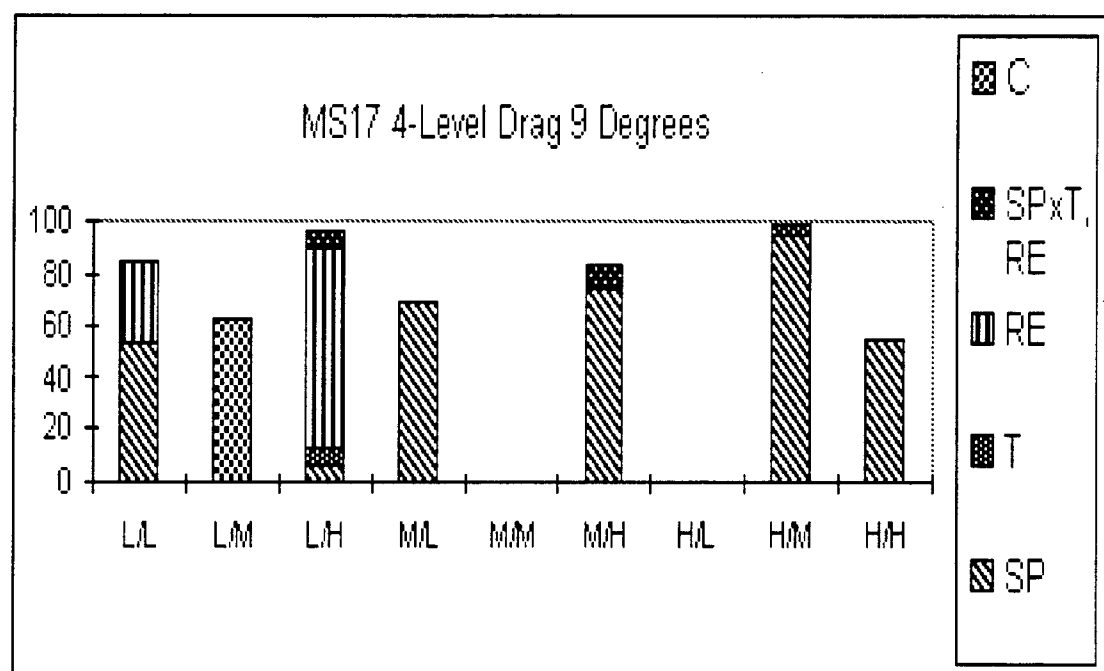
Fig. 5-10   4-Level Test, MS17 9° Lift Error

Fig. 5-11   4-Level Test, MS17 9° Drag Error

Having determined that spacing is the most significant factor in calculating drag error and lift error, a 4-level test can be conducted where the low spacing division is now spacing values 2, 3, 4, and 5, (which corresponds to wall spacings of 3×10^{-7} to 1×10^{-6}) medium spacing is now values 6, 7, 8, and 9, (grid spacings of 2×10^{-6} to 2×10^{-5}) and the high spacing is composed of grid values 10, 11, 12, and 13 (grid spacings of 4×10^{-5} to the highest spacing of 1×10^{-4}). Spacing value 1 usually halted during the CFD run, perhaps because of the extremely high grid aspect ratio so it is not used as a spacing factor. The low, medium, and high Reynolds number ranges stay the same as in Fig. 5-2 and Fig. 5-3. Again separate tests are performed at different combinations of Reynolds number and spacing but now the result includes better definition of spacing since four values are in each group. Fig. 5-10 and Fig. 5-11 show a different example of expressing the results, keeping the factors as the plotted variable instead of the subtest. The factor "C" represents the confounding, or mixing, of all the other factors. This happens in a low resolution 4-level experiment with more than two main factors. Any Reynolds number/wall spacing region that has a high value of the factor "C" would have large interactive effects.

From these plots it is clear that most of the significant factors are concentrated on either end of the curve, which is what was observed in the discussion of Chapters 3 and 4. Also, the Reynolds number is not a factor at the high Reynolds number end of the data, again agreeing with prior conclusions. This information cannot tell us that the spacing (or y^+) must be scaled with a power of the Reynolds number (see Chapter 3) to be consistent, but it gives us a clue about the regimes to concentrate in by pointing out regions that donyt involve Reynolds number. Lift seems dominated by the main factors alone while drag has more interactive effects. This is probably due to the viscous terms which depend more upon the action of Reynolds number, wall spacing, and turbulence model. It is interesting that the statistical tests can highlight this effect and help explain CFD's difficulty in calculating drag.

This type of data parsing may be very valuable in many areas of code development and validation and experimentation - if nothing else than to cut down on the required number of computer runs. It agrees well with the original plots which hints that the methods

are valid and correct. The Taguchi Technique may be an excellent way to analyze and evaluate not only the results of these tests but many types of CFD results as well.

Chapter 6   High Lift Multi-Element Airfoils

6.1 Introduction

In addition to being difficult problems for CFD codes to compute, high lift airfoils have not been tested much over a wide Reynolds number range. This is slowly beginning to change as researchers attempt to increase the applicability of their algorithms, but for this study it was very difficult to find acceptable wind tunnel tests of two-dimensional flapped and slatted airfoils. Some tests do not report the drag data at all, even if there was an adequate spread of Reynolds number. Fig. 6-1 illustrates a common high lift configuration and one that will be discussed here. Fig. 6-2 and Fig. 6-3 are two further examples of the grids that can be created as a result of this work.
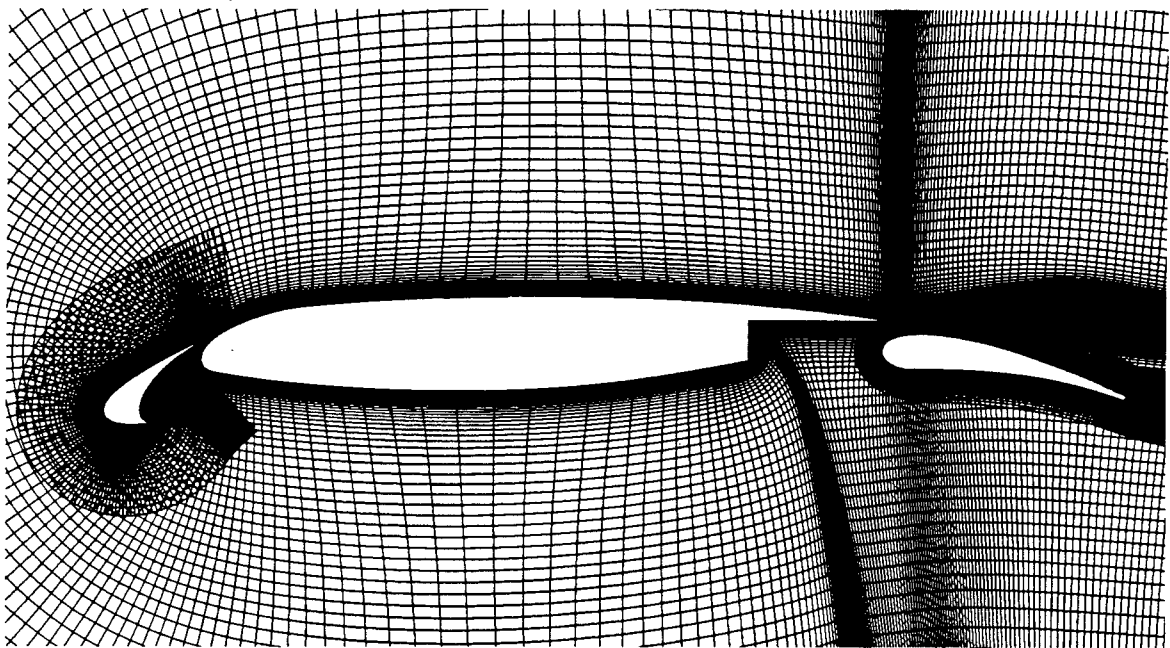
Fig. 6-1   High Lift Airfoil Section Using Chimera Gridding

This configuration is set for take-off with the flap at $10°$ and the slat at $20°$. Chimera gridding is used by overlaying the grids for the slat and the flap over holes cut in the

main wing grid by NASA's PEGSUS[57] software. As part of this research, a method was adapted from Rogers at NASA Ames to create a UNIX Script file that creates the entire grid from a single input file using the HYPGEN[58] grid generator to create the three different grids. To keep commonality between the plain airfoil results and the high lift results, the grid and solver inputs will stay the same for all runs unless stated specifically. The grid density, once calculated to create satisfactory grids, will also stay the same. The slat grid has a density of 181 x 61, the main grid is 397 x 161, and the flap is also 181 x 61. The overlaying points are interpolated between grids points since none of grid points on one grid lays precisely over the grid point on the neighboring grid. In order to insure adequate coverage, some grid parameters around the slat or flap such as the outer boundary distance must be changed slightly.
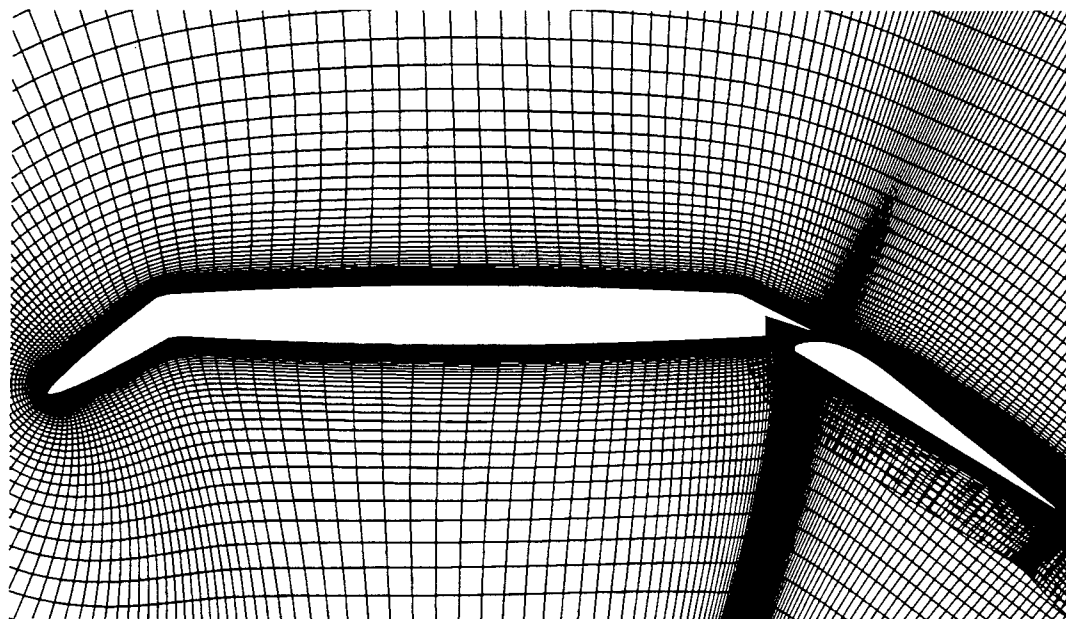
Fig. 6-2   McDonnell Douglas F-18 Airfoil with Drooped Nose and 40° Flap
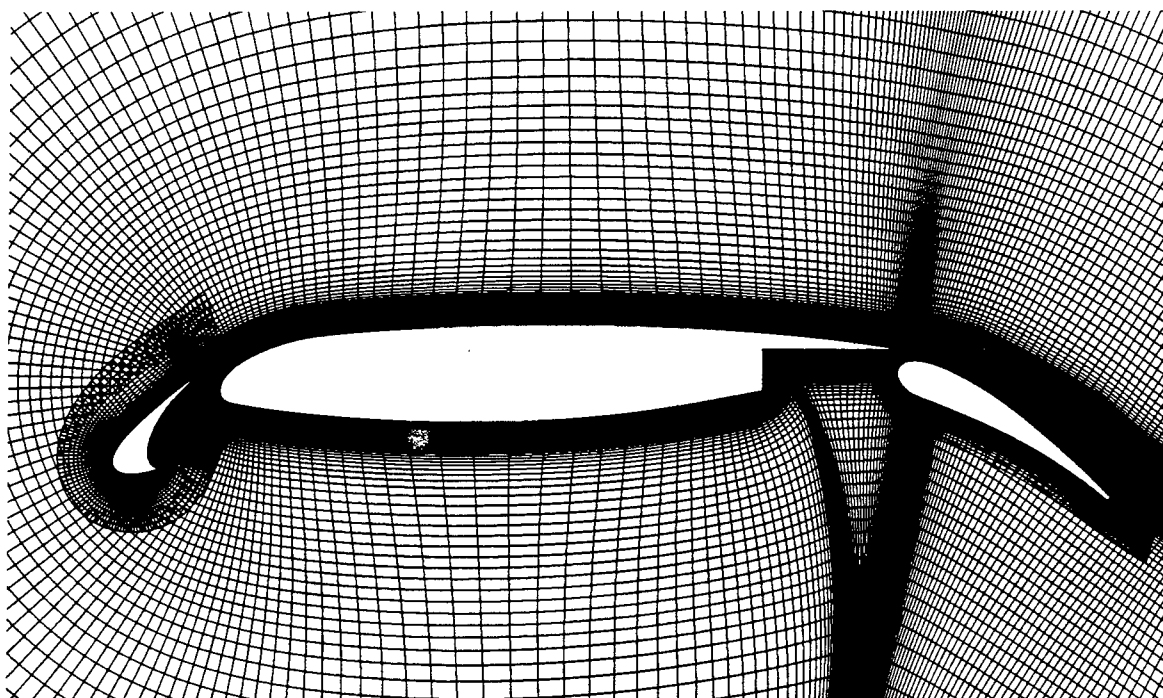
Fig. 6-3   Configuration of Figure 6-1 with 30° Slat and Flap

To the maximum extent possible, no grid parameters except wall spacing are changed. The wall spacing is specified by the user as before and stays the same on all surfaces. The value of y^+ is calculated for each of the three surfaces as well as an average of the three. Before the grid is generated, a preprocessor was created to place the surface coordinates of the three airfoil parts at the correct location and orientations. For example, in Fig. 6-1, the given surface input information includes the surface coordinates at $0°$ orientation for each of the three surfaces. The preprocessor turns the flap and slat surfaces to the correct angles and sets the gap between the bodies and the overhang of the leading and trailing edges before it is submitted to the grid generator.

Neither of these two turbulence models (Baldwin-Lomax has been dropped) is specifically cast for a problem of this type. Studies have been done on high lift airfoils with different turbulence models, including the two turbulence models used in this study[39]. They perform reasonably well overall, although as mentioned previously, neither model is

superior over all points of this extremely complex flow problem. The challenge here will be to see if the consistency of solution is obtained over different angles of attack, Reynolds numbers, and airfoils as it was with the single element airfoil. Computer run time is also much more of an issue on these high lift cases. Six grids were created with wall spacings from 10^{-7} to 10^{-4} instead of thirteen on the simple airfoil. A run involving all six grids at one angle of attack and four Reynolds numbers (24 runs at 200 iterations per run) used an average of approximately 20,000 CPU seconds on the Silicon Graphics Power Challenge Array at the National Center for Supercomputing Applications at the University of Illinois - Urbana Champaign. Again, should this method prove promising, some amount of value must be placed on the high Reynolds number trend data so the engineer and his company can determine if it is worthwhile to take the computer time required to generate the trend data. Use of a method such as the Taguchi Technique would be particularly welcome here if it could reduce the number of required computer runs.

No changes were made in the solver/turbulence model input parameters except for the boundary conditions for the new grid, the flow variables and the angle of attack. These results are purely incompressible as before; no Mach effects are considered or predicted. No presumption is made about the applicability of the simple airfoil method; the same procedures are used and the same data is collected. No attempt was made to try to calculate coefficient or trend data for the slat, flap and main airfoil separately, although this is possible if required. Most experimenters who report overall lift and drag coefficients do so also for the components separately. For some phases of flight, such as a stalled slat when the wing and flap are still flying, may need high Reynolds number data for the components separately. Fig. 6-4 shows the lift and drag plots for this high lift airfoil at $14°$ angle of attack run at Reynolds numbers of 5, 9, 16 and 20 x 10^6.
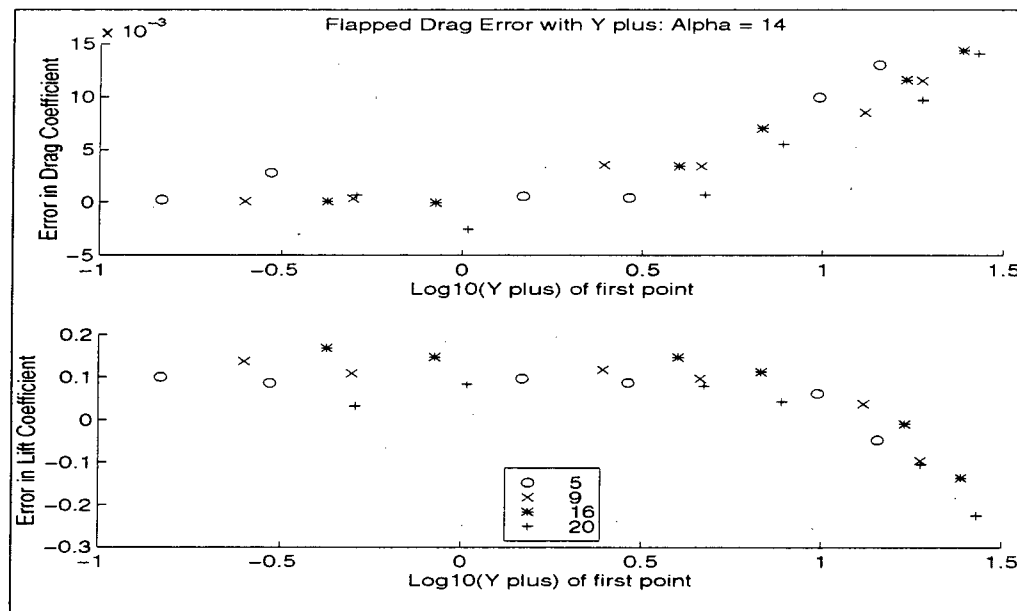
Fig. 6-4   High Lift 20slat/10flap Configuration 14° Angle of Attack, BBT Model

Fig. 6-4 was made with the Baldwin-Barth turbulence model and was plotted against the average y^+ of the three airfoil sections. Several items are noteworthy on this plot. First of all similar trends are evident to those observed in the single airfoil plots. The data convergence is not as sharp as previously seen but the effects with y^+ are similar. This plot graphs the average y^+ of the three surfaces but if plotted versus either of the three y^+ values separately there is no observable change in the plots except for the x-axis scale.
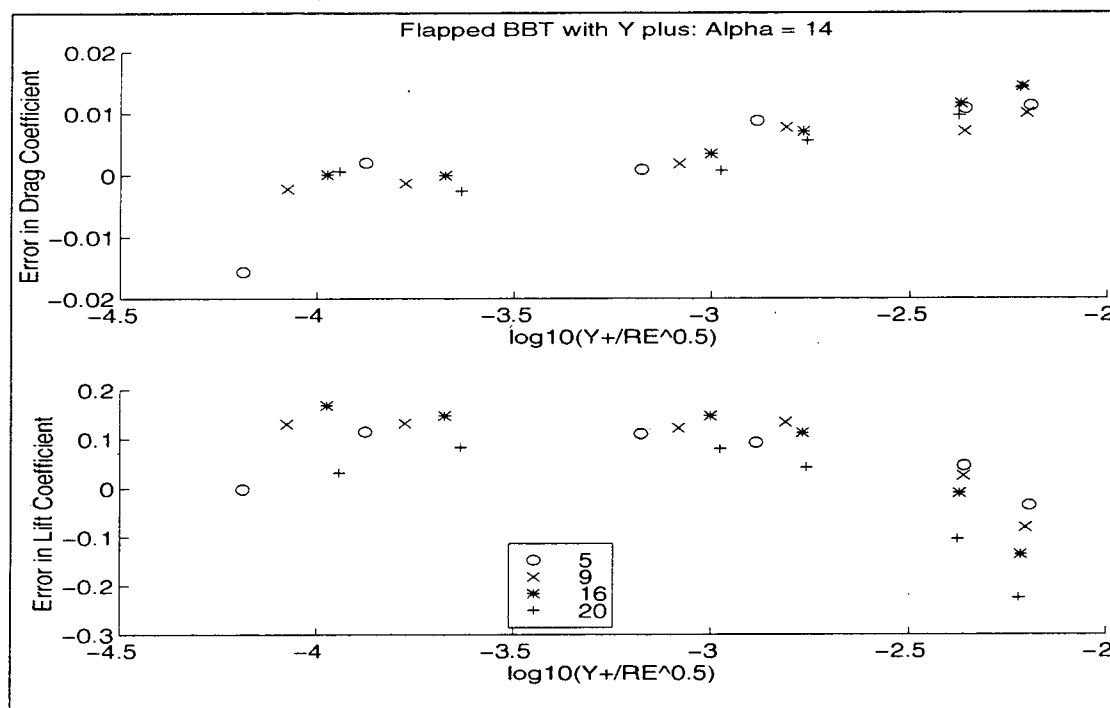
Fig. 6-5   High Lift 20slat/10flap Configuration 14° Angle of Attack, BBT Model, Different X scale

Interestingly, the drag error is better when plotted against $y^+/\sqrt{Re}$ in Fig. 6-5 but the lift is better against y^+. Fig. 6-6 and Fig. 6-7 are the same case but with the SPT model and with both X-axis scales.
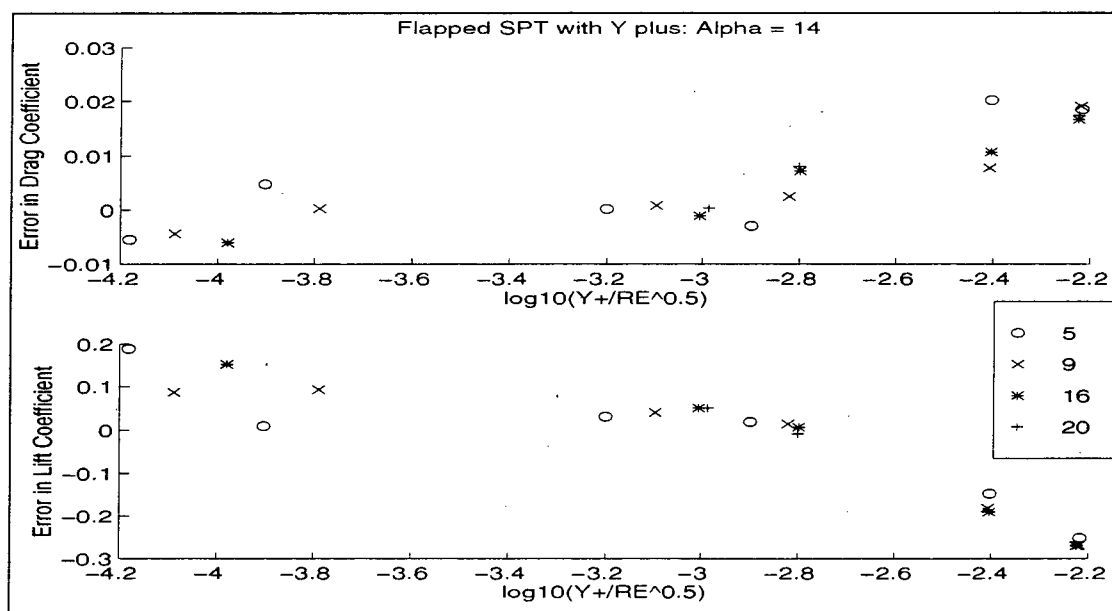
Fig. 6-6   High Lift 20slat/10flap Configuration 14° Angle of Attack, SPT Model, Different X Scale
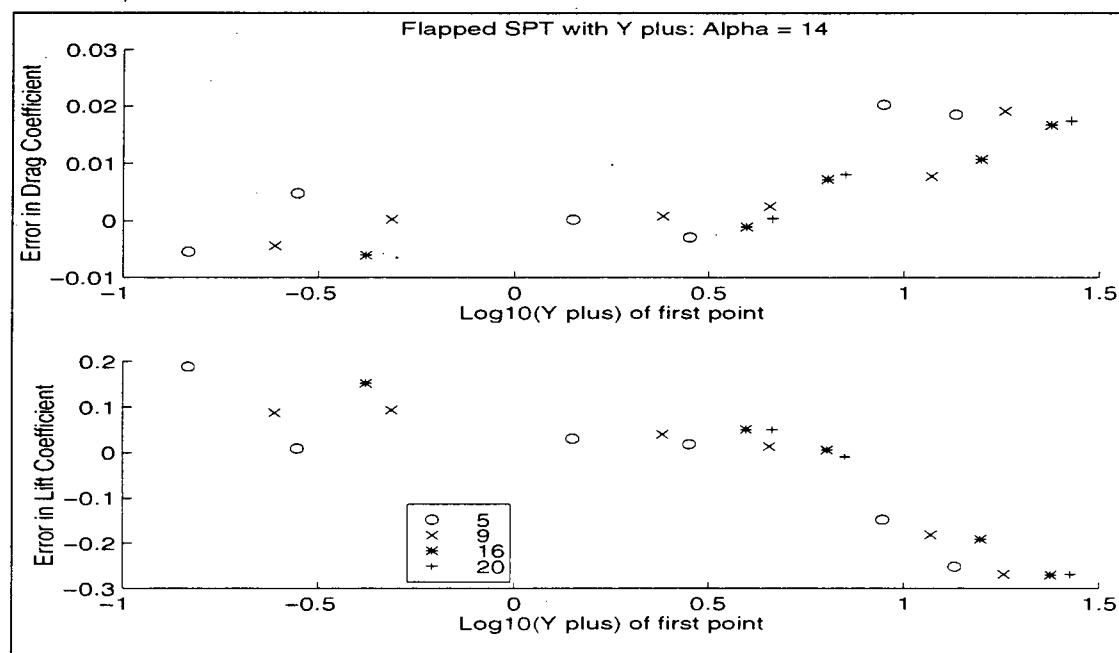
Fig. 6-7   High Lift 20slat/10flap Configuration 14° Angle of Attack, SPT Model

The Spalart model seems more consistent by plotting versus $y^+/\sqrt{Re}$, as it was for any moderate to high angle of attack on the simple airfoils. The SPT model seems the more likely of the two to be able to be extended to lift and drag trend data on high lift airfoils. When only y^+ is used, the best trend data remains at $y^+ \sim 3$ or so, which would not have seemed reasonable beforehand, given the complexity of the flowfield.

Chapter 7   Conclusions and Recommendations for Future Study

7.1 Introduction

This section presents the major findings of this study including those items which are newly presented here. In addition some recommendations for future study are suggested.

7.1.1 Grid Refinement

In agreement with studies of transonic airfoils, this study has found that the spacing in the normal direction is much more important than that along the surface of the airfoil for incompressible tests. The Taguchi Technique amplifies this by showing that it is the most important parameter of all in certain cases, more important than Reynolds number or turbulence model. A new discovery to this study is that this distance is the most important parameter across a wide range of Reynolds numbers and even angles of attack. It has been shown that the parameter $y^+/\sqrt{Re}$ can be used to pinpoint desired lift and drag errors across a wide Reynolds number and angle of attack range. This parameter points to constant lift and drag error across the entire Reynolds number range for medium and higher angles of attack. This compares favorably with the inverse Reynolds number power of the NACA0012 compilation[10]. For low angles of attack, y^+ alone can be used. The scaling factor $1/\sqrt{Re}$ on y^+ may be a correction for pressure effects at medium to high angles of attack but it definitely allows the data to capture the turbulent data dip which does appear in the pressure drag coefficient.

7.1.2 Reynolds Number Trend

A new relationship between CFD and wind tunnel testing has been explored which may allow low to medium Reynolds number data to be extended to higher values. By run-

ning CFD codes and suitable grids at the same Reynolds numbers as the wind tunnel tests, the values of C_d and C_l error converge to a single curve from which higher Reynolds number solutions from CFD alone can be used to predict high Reynolds number data. This method involves keeping the CFD solver in one configuration and changing only the wall spacing in the grid, the Reynolds number, the angle of attack, and the turbulence model if desired. Both the Baldwin-Barth and Spalart-Allmaras were satisfactory for most Reynolds number/angle of attack combinations but the Spalart-Allmaras model is better at the extreme cases, which includes the high lift airfoil. Another new discovery was that in the low angle of attack cases, the grids at high wall spacings ($y^+ \geq 5$) can be used to extend the Reynolds number data since this end of the curve shows better convergence properties at low angle of attack. The initial work, as explained in Chapter 2 was able to demonstrate the ability of a constant y^+ value to mimic not only the wind tunnel drag values of the sharp NACA0012, but the drag trend as well. This relationship does not hold for blunt airfoils due to the more viscous nature of the vortical trailing edge flow. At low angles of attack, before the pressure field around the airfoil changes too much it still holds but as stated, the consistent lift and drag errors are found at $y^+ \sim 5$ to 10.

7.1.3 Turbulence Model Performance

In both turbulence models of interest in this study, but more so in the Spalart-Allmaras model there is an interesting traveling discontinuity in the lift and drag data. At a value of $y^+/\sqrt{Re}$ that is constant across the Reynolds number at a given angle of attack but that increases with angle of attack there is a slight discontinuity in both the drag and lift coefficients. Because it is evident in the pressure drag only, it is surmised that this effect is manifested through the velocity gradients that are amplified at certain grid spacings at the right angle of attack. It does not affect the ability to predict higher Reynolds number data. The Spalart model is either more sensitive to pressure gradient effects or causes non-physical pressure sensitivities at certain grid spacings. This was evident, but less so, in the Baldwin-Barth model. In the excursions to the basic method, the Baldwin-Lomax model was compared in a new way, across Reynolds numbers and spacing for lift and drag error

and was shown to be unsatisfactory when compared to the other two models. New comparisons of the remaining turbulence models were made on different grids and airfoil trailing edges when run across the range of spacings and Reynolds numbers.

7.1.4 Taguchi Techniques

This work is the first use of the Taguchi Technique statistical tool as a method of helping to evaluate the performance of a CFD solver itself, rather than a hardware design. This technique helps in the design of the experiment and identifies those factors that are important to the result being studied and under what circumstances they are important. Not only main factors but interactions between factors are highlighted by this technique which may allow developers and experimenters to more intelligently apply limited and valuable computer resources and time. The Taguchi Techniques agreed with and amplified in some cases the results of the current work as shown in the discussion of Chapters 3, 4, and 5. It is a very flexible tool and may have a role to play in code validation, turbulence model evaluation, and other areas where a large matrix of runs is required.

7.1.5 High Lift Airfoils

This study has determined that the first wall normal spacing point seems to also be a very important point in the solutions of a three element high lift airfoil system across a wide Reynolds number range. When applied to trend information, it seems to have little or no effect which airfoil element is chosen to calculate y^+. The characteristics of Reynolds number, angle of attack and y^+ that were evident in the single airfoil are also in evidence for the high lift case, although the data convergence of lift and drag error are not so sharp at higher Reynolds number. The turbulent scaling parameter for y^+ seems to be consistent for the high lift airfoils. The Spalart-Allmaras method is more clearly better able to predict consistent values of lift and drag error than it was for the simple airfoils. It is also quite surprising at how accurate this solver/turbulence model combination is for drag and lift error at tight wall spacing over this very complicated flow. If the 20×10^6 Reynolds num-

ber case were the high Reynolds number unknown, this method would have predicted it within 5%.

7.1.6 Absolute Accuracy

CFD solvers must deal with a multitude of accuracy issues including modeling error (are the governing equations correct?), round-off errors, truncation errors, and consistency. This work adds absolute error - the absolute difference between the wind tunnel solution and CFD - and demonstrates that it can be tracked successfully across a wide Reynolds number range for different airfoils at various angles of attack.

7.2 Recommendations for Future Study

The results presented in this work are based on only the combination of INS2D and the two turbulence models noted. The Taguchi Technique, which belongs to the family of techniques that includes neural networks and regression models is but one of several statistical methods. The Taguchi Technique assumes linearity, in that the effect of 'A' + the effect of 'B' = the effect of 'A+B'. Other techniques may operate differently when used against CFD solvers. Ideally, the use of the chosen statistical method should point toward selection of solver parameters. Since Taguchi Techniques were used here for the first time on the solver, this avenue was not pursued, although it is an excellent area for future research since the Taguchi Techniques seem to be able to point out solver interactions. Any further work should attempt to extend the assumptions contained in the current research. The Reynolds number trend method shows promise in its use for high lift airfoils, although perhaps the solver/turbulence model combination must be optimized for the more complex cases.

References

1. Ok, Honam, "Development of an Incompressible Navier-Stokes Solver and its Application to the Calculation of Separated Flows", Ph.D. Thesis, 1993.

2. Kim, Byoungsoo, "Automatic Multi-Block Grid Generation about Complex Geometries", Ph.D. Thesis, 1994.

3. Rodgers, S. E., and Kwak, D., *An Upwind Differencing Scheme for The Time-Accurate Incompressible Navier-Stokes Equations,* AIAA Paper 88-2583, 1988.

4. Rogers, S. E., and Kwak, D., *An Upwind Differencing Scheme for the Incompressible Navier-Stokes Equations,* NASA-TM-101051, 1988.

5. Rogers, S. E., and Kwak, D., *Steady and Unsteady Solutions of the Incompressible Navier-Stokes Equations,* AIAA Paper 89-0463, 1989.

6. Elsenaar, A., (Chairman, CFD Working Group), "A Selection of Experimental Test Cases for the Validation of CFD Codes", AGARD-AR-303 Vol I and II, 1994.

7. McGhee, R. J., and Beasley, W. D., *Low-Speed Aerodynamic Characteristics of a 13-Percent-Thick Medium-Speed Airfoil Designed for General Aviation Applications,* NASA-TP-1498, 1979.

8. McGhee, R. J., and Beasley, W. D., *Low-Speed Aerodynamic Characteristics of a 17-Percent-Thick Medium-Speed Airfoil Designed for General Aviation Applications,* NASA-TP-1786, 1980.

9. Harris, C. D., *Two-Dimensional Aerodynamic Characteristics of the NACA0012 Airfoil in the Langley 8 Foot Transonic Pressure Tunnel,* NASA-TM-81927, 1981.

10. McCroskey, W. J., *A Critical Assessment of Wind Tunnel Results for the NACA0012 Airfoil,* NASA-TM-100019, 1987.

11. McGhee, R. J., et al., *Wind Tunnel Results for an Improved 21 Percent Thick Low Speed Airfoil Section,* NASA-TM-78650, 1978.

12. Noonan, K. W., et al., *Low-Speed Aerodynamic Characteristics of a 9.3 Percent Thick Supercritical Airfoil Section,* NASA-TM-X-72763, 1982.

13. Loftin, L. K., Jr., and Bursnall, W. J., *The Effects of Variations in Reynolds Number Between 3.0x10^6 and 25.0x10^6 Upon the Aerodynamic Characteristics of a Number of NACA 6-Series Airfoil Sections*, NACA Report 964, 1950.

14. Ferris, J. C., McGhee, R. J., and Barnwell, R. W., *Low-Speed Wind-Tunnel Results for Symmetrical NASA LS(1)-0013 Airfoil*, NASA-TM-4003, 1987.

15. Van den Berg, B., *Boundary Layer Measurements on a Two-Dimensional Wing with Flap*, NLR-TR-79009U, 1979.

16. Valarezo, W. O., et al., *Multi-Element Airfoil Optimization for Maximum Lift at High Reynolds Number*, AIAA-91-3332-CP, 1991.

17. Hobbs, C. R., et al., *High Lift Research Program for a Fighter-Type Multi-Element Airfoil at High Reynolds Number*, AIAA 96-0410, 1996.

18. Moir, I. R. M., Foster, D. N., and Holt, D. R., *The Measurement and Analysis of the Profile Drag of a Wing with a Slotted Flap*, RAE-CP-1233, 1972.

19. Foster, D. N., Irwin, H. P. A., and Williams, B. R., *The Two-Dimensional Flow Around a Slotted Flap*, ARC-R/M-3681, 1971.

20. Chin, Vincent D. et al., *Flowfield Measurements About a Multi-Element Airfoil at High Reynolds Number*, AIAA 93-3137, 1993.

21. Hobbs, C. R., <u>Effect of Reynolds Number on MDA F/A-18E/F Airfoil Section,</u> Informal Transmission (Wind Tunnel Test Data), McDonnell-Douglas, 1996.

22. Valarezo, W. O., Dominik, C. J., and McGhee, R. J., *Reynolds and Mach Number Effects on Multi-Element Airfoils*, AIAA 93-27446, 1993.

23. Berkowitz, B. M., Potapczuk, M. G., Namdar, B. S., and Langhals, T. J., *Experimental Ice Shape and Performance Characteristics for a Multi-Element Airfoil in the NASA Lewis Research Tunnel*, NASA-TM-105380, 1991.

24. Luh, R. C., and Mack, M. D., *A Numerical Procedure to Predict the Effects of Reynolds Number and Trip Strip Variation on Three-Dimensional Wing Lift and Pitching Moment*, AIAA 84-0255, 1984.

25. Rogers, S. E., *Progress in High-Lift Aerodynamic Calculations*, Journal of Aircraft Vol. 31 No. 6, Nov-Dec 1994.

26. Kusunose, K., and Cao, H. V., *Numerical Prediction of Reverse Reynolds Number Effects for Multi-Element Airfoils*, 9th International Conference on Numerical Methods in Laminar and Turbulent Flow, 1995.

27. Kusunose, K., *The Importance of Flow Physics in CFD*, Asymptotic and Computational Methods for Applications Conference, Troy, NY, October 1995.

28. Lynch, F. T., Potter, R. C., and Spaid, F. W., *Requirements for Effective High Lift CFD*, Informal Transmission (ICAS Paper), 1996.

29. McMasters, J., *What the Heck Is a Reynolds Number?*, AIAA Newsletter, Pacific Northwest Section, Vol. 25 No. 1, 1995

30. Bushnell, D. M. et al., *Reynolds Number Influences in Aeronautics*, NASA-TM-107730, 1993.

31. Mack, M.D. & McMasters, J.H., *High Reynolds Number Testing in Support of Transport Airplane Development*, AIAA Paper 92-3982, 1992.

32. Bobbitt, P. J., *The Pros and Cons of Code Validation*, AIAA Paper 88-2535, 1988.

33. Rogers, S. E., Wiltberger, N. L., and Kwak, D., *Efficient Simulation of Incompressible Viscous Flow Over Multi-Element Airfoils*, NASA-CR-193000, 1992.

34. Georgiadis, N. J., and Dudek, J. C., *Grid Resolution and Turbulent Inflow Boundary Condition Recommendations for NPARC Calculations*, NASA-TM-106959, 1995.

35. Zingg, D. W., *Grid Studies for Thin-Layer Navier-Stokes Computations of Airfoil Flowfields*, AIAA Journal, Vol 30, No. 10, Technical Notes, 1992.

36. Abdol-Hamid, K. S. et al, *Application of Navier Stokes Code PAB3D with Kappa Epsilon Turbulence Model to Attached and Separated Flows*, NASA-TP-3480, 1995.

37. Nettelhorst, Heather L. et al, *Grid Resolution and solution Convergence for Mars Pathfinder Forebody*, NASA-TM-109173, 1994.

38. Jameson, Antony, *Re-Engineering the Design Process through Computation*, AIAA Paper 97-0641, 1997.

39. Kern S., *Evaluation of Turbulence Models for High-Lift Military Airfoil Flowfields,* AIAA Paper 96-0057, 1996.

40. Wilcox, D. C., *Comparison of Two-Equation Turbulence Models for Boundary Layers with Pressure Gradients,* AIAA Journal Vol. 31, No. 8, 1993.

41. Londenberg, W. K., *Turbulence Model Evaluation for Use with Supercritical Airfoils,* AIAA Paper 93-0191, 1993.

42. Baldwin, B. S., and Lomax, H., *Thin Layer Approximation and Algebraic Model for Separated Turbulent Flows,* AIAA Paper 78-257, 1978.

43. Baldwin, B. S., and Barth T. J., *A One-Equation Turbulence Transport Model for High Reynolds Number Wall-Bounded Flows,* AIAA Paper 91-0610, 1991.

44. Spalart, P. R., and Allmaras, S. R., *A One-Equation Turbulence Model for Aerodynamic Flows,* AIAA Paper 92-0439, 1992.

45. Johnson, D. A., and King, L. S., *A Mathematically Simple Turbulence Closure Model for Attached and Separated Turbulent Boundary Layers,* AIAA Paper 84-0175, 1984.

46. Follett. W., *Optimization Methodology for Unconventional Rocket Nozzle Design,* NASA-CP-3332-Vol-1, 1996.

47. Acheson, K.E., et al, *Design Optimization Study for F-15 Propulsion/Forward Fairing Compatibility,* AIAA Paper 93-3484, 1993.

48. Haines, A. B., and Young, A. D., (Editor), "Scale Effects on Aircraft and Weapon Aerodynamics", AGARD-AG-323, 1994.

49. Munson, B. R., Young, D. F., and Okiishi, T. H., "Fundamentals of Fluid Mechanics", Wiley, 1990.

50. Anderson, D. A., Tannehill, J. C. and Pletcher, R. H., "Computational Fluid Mechanics and Heat Transfer", McGraw-Hill, 1984.

51. Abbot, I. H., Von Doenhoff, A. E., "Theory of Wing Sections", Dover, 1959

52. Schlichting, H., Dr, "Boundary Layer Theory (Seventh Edition)", McGraw-Hill, 1979.

53.   Hoerner, S. F., Dr, "Fluid Dynamic Drag", Hoerner, 1965.

54.   Tennekes, H. and Lumley J. L., "A First Course in Turbulence", MIT Press, 1972.

55.   Ross, Phillip J., "Taguchi Techniques for Quality Engineering (second edition)", McGraw-Hill, 1996.

56.   Belavendram, Nicolo, "Quality by Design, Taguchi Techniques for Industrial Experimentation", Prentice Hall, 1995.

57.   Suhs, N. E. and Tramel, R. W., "PEGSUS 4.0 Users Manual", AEDC-TR-91-8, 1991.

58.   Chan, W. M., Chiu, I., and Buning, P. G., *User's Manual for the HYPGEN Hyperbolic Grid Generator and the HGUI Graphical User Interface,* NASA-TM-108791, 1993.

59.   McGhee, R. J. and Harris C. D., NASA Langley Research Center, Personal Electronic Mail Conversations, 1995-1997.

60.   Breidenthal, R., Class Notes AA508, Viscous Flow III, University of Washington, 1995.